U.PORTO
FEUP FACULDADE DE ENGENHARIA
UNIVERSIDADE DO PORTO

Preparation, Characterisation and Stability Evaluation of Perovskite Solar Cells

Dissertation presented to the Faculty of Engineering of
University of Porto for obtaining the degree of
Doctor in Chemical and Biological Engineering
by

Isabel Tavares de Mesquita

Luísa Manuela Madureira Andrade Silva, Assistant Researcher – Supervisor

Adélio Miguel Magalhães Mendes, Full Professor – Co-supervisor

lepabe
Laboratory for Process Engineering, Environment, Biotechnology and Energy

Department of Chemical Engineering,
Faculty of Engineering, University of Porto, Portugal

2019

This thesis was financially supported by Foundation for Science and Technology (FCT) through the PhD grant PD/PB/105985/2014 and by projects: i) GOTSolar (no. 687008) funded by European Union's Horizon 2020 Programme through a FET Open research and innovation action; ii) SolarPerovskite (NORTE-01-0145-FEDER-028966) funded by FEDER (European Regional Development Fund) funds, under Norte Portugal Regional Operational Programme (NORTE 2020), and national funds through FCT/ MCTES (PIDDAC); iii) WinPSC (POCI-01-0247-FEDER-017796) co-funded by FEDER, through the Operational Programme for Competitiveness and Internationalisation (COMPETE 2020), under Portugal 2020 Partnership Agreement; iv) BI-DSC (no. 321315) funded by the European Commission through the 7th Framework Programme, the Specific Programme "Ideas" of the European Research Council as part of an Advanced Grant; v) SunStorage (POCI-01-0145-FEDER-016387) funded by ERDF through COMPETE 2020 - Operational Programme for Competitiveness and Internationalization (POCI), by FCT; vi) UID/EQU/00511/2019 – LEPABE (Laboratory for Process Engineering, Environment, Biotechnology and Energy) funded by national funds through FCT/MCTES (PIDDAC); vii) POCI-01-0145-FEDER-006939 (LEPABE-UID/EQU/00511/2013), funded by ERDF, through COMPETE 2020 and by nationals funds through FCT; and viii) NORTE-01-0145-FEDER-000005-LEPABE-2-ECO-INNOVATION, funded by NORTE 2020, under Portugal 2020 Partnership Agreement, through ERDF.

Isabel Tavares de Mesquita
Laboratory for Process Engineering, Environment, Biotechnology and Energy
University of Porto – Faculty of Engineering
Rua Dr. Roberto Frias s/n, 4200-465 Porto, Portugal

Acknowledgements

First of all, I am grateful to my supervisors Doctor Luísa Andrade and Professor Adélio Mendes for all the support, availability and for always trusting me and in my work. This thesis is also yours. I like to express my huge gratitude to Doctor Luísa for all the motivation, guidance and friendship, for being always available to help me and advise me wisely in the good and bad moments. Above all things, I would like to thank for all the transmitted knowledge and optimism, without that this thesis would not be possible. I also thank my co-supervisor Professor Adélio Mendes for his great and enormous capacity of work and for always organized time for me in his crazy schedule. Thank you for giving me the opportunity to work in this group, full of fantastic people.

I gratefully acknowledge Professor Michael Grätzel for accepting me in his research group at EPFL and Doctor Shaik Zakeeruddin for all the patience and constant guidance. Thanks to all LPI members for welcoming me and for always being available to help me and for deep discussions. I learned a lot from you!

Many thanks for my lab mates from the Solar Group in UPTEC led by Professor Mendes. It is an outstanding group, full of friendly and fun people that always provided me a relaxed and calm environment to perform my work. Special thanks to my friends from the beginning, Ana Pereira, Andreia Cruz, Joana Ângelo, Paula Dias, Rute Santos, Seyedali Emami, António Vilanova, Pedro Magalhães and Sérgio Miranda for all the great moments, complicity and friendship. Friends for life! I am also very grateful to my “perovskite girls”, Cristina Teixeira, Mafalda Pereira and Vera Duarte for being a very cohesive group, always ready to help in the difficult moments of the work. To Verena Stockhausen for starting this new and long journey with me on the perovskite solar cells field. To Rita Arnaldo, for being an excellent deskmate, dividing her space, music and news with me. Your secrets are safe with me! I also acknowledge to Margarida Catarino for always being available to help me in the assemble of glove box and all other things. Your knowledge is huge! I want also to thanks Cecilia Pedrero for all the friendship and help in the “more chemistry”

doubts and Tânia Lopes for friendship, advices and for always saving me from the crises of potentiostat.

To Amaral/Crispim family, Teresa, Hélder, Sofia and Francisco, for receiving me in your house as a member of your family, during my stay in Switzerland.

I cannot forget my childhood friends Aurora, Micaela, Sandra and Vanessa, that are still an important part of my life. The jobs put us in different countries, but the good stories and laughs are guaranteed whenever we get together.

A special and huge thanks to my family, for their endless support and love. A heartfelt thanks to my parents, Fátima and Rodolfo Mesquita for your unconditional love and for always being present in all the most important moments of my life. Without your support none of this would have been possible. You are examples of strength and inspiration. To my grandparents, Alice Ventura and Armando Mesquita for all the knowledge transmitted in the first years of my life and for raising me with good values, as a person and as a woman. I cannot forget my aunt, Isabel Silva, and my cousin, João Azevedo, for all the good discussions and moments passed around the table. With you I am always learning things, useful or not! You are the best family that I could ever had!

Last but not least, I want to sincerely thank to my boyfriend João Cunha for all these years by my side and for never let me down in any moment. Thank you for making me laugh every day, you know what you mean to me.

To all who have been part of this tireless journey and I may have forgotten, my sincere and humble thanks!

To my lovely family
and friends…

Preface

The present work was developed at the Laboratory for Process Engineering, Environment, Biotechnology and Energy (LEPABE) facilities, in the Chemical Engineering Department of the Faculty of Engineering - University of Porto (FEUP), between 2015 and 2019 and under the FCT (Foundation for Science and Technology) grant PD/PB/105985/2014. The work was supervised by Doctor Luísa Andrade and co-supervised by Professor Adélio Mendes, both from LEPABE - FEUP.

The initial knowledge that allowed the expansion of the thesis was acquired at the Laboratory of Photonic and Interfaces (LPI) in École Polytechnique Fédéral de Lausanne (EPFL), in Switzerland, under the supervision of Professor Michael Grätzel and Doctor Shaik Mohammed Zakeeruddin.

This thesis presents five chapters: one introduction chapter; three scientific papers, each paper represents one independent chapter; and a final chapter with the general conclusions and perspectives of future work.

CONTENTS

CHAPTER 2

INSIGHTS IN PEROVSKITE SOLAR CELL FABRICATION: UNRAVELLING THE HIDDEN CHALLENGES OF EACH LAYER

CHAPTER 3

TEMPERATURE IMPACT ON PEROVSKITE SOLAR CELLS UNDER OPERATION

CHAPTER 4

CHAPTER 5

ABSTRACT

Worldwide energy demand grew 2.3 % in the last year, where electricity accounted with 23 000 TWh, and the CO_2 emissions increased 1.7 %. This fast growth pushed the electricity towards a 20 % share in the total final consumption energy during 2018. The power conversion of energy from renewable sources is the only way to address this great increase of energy demand, which represents already 25 % of the generated energy and it is forecasted to rise 40 % until 2040 (International Energy Agency data). Several renewable sources can be explored; in particular, the sun represents a powerful energy source, easily affordable for humans and by means photovoltaic solar cells display an efficient way for producing electricity. This work aims at to study a thin-film photovoltaic technology - perovskite solar cells (PSCs) - claimed by the scientific community as the top star of the 3rd generation family of solar cells. This technology displays efficiencies higher than 24 %, facile fabrication protocols and diversity of applications, rivalling already with commercialised photovoltaic technologies.

The scaling up and industrialisation of PSC rest in three main pillars: efficiency, stability and cost. The first received already much attention from scientists, which put already PSCs in the forefront of photovoltaic technologies in terms of efficiency boost in a timeframe of a single decade. Since PSCs are a thin-film solvent-processing technology, reduction of costs is already an important advantage. For further contributing to the establishment of PSCs as a competitive technology in the photovoltaic market, a simple protocol is proposed within this work, aiming to achieve reproducible and moderate mesoporous triple-cation perovskite efficient cells with spiro-OMeTAD as hole extraction layer and with a power conversion efficiency of (14.8 ± 1.0) %. All materials, methods and equipment are described and a step-by-step analysis of each layer is provided with several fabrication techniques compared in terms of efficiency optimisation. Still, stability needs further attention and this was the main focus of the present work. So, the effect of temperature, humidity and oxygen were assessed. The photovoltaic performance was evaluated *in-situ* to

reproduce real operating conditions in a temperature range between -5 °C and 80 °C. The impact of the temperature during PSC operation is mainly in the hole extraction layer (HEL), particularly in its additives evaporation. The main HELs used in PSCs were investigated and their irreversible losses after thermal-stress were assessed. The effect of humidity and oxygen was evaluated following two strategies: one during the preparation of the perovskite and hole extraction layers and the second in the long-term stability of the fully devices, stored under inert and ambient atmospheres. The deposition of perovskite layer was studied in two different atmospheres (nitrogen and air) in the relative humidity range of 0 - 50 %. The stability of the devices was recorded weekly during 1000 h. These tests were also important to understand the limiting conditions dominating the deposition steps of the HEL and perovskite layer. These less restrictive conditions will directly impact on the manufacturing costs of the devices when the design of a PSC production plant is in view.

SUMÁRIO

O consumo mundial de energia cresceu 2,3 % no último ano, onde a eletricidade contabilizou 23 000 TWh e as emissões de CO_2 aumentaram 1,7 %. Este rápido crescimento fez com que a eletricidade representasse 20 % da energia total consumida durante 2018. A produção de energia a partir de fontes renováveis permite dar resposta a este aumento da procura energética, representando já 25 % da geração de energia e prevendo-se um crescimento de 40 % até 2040 (dados da Agência Internacional da Energia). Diversas fontes de energia renovável podem ser exploradas; em particular, o sol representa uma poderosa fonte de energia, facilmente acessível ao Homem e que, por meio de células fotovoltaicas, permite converter de forma eficiente energia solar em energia elétrica. Este trabalho foca-se no estudo de uma tecnologia fotovoltaica de filme fino - células solares de perovskita (PSCs) - designada recentemente pela comunidade cientifica como "*top star*" da família de células solares de 3ª geração. Esta tecnologia apresenta eficiências superiores a 24 %, processos de fabrico simples e possibilidade de diversificação de aplicações, rivalizando com as tecnologias fotovoltaicas já comercializadas.

O aumento de escala e sua respetiva comercialização assenta em três pilares principais: eficiência, estabilidade e custo. O primeiro tem recebido muita atenção por parte da comunidade cientifica, que conseguiu colocar as PSCs na vanguarda das tecnologias fotovoltaicas em termos de eficiência em menos de uma década de existência. Sendo as PSCs passíveis de serem depositadas através de técnicas de processamento de solvente, a redução de custos é já uma vantagem muito importante. Para contribuir ainda mais para o estabelecimento das PSCs como uma tecnologia competitiva no mercado fotovoltaico, neste trabalho é apresentado um protocolo simples que permite alcançar células de perovskita triplo-catião com arquitetura mesoporosa e spiro-OMeTAD como transportador de lacunas, atingindo eficiências de (14.8 ± 1.0) %. Todos os materiais, métodos e equipamentos são descritos e uma análise passo-a-passo de cada camada é fornecida comparando várias

técnicas de preparação em termos de eficiência. Ainda assim, a estabilidade necessita de mais atenção por parte da comunidade científica e por essa razão tornou-se o foco do presente trabalho, que avalia o efeito de varáveis como a temperatura, humidade e oxigénio no desempenho das PSCs. O desempenho fotovoltaico dos dispositivos foi avaliado *in-situ* de forma a reproduzir as condições de operação real, numa gama de temperaturas entre - 5 °C e 80 °C. O impacto da temperatura durante o funcionamento da PSC é maioritariamente na camada transportadora de lacunas, particularmente responsável pela evaporação dos seus aditivos. Os transportadores de lacunas mais usados na literatura foram estudados e foram determinadas as suas perdas irreversíveis de desempenho, após os testes de *stress* térmico. O efeito da humidade e do oxigénio foi avaliado de duas formas: em primeiro lugar, durante a preparação das camadas de perovskita e do transportador de lacunas, e em segundo lugar, em termos de estabilidade a longo prazo dos dispositivos preparados, mantidos numa atmosfera ambiente ou inerte. A deposição da camada de perovskita foi estudada em duas atmosferas diferentes (azoto e ar) com valores de humidade relativa entre 0 e 50 %. A estabilidade dos dispositivos foi registada semanalmente durante 1000 h. Estes testes são também importantes para perceber as condições limite que podem ser usadas na deposição das camadas de perovskita e do transportador de lacunas. Estas condições menos restritivas têm um impacto direto nos custos de produção quando se tem em vista o projeto de uma unidade de produção de PSCs.

LIST OF ABBREVIATIONS AND SYMBOLS

Abbreviations	Definition	Units
5-AVA	5-ammoniumvaleric acid	
ALD	atomic layer deposition	
BIPV	building integrated photovoltaics	
c-Si	crystalline silicon	
CuPc	copper phthalocyanine	
CuSCN	Copper(I) thiocyanate	
CV	cyclic voltammetry	
DC	direct current	
DMF	N,N-dimethylformamide	
DMSO	dimethyl sulfoxide	
DSC	dye-sensitized solar cell	
DSVP	dual-source vapor deposition	
D-*t*-BP	2,6-di-*tert*-butylpyridine	
e^-	electrons	
E	energy	eV
FA	formamidinium	
FAI	formamidinium iodide	
FDT	2',7'-bis(bis(4-methoxyphenyl)amino)spiro [cyclopenta[2,1-b:3,4-b']dithiophene-4,9'-fluorene]	
FF	fill factor	
FK209	tris(2-(1H-pyrazol-1-yl)-4-tert-butylpyridine) cobalt(III) tri[bis(trifluoromethane)sulfonimide]	
FTO	fluorine-doped tin oxide	

GBL	*γ*-butyrolactone	
GIWAXS	grazing incidence wide-angle x-ray scattering	
h	Planck constant	J·s
h^+	holes	
HEL	hole extraction layer	
HOMO	highest occupied molecular orbital	
ICBA	1′,1″,4′,4″-Tetrahydro-di[1,4] methanonaphthaleno [1,2:2′,3′,56,60:2″,3″][5,6]fullerene-C60	
IMPS	intensity-modulated photocurrent spectroscopy	
IPCE	incident photon to current efficiency	
I-V	current-potential characteristics	
J_{sc}	short-circuit current density	$mA \cdot cm^{-2}$
Li-TFSI	lithium bistrifluoromethane sulfonimidate	
MABr	methylammonium bromide	
MPP	maximum power point	
P3HT	poly(3-hexylthiophene-2,5-diyl)	
PCBM	[6,6] phenyl C61 butyric acid methyl ester	
PCE	power conversion efficiency	
PDPPDBTE	poly[2,5-bis(2-decyldodecyl)pyrrolo[3,4-c]pyrrole-1, 4(2H,5H)-dione-(E)-1, 2-di (2,2′-bithiophen-5-yl) ethene]	
PEA	phenylethylammonium	
PEDOT	poly (3,4-ethylenedioxythiophene)	
PEDOT:PSS	poly(3,4-ethylenedioxythiophene) polystyrene sulfonate	
PEIE	ethoxylated polyethylenimine	
PLMF	perovskite-like metal formate	
poly-Si	polycrystalline silicon	

PMMA	poly(methyl methacrylate)	
PSC	perovskite solar cell	
PTAA	poly(triaryl amine)	
PV	photovoltaic	
q	scattering vector	nm^{-1}
RH	relative humidity	
SEM	scanning electron microscopy	
Spiro-OMeTAD	2,2',7,7'-tetrakis(N,N-di-p-methoxyphenyl-amine)9, 9'-spirobifluorene	
T	temperature	ºC
t-BP	4-*tert*-butylpyridine	
TCO	transparent conductive oxide	
TFB	poly[(9,9-dioctyl-fluorenyl-2,7-diyl)-co-(4,4′-(N-(4-sec butylphenyl) diphenylamine)]	
ToF-SIMS	time-of-flight secondary ion mass spectrometry	
UV	ultraviolet	
V_{oc}	open-circuit potential	V
XPS	x-ray photoelectron spectroscopy	
XRD	x-ray diffraction	

Greek symbols	Definition	Units
α	alfa phase of perovskite crystal	
β	beta phase of perovskite crystal	
γ	gama phase of perovskite crystal	
∇	heat	
η	solar to energy conversion efficiency	%
υ	frequency	

Subscripts	Definition
oc	open-circuit
sc	short-circuit
CB	conduction band
VB	valence band
p	peak
i	initial value

CHAPTER 1

INTRODUCTION

Adapted from the peer-reviewed article

Mesquita, I., Andrade, L., Mendes, A., *Perovskite solar cells: Materials, configurations and stability*, Renewable and Sustainable Energy Reviews **82** (2018), p:2471-2489.

1

INTRODUCTION

The accelerated world population growth and post-industrial era bring to attention an unprecedented energy demand, responsible for environmental problems, sustainable development concerns as well as economic challenges. At present, fossil fuels are the source for more than 80 % of the world primary energy and responsible for most of the greenhouse gas emissions.[1] Technologies that take advantage of renewable energy sources such as sun, wind, biomass, hydraulic and geothermal are being studied and developed. Sunlight has an enormous potential as energy source with an irradiance 1.8×10^{14} kW at earth's surface,[2] which can be transformed in electricity and heat with minimal environmental impact.[3] Photovoltaic (PV) solar cells are one of the most promising technologies for producing electricity from sunlight; in particular, photovoltaic panels based on silicon technology (c-Si and poly-Si) are widely installed showing normal efficiencies of 15 - 20 %[4,5] with a record-breaking efficiency of 26.6 %.[6] However, PV-grade silicon fabrication uses harmful chemicals in a complex purification process.[7] For building integrated photovoltaic (BIPV), silicon-based panels are generally unaesthetic and display significantly lower real efficiencies when used in facades, mostly due to the difficulty in harvesting diffuse light. The third generation of solar cells emerged with dye sensitized solar cells (DSCs); they can be easily adapted to the facades of buildings, display different colors and patterns and with the interesting feature of harvesting efficiently diffuse light. The power conversion efficiency (PCE) of this type of cells reached 14.3 % with organic-based dyes and cobalt (III/II)

complex redox electrolyte in a lab device.[8] Following these achievements, Kojima *et al*.[9] presented for the first time in 2009 a DSC using a perovskite as light absorber with 3.8 % PCE. The organometal halide perovskite material used, with the generic structure of $CH_3NH_3PbX_3$, soon proved to have an astonishing high-efficiency as light absorber displaying also very high hole and electron conductivities.[10,11,12,13] This disruptive finding led to the emergence of a new thin-film photovoltaic family - the perovskite solar cells (PSCs) - presently one of the most investigated families of solar cells. The sudden interest on the PSC is related to the great increase on energy conversion efficiency that this technology experienced in the pasted 10 years, from 3.8 % in 2009 to 25.2 % in 2019.[14] Moreover, PSCs are easy to produce and display a great potential for BIPV allowing colour[15,16] and transparency.[17] Until now, the highest certificated PCE belongs to a collaboration, between the Korean Research Institute of Chemical Technology (KRICT) and Massachusetts Institute of Technology (MIT), that have reached 25.2 %.[14] However, the structure of this certified perovskite device and its architecture are still unknown. As far as the author knows, the highest PCE reported in a scientific article was presented by Jung *et al*.[18] using P3HT without any dopants in a wide-bandgap halide achieving 22.7 % PCE, that retained 95 % of initial PCE after 1390 h under 1 sun illumination at room temperature (encapsulated device). This astonishing stability result, was only surpassed by Grancini *et al*.[19] that prepared a 2D/3D perovskite module (10 x 10 cm^2) with a carbon back contact. The module maintained the initial efficiency for more than one year, kept under 1 sun and at short circuit conditions. Although the astonishing power conversion efficiencies reached by now, two major obstacles are still limiting the commercialisation of PSC: moisture and oxygen sensitivity responsible for the degradation of the perovskite absorber, and the presence of lead (Pb) in the composition of the most efficient perovskite absorbers.[20,21,22] These major challenges are boosting the research community to develop effective hermetic encapsulating solutions and to produce efficient lead-free absorbers.

This chapter reviews the PSC working principles and the most studied configurations, as well as the role of each layer in the different architectures. Degradation mechanisms due to temperature, oxygen, UV radiation and

moisture, the role of deposition methods and hysteresis phenomenon effect in the PSC stability are also reviewed. Finally, it is presented the most recent lead-free materials reported and the innovative sealing processes that can lead to PSC commercialisation in few years. This review aims to offer an important tool for driving future research.

1.1 Device operation

"Perovskite" refers to the absorber material of PSC devices, which adopts the crystal structure of ABX_3.[23] The perovskite family typically used is based on organic-inorganic lead perovskites with the polycrystalline structure $CH_3NH_3PbX_3$, where X is a halide atom (I, Cl, Br or a combination of some of them). This type of materials shows advantageous properties to be used as a PV absorber, namely: 1) strong optical absorption due to s-p anti-bonding coupling; 2) high electron and hole mobilities and diffusion lengths; 3) superior structural defect tolerance and shallow point defects; 4) low surface recombination rate; and 5) favorable grain boundaries since they do not promote the electron-hole recombination.[24,25] In fact, comparing to the most common photovoltaic systems - Table 1.1 - perovskite semiconductors show tunable band gap, balanced electron/hole transportation, low recombination rate, carrier lifetime over 100 ns and a diffusion length over 1000 nm.[26] The high absorption coefficient of the perovskite nanocrystals makes the perovskite layer within the PSCs to be very thin, in the range of *ca*. 400 nm.

Table 1.1. Physical properties of most common photovoltaic materials.[26,27,28]

	Perovskite	Si	CIGS	GaAs	CdTe
Band gap / eV	1.5 (tunable)	1.1	1.12	1.43	1.5
Absorption coefficient / cm^{-1}	10^4-10^5	10^3	10^4-10^5	10^4-10^5	10^3
Carrier mobility / $cm^2 \cdot V^{-1} \cdot s^{-1}$	Up to 2000	1500	<10	8500	10
Carrier concentration / cm^{-3}	10^{16}-10^{17}	10^{16}	10^{15}-10^{16}	10^{17}	10^{14}-10^{15}
Carrier lifetime	>100 ns	ms	50-200 ns	<100 ns	20 ns

Perovskite solar cells present a very similar structure to typical DSCs and the most common configuration is composed by six main layers: 1) transparent conductive oxide (TCO) glass substrate; 2) a semiconductor compact layer (typically called blocking layer); 3) a mesoporous semiconductor film (scaffold); 4) a perovskite absorbing material; 5) a hole extraction material; and 6) an electrical conductive back contact. The corresponding architecture of this type of devices is sketched in Figure 1.1. The blocking layer is normally made of titanium dioxide (TiO_2), a n-type material that forms a n-i junction selective to the passage of the electrons. The mesoporous layer serves to drive the photoinjected electrons to the blocking layer, however it is not essential in the PSC operation, since there are evidences that the main role is to serve as a scaffold for the perovskite deposition.[13] The perovskite layer is the light absorber material that produces the charge separation driving electrons to the n-i junction and holes to the i-p junction. The hole transport material is a p-type material that forms an i-p junction selective to the holes' transport. For an efficient charge extraction, the band alignment of the perovskite with n- and p-type selective materials is very important: the conduction band edge of the electron transport layer must be lower than the perovskite conduction band and the valence band edge of the hole transport layer must be higher than the perovskite valence band - see Figure 1.2.

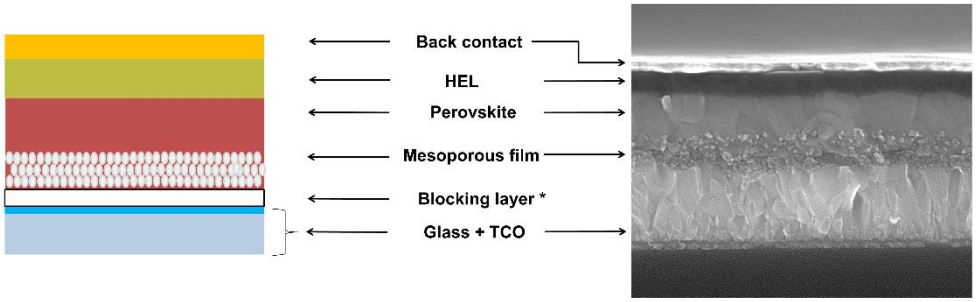

Figure 1.1. Typical mesoporous perovskite solar cell: a) sketch illustrating the multilayer arrangement and; b) a scanning electron microscopy (SEM) image (* the blocking layer is so thin that is imperceptible in SEM image).

In the typical configuration of a PSC device, as the perovskite absorbs light, an electron-hole pair is created – eq.(1.1); photogenerated electrons are injected into the mesoporous semiconductor and the holes are driven into the hole extraction layer (HEL) - eq.(1.2). The injected electron goes through the external circuit until the back contact, and the hole is transported by a hopping mechanism (electronic conduction) until the same contact. At the interface HEL/back contact the hole and electron recombine regenerating the system - Figure 1.2a. The p-n junctions are responsible for the creation of a built-in electric field that allow the charges separation, where electrons move to the mesoporous TiO_2 and holes move to the HEL.[29] Since both materials have different Fermi levels, charges flow until equilibrium is reached; a space-charge region appears at the respective interface and consequent band-bending is observed - Figure 1.2b.

$$\text{Perovskite} + h\nu \rightarrow (\text{e}^- \ldots \text{h}^+)_{\text{perovskite}} \quad (1.1)$$

$$(\text{e}^+ \ldots \text{h}^+)_{\text{perovskite}} \rightarrow \text{e}^-_{\text{CB}}(\text{TiO}_2) + \text{h}^+(\text{HEL}) \quad (1.2)$$

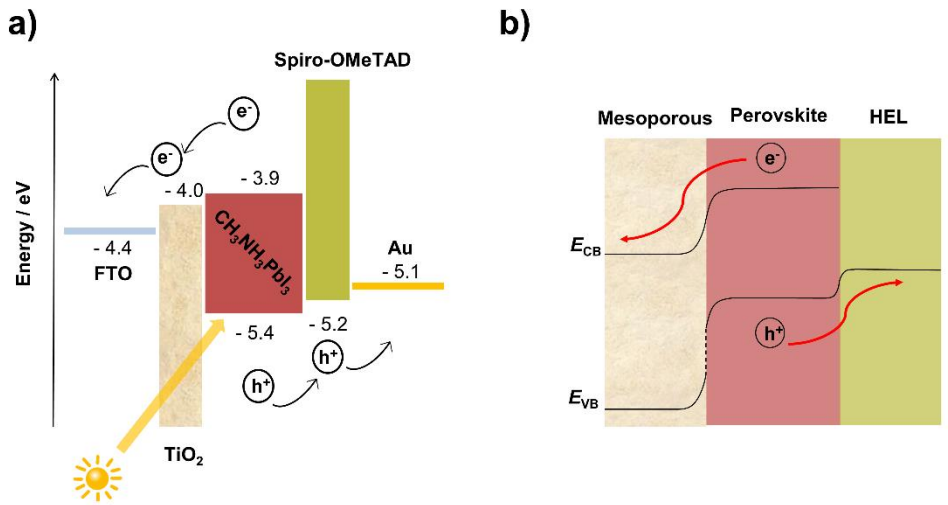

Figure 1.2. a) Energy diagram of a typical PSC representing the energy levels of typical materials used in the different layers and b) band-bending of energy levels during separation of charges.

However, undesired reactions may occur, competing with the extraction of photogenerated charges. The main back reactions are: exciton annihilation by photoluminescence - eq.(1.3); non-radiative recombination - eq.(1.4) - and recombination of the charge carriers at the interfaces (TiO_2 surface, HEL surface and TiO_2/HEL interface) - eq.(1.5-1.7) - with consequent heat release.

$$(\mathrm{e}^- \ldots \mathrm{h}^+)_{\mathrm{perovskite}} \rightarrow h\nu' \quad (1.3)$$

$$(\mathrm{e}^- \ldots \mathrm{h}^+)_{\mathrm{perovskite}} \rightarrow \nabla \quad (1.4)$$

$$\mathrm{e}^-_{\mathrm{CB}}(\mathrm{TiO_2}) + \mathrm{h}^+(\mathrm{perovskite}) \rightarrow \nabla \quad (1.5)$$

$$\mathrm{h}^+(\mathrm{HEL}) + \mathrm{e}^-(\mathrm{perovskite}) \rightarrow \nabla \quad (1.6)$$

$$\mathrm{e}^-_{\mathrm{CB}}(\mathrm{TiO_2}) + \mathrm{h}^+(\mathrm{HTM}) \rightarrow \nabla \quad (1.7)$$

1.2 PSC architectures and materials

In the thin-film solar cells family, the preparation method and the device architecture are key factors for high-efficient light-to-electricity conversion processes. In the case of PSC there are five different configurations: mesoporous-conducting semiconductor scaffold; mesoporous-insulating oxide; planar; HEL-less and inverted. Until now, the best-performing PSCs is not confined to a single architecture[30] depending heavily on the type of perovskite material used. The configurations that have been reported with higher values of power conversion efficiencies are the mesoporous and planar. In the National Renewable Energy Laboratory (NREL) efficiencies plot the most efficient certified cell presents 25.2 %, however the configuration and the detailed materials used remain unknown.

1.2.1 Mesoporous conductive semiconductor PSC device

Presently, the most studied architecture of perovskite solar cells is the mesoporous type – Figure 1.1. Perovskite $CH_3NH_3PbI_3$ nanocrystals filling the inner porosity of the TiO_2 mesoporous layer were first used to enhance the light absorption in liquid DSCs, resulting in an PCE of 3.8 %.[9] In 2011, Im *et al*.[31] proposed a quantum dot (QD) sensitized solar cell using $CH_3NH_3PbI_3$ perovskite reaching the highest efficiency among the reported inorganic QD sensitizers (6.5 %). However, liquid solar cells presented two major challenges, the deposited perovskite corrosion by redox mediator and the low performing encapsulation strategies, which allowed electrolyte leakage.[32] Kim *et al*.[33] reported for the first time the use of an amorphous organic hole-transport material, 2,2′,7,7′-tetrakis(N,N-di-p-methoxyphenyl-amine)9,9′-spirobifluorene, known as spiro-OMeTAD, having reached a PCE of 9.7 %; this hole extraction material was used for the first time in the context of solar cells by Bach *et al*.[34] The use of spiro-OMeTAD avoids the use of a liquid electrolyte and opened the door for a new era of perovskite solar cells. The advantage of the solid-state over liquid devices are obvious: need less manufacturing steps, easy interconnection of monolithically modules, easier encapsulation process and

therefore lower fabrication costs; all these benefits contribute also for easier scaling-up.[35]

The mesoporous architecture considers the use of a mesoporous layer for allowing a rapid extraction of the photoinduced electrons from the perovskite, shortening the electron transport length, and not requiring high crystal quality for an efficient light harvest.[36] However, when compared with other configurations, mesoporous perovskite solar cells commonly present lower open-circuit potential (V_{oc})[37] and lower light absorbance at wavelengths higher than 700 nm.[38] Another disadvantage is the need of a perovskite overlayer to avoid contact between the mesoporous layer and HEL, frequently responsible for short-circuits.[30] Moreover, the role of the mesoporous layer is still a matter of discussion also in view of the high efficiencies of the planar PSC devices, already displaying 21.3 %.[39]

TiO_2 is normally used as mesoporous layer since it has a wide band gap energy of *ca*. 3.2 eV, high chemical and thermal stabilities, photostability, non-toxicity and low cost.[40,41] The perovskite polycrystals can infiltrate into the pores of TiO_2 - Figure 1.3 - but this pore filling is highly dependent on the thickness of the mesoporous layer. Leijtens *et al*.[42] found that a TiO_2 mesoporous layer with thickness between 260 nm and 440 nm is enough for complete pore filling - Figure 1.4; it can then be concluded that the optimum for balancing the maximum light absorption and minimum recombination caused by the path length is between these two limits. The corresponding photovoltaic performance was assessed and the high performance of thinner mesoporous TiO_2 device is associated to high electron density in TiO_2, improving the charge transport rates and collection efficiency.[30]

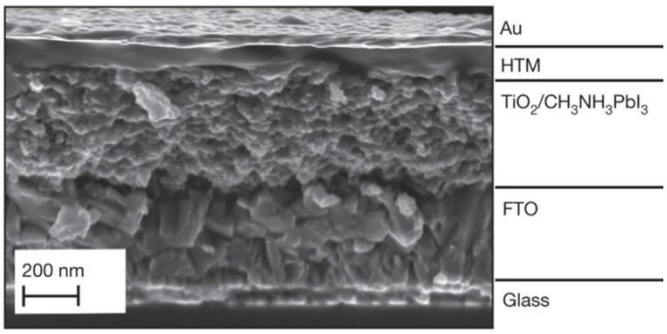

Figure 1.3. Cross-sectional SEM image of a perovskite solar cell prepared by Burschka *et al.* Reprinted by permission from Macmillan Publishers Ltd: Nature [43], copyright 2013.

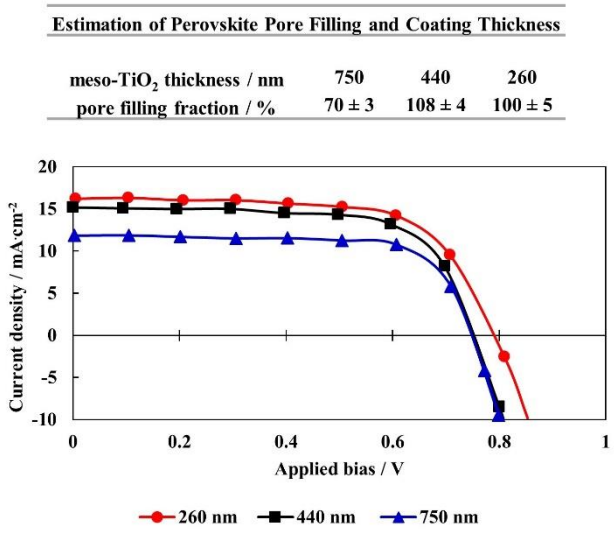

Figure 1.4. Estimation of perovskite pore filling and coating thickness and respective device *I-V* curves. Adapted with permission from [42]. Copyright 2014 American Chemical Society.

Although the good performances of TiO_2 as mesoporous layer, other semiconductor materials are being studied. ZnO has been widely tested as TiO_2 substitute and, apart its higher electron mobility (space charge limited current mobility of thin films > 0.6×10^{-3} $cm^2 \cdot V^{-1} \cdot s^{-1}$)[44] compared with TiO_2 and low

temperature of sintering, the cells fabricated with ZnO suffer from lower performance due to more recombination losses.[45,46] In particular, ZnO nanorods grown on the ZnO seed layer showed a PCE of more than 11 % using $CH_3NH_3PbI_3$ absorber.[46] In 2015, a significant PCE improvement of $CH_3NH_3PbI_3$ perovskite solar cells was observed (15.7 % the best cell) inserting a self-assembling monolayer of 3-aminopropanoic acid between the ZnO and the perovskite.[47] The presence of 3-aminopropanoic acid decreases the presence of pinholes and density trap states in the perovskite layer, allowing to obtain a highly crystalline $CH_3NH_3PbI_3$ film. More recently, Zheng *et al*.[44] proposed a combustion synthesis in order to produce dense and high quality ZnO films with high crystallinity and low quantity of organic impurities, favoring the growth of large and highly interconnected perovskite grains. The devices prepared with this material presented remarkable PCE of 17.14 % (with $CH_3NH_3PbI_3$), 18.82 % (with $Cs_{0.05}FA_{0.81}MA_{0.14}PbI_{2.55}Br_{0.45}$) and 19.84 % (with $Cs_{0.1}FA_{0.9}PbI_3$).

Active scaffold layers could be also decorated with quantum dots in order to improve the photon harvesting and assist the charge transport from the perovskite to TiO_2, this is the case of graphene that showed an impressive PSC efficiency of 20.45 %.[48]

As far as the author knows, the best record efficiency of a mesoporous architecture using TiO_2 was obtained with a doped spiro-OMeTAD with 4-*tert*-butylbenzylamonium hydroiodide as additive. The device presented a PCE of 23.25 % and a V_{oc} of 1.122 V. This result was disclosed in the ABXPV conference in the framework of GOTSolar project (Rennes, 2018).

1.2.2 Mesoporous insulating PSC device

Mesoporous insulating PSC device presents a similar structure to the mesoporous TiO_2-based devices except that the mesoporous layer is now made of an insulating material - Figure 1.5. In a mesoporous conductive PSC, electrons flow through the conductive oxide until reaching the contact, whereas in the case of mesoporous insulating PSC devices the responsible for this electron conduction is the perovskite. Indeed, the insulating layer works as an

inert scaffold and the light absorber works as an ambipolar electron and hole transporters.

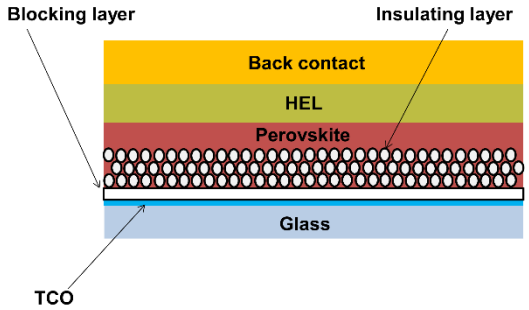

Figure 1.5. Mesoporous insulating-oxide based PSC.

Lee *et al.*[13] evidenced that a specific perovskite - $CH_3NH_3PbI_2Cl$ - used with a TiO_2 scaffold presented 8 % of PCE but replacing this mesoporous scaffold by an insulating framework of Al_2O_3 the PCE improved to 11 %. This perovskite is much better electron conductor than TiO_2 semiconductor and the charge collection in Al_2O_3-based devices was enhanced by a factor of more than 10 when compared with TiO_2-based devices. As mentioned above, Al_2O_3 only acts as a scaffold to provide surface area to the perovskite settling.

Following these exciting results, it was found that the substitution of TiO_2 by Al_2O_3 enables the device to be more stable under continuous illumination because alumina does not suffer from light-induced desorption of surface-adsorbed oxygen. Leijtens *et al.* [38] showed stable photocurrent for over 1000 h continuous exposure and operation under full spectrum simulated sunlight. This stability enhancement, combined with the photovoltage increase verified by Lee *et al.*[13] in the Al_2O_3-based cells, is attributed to the variation in chemical capacitance of the oxide, which is related to the charge storing capacity caused by the presence of sub-band gap states.[30] Another advantage of using Al_2O_3 in comparison to TiO_2 is the reduction of fabrication costs and processing time, since this material does not need high sintering temperatures.[49] The same group, in 2013, found that Al_2O_3 particles could be deposited from a simple binder-free colloid calcined at *ca*. 150 °C and achieved 12.3 % of PCE with an

optimum Al_2O_3 film thickness of *ca*. 400 nm.[50] The increase of alumina thickness until 400 nm improved the V_{oc} and *FF* (fill factor) due to the buffer layer effect that inhibits leakage current between the electrodes and improves the uniform coating of the perovskite. However, beyond the 400 nm, all the solar cell parameters (*FF*, V_{oc} and J_{sc}) decrease because of the increasing competition between recombination and charge collection.[50] Though, PCE values as high as 15.9 % (V_{oc} = 1.02 V; *FF* = 0.71; J_{sc} = 21.5 mA·cm^{-2}) have been reached for this architecture.[51]

Mesoporous-based PSCs, independently of being conductive or insulating, need to be coupled to a HEL to transport the holes generated in the perovskite absorber. A good HEL needs to present four requirements: 1) high hole mobility; 2) an optimal HOMO energy level; 3) good solubility and film forming properties; and 4) low cost. Spiro-OMeTAD is the most commonly used HEL in PSCs but it presents two huge disadvantages: it is very expensive mainly due to its lengthy and low yielding synthesis and it is thermally unstable.[52] For those reasons, investigation on new hole transport materials is very important. Inorganic hole-transporter materials, CuI (η = 6 %)[53] and CuSCN (η = 12.4 %)[54] are quite stable under ambient conditions and display a cheap synthesis route. However, these HELs show inferior performance compared with spiro-OMeTAD since they have no flexibility in tuning the oxidization potentials.[30] Polymeric HELs, like poly(triarylamine) (PTAA) and poly(3-hexylthiophene-2,5-diyl) (P3HT), are also interesting in terms of hole mobility and good film forming properties. A PCE of 17.9 % was certified for a device with PTAA as HEL conjugated with a mixed-halide perovskite, $(FAPbI_3)_{0.85}(MAPbBr_3)_{0.15}$.[55] Also Saliba *et al*.[20] reached an astonishing result in a quadruple cation perovskite composition (rubidium/cesium/ methylammonium/formamidinium) combined with PTAA hole transport material reaching a stabilized PCE of 21.6 %. Moreover, the device retained 95 % of its initial power conversion efficiency after a severe aging protocol at 85 °C for 500 h under full solar illumination and maximum power point (MPP) tracking. Recently, Jung *et al*.[18] proposed the use of P3HT without any dopants in a wide-bandgap halide and achieved 22.7 % of PCE; the devices maintained 95 % of the initial PCE after 1390 h of 1 sun illumination at room temperature (encapsulated device). Its low cost and facile production protocol

allied to high PCE makes the P3HT one of the most promising substitute of spiro-OMeTAD.

1.2.3 Planar PSC device

The planar perovskite solar cell has a very simple device structure because it does not present the mesoporous semiconductor or scaffold, contacting the perovskite directly to the n-type blocking layer - Figure 1.6. This type of architecture is suitable to better understand the working mechanism behind the charge separation and transport in the perovskite material. On the other hand, the absence of the mesoporous layer is particularly interesting since infiltration problems of the perovskite and HEL into the porous layer are eliminated and allows the use of flexible substrates since no high temperature treatments are involved. This configuration has, however, some disadvantages such as photovoltage loss due to the high density of trap states resulting in non-radiative electron-hole recombination,[56] and usually exhibits more severe current-voltage (*I-V*) hysteresis than mesoporous configuration.[57]

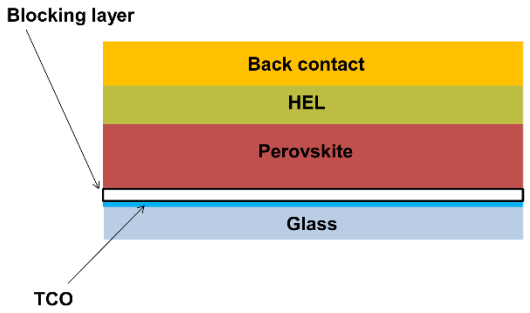

Figure 1.6. Planar perovskite solar cell structure.

The fabrication of this planar devices presents challenges such as avoiding direct contact between HEL and blocking layer. So, some new procedures were developed substituting the typical spin-coating deposition to vapor-based processes.[58,59,60,61,62] Although, a wide range of publications demonstrated that mesoporous TiO_2 is essential for high efficient PSC, Dar *et al*.[63] showed that reducing the thickness of a less porous TiO_2 layer and optimizing the thickness

of the perovskite layer, it is possible to obtain devices with reduced complexity without sacrificing the performance of the device.

In planar configuration the blocking layer gains a critical role. Thus, the research community also started studying alternative compact layers for planar PSCs, having considered the use of ZnO due to its high electron mobility. Liu and Kelly[64] reported a device with 15.7 % of PCE with high reproducibility and V_{oc} of 1.0 V. CdSe nanoparticles were tested by Wang *et al.*[65] with a low temperature solution-processed CdSe/$CH_3NH_3PbI_3$/spiro-OMeTAD/Ag planar device, reaching 11.7 % of efficiency. Anaraki *et al*.[66] reported the planar PSC with highest PCE of 20.7 %.The device presents an electron selective layer of SnO_2 deposited by a combined spin-coating and chemical bath post-treatment that allows to achieve higher *FF* than with ALD (atomic layer deposition) method. Recently, Cui *et al*.[39] proposed a p-type perovskite/n-type perovskite homojunction, enhancing the PCE of planar devices to 21.38 %. The combination of a thermally evaporated p-type perovskite with a solution-processed n-type layer promotes oriented transport of the photo-induced carriers, reducing carrier recombination losses. The n- and p-type doping was induced controlling the stoichiometry of the perovskite precursors.

In this architecture some researchers used an interlayer to assist charge injection and extraction at the metal-semiconductor interfaces, creating a quasi-ohmic interfacial contact that increases the *FF* and decreases the series resistance. Ethoxylated polyethylenimine (PEIE) and [6,6]-phenyl-C61-butyric acid methyl ester (PCBM) are some examples; the first one was suggested to reduce the work function of the ITO layer from 4.6 to 4.0 eV;[60] the PCBM, placed between ZnO blocking layer and perovskite, reduces the trap-assisted charge recombination at the ZnO interface and in the bulk of the perovskite.[67]

The most popular HEL used in planar cells is still spiro-OMeTAD, but P3HT can also be used. Guo *et al*.[68] achieved a value of PCE of 12.4 % with a $CH_3NH_3PbI_{3-x}Cl_x$ perovskite layer replacing the common HEL additive, 4-*tert*-butylpyridine (*t*-BP), by 2,6-di-*tert*-butylpyridine (D-*t*-BP). Recently, company Dyenamo launched a low-cost high-performance hole conductor coded as X-60, which enabled Xu *et al*. [69] to produce a PSC with efficiencies of 19.8 % and almost no hysteresis - Figure 1.7.

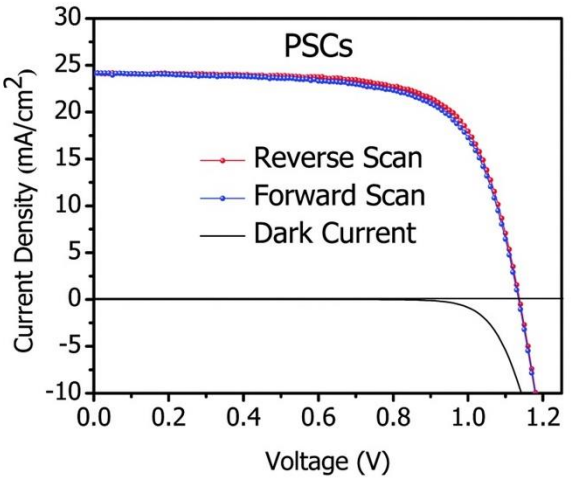

Figure 1.7. *I-V* curves of best PSC devices using X60 as HEL, measured under 100 mW·cm^{-2} AM 1.5G solar illumination. Reproduced from [69] with permission of The Royal Society of Chemistry.

1.2.4 HEL-less PSC device

As referred before, perovskites are also able to transport free holes through their valence band; other architectures were then developed considering no HEL - Figure 1.8a. A HEL-less PSC is simpler and its stability is not limited by the stability of the HEL. In this case, the perovskite layer should display a dense and uniform overlayer to avoid shunt pathways resulting from the contact between mesoporous TiO_2 and back contact layer.

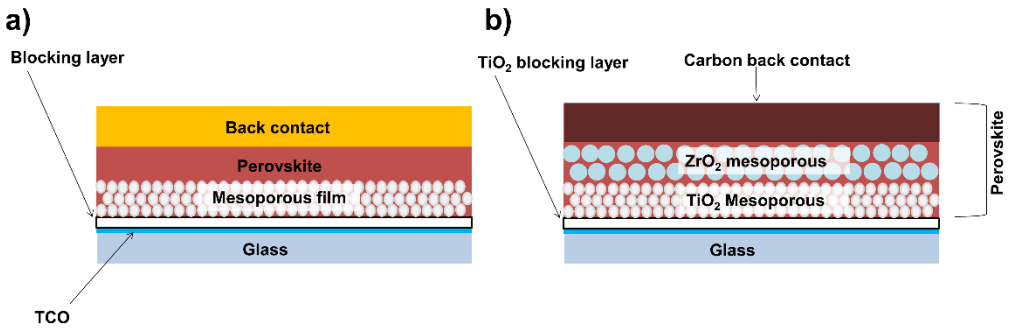

Figure 1.8. HEL-less perovskite solar cell with: a) single mesoporous layer structure, b) double (TiO_2 and ZrO_2) mesoporous layer structure and carbon back contact.

The first HEL-less PSC was reported by Etgar *et al.* [12] and considered a mesoporous TiO_2 layer loaded with $CH_3NH_3PbI_3$ perovskite; the cell presented a PCE of 5.5 %. In 2014, Mei *et al.*[70] fabricated a perovskite solar cell with a scaffold made of two layers, first of TiO_2 followed by ZrO_2; the ZrO_2 layer was added to prevent the short-circuit of the back-contact with the TiO_2 - Figure 1.8b. Using the perovskite $CH_3NH_3PbI_3$ the authors achieved a certified PCE of 12.8 %. As demonstrated, the HEL can be easily replaced by a back contact displaying a work function matching with the energy level of the hole, such as gold or carbon.[71,72] A record efficiency of HEL-less PSC was achieved by Zhang *et al.*[73] introducing a eco-friendly material, $SrCl_2$, as precursor. The introduction of this precursor tuned the perovskite crystallization kinetics and facilitated the growth of the film without defects, enabling a PCE of 15.9 %.

For all the previously described architectures the back contact is, normally, a metal (Ag or Au).[33,74] However, the use of these materials increases the cost of the devices and removes the significance of low cost required to the PSC. Nowadays, carbon electrodes are emerging as a better approach for replacing these materials. Ku *et al*.[75] prepared a PSC with a screen-printed mesoporous carbon electrode above a double layer of mesoporous TiO_2 and ZrO_2; the perovskite was then infiltrated through the carbon layer made of carbon black particles; this design reached a PCE of 6.6 %. This PCE value was further improved incorporating 5-ammoniumvaleric acid (5-AVA).[70] The 5-AVA allow to form $(5\text{-AVA})_x(MA)_{1-x}PbI_3$ perovskite crystals with lower defect concentration and better contact with TiO_2 mesoporous; the perovskite showed longer exciton lifetime when compared to $CH_3NH_3PbI_3$ and higher quantum yield.[76] The record of HTM-less device with carbon contact belongs to Tian *et al*.,[77] that increased the oxygen content of carbon black of the counter electrode in order to elevate its energy level and enhance the hole extraction efficiency at the perovskite/back-contact interface. Recently, devices with the low cost HEL poly (3,4-ethylenedioxythiophene), commonly called PEDOT, and a carbon back contact were prepared by Jiang *et al*. reaching efficiencies of 17 %.[78]

1.2.5 Inverted PSC device

Back to 2013 a quite different PSC architecture emerged, the so-called inverted planar perovskite solar cell. This type of cell got inspiration on the organic solar cells and uses p-type and n-type materials as bottom (HEL) and top (ETL - electron transport layer) charge transport layers, respectively - Figure 1.9.

Figure 1.9. Schematic image of an inverted planar perovskite solar cell: HEL - hole extraction layer; ETL - electron transport layer.

The first inverted device was proposed by Jeng *et al*.[79] It was made of a PEDOT:PSS layer as hole extraction and C_{60} derivatives such as PCBM and indene-C_{60} bisadduct (ICBA) as electron transport layer; a PCE of 3.69 % was reported. However, in a short period of time this value was enhanced up to 16 %.[80] PEDOT:PSS, similarly to spiro-OMeTAD in regular PSCs, is the most used HEL in inverted PSC cells though it is highly hygroscopic, which compromises the long term stability of these devices. To overcome this difficulty, Docampo *et al*. [81] applied NiO as HEL but without success, probably due to poor perovskite film formation and poor surface coverage. Later, it was discovered that UV-ozone treatment improves the surface wetting properties and energy alignment between NiO and perovskite, allowing to produce devices with more than 7 %.[82,83]

In 2015, Chen *et al*.[84] reported a large size (> 1 cm^2) inverted PSC made of inorganic charge extraction layers. They developed heavily p-doped $Ni_xMg_{1-x}O$ and n-doped TiO_x contacts, substituting $Ni(Mg)^{2+}$ ions and Ti^{4+} ions on the

$Ni_xMg_{1-x}O$ lattice and TiO_x matrix with Li^+ and Nb^{5+} ions, respectively. The devices maintain more than 90 % of the 16.2 % initial PCE value after 1000 h of light soaking. As far as the author knows, the best power conversion efficiency for this device structure was reported by Yang *et al*.[85] in 2019, displaying 20.2 % and retained 90 % of its initial PCE after 30 days stored in ambient air. The device employs poly[(9,9-dioctyl-fluorenyl-2,7-diyl)-co-(4,4′-(N-(4-secbutylphenyl) diphenylamine)] (TFB) as HEL. Several other metal oxides such as V_2O_5[81] seem to be an option for HEL, however, they are not stable in contact with the perovskite precursor CH_3NH_3I, because of its acidity. This is not the case of CuSCN, which allows producing a high stable inverted PSC with 16.6 % of PCE.[86]

Bearing in mind all the above-described architectures, in the last 7 years remarkable PCE results have been attained by different research groups - Table 1.2. Although perovskite solar cells present better efficiencies than conventional DSCs and PCEs very close to silicon technology, some challenges are still needed to be resolved. Among these challenges are the toxicity of the lead-perovskites, the low stability of the used perovskites and hole transport materials, as well as the encapsulation of the cell, crucial for minimizing exterior contamination and for benefiting the scalability of the technology. These specific topics are now overviewed in the next sections.

Table 1.2. History of the PSC highest power conversion efficiencies.

Research Group	Year	Architecture	η / %	Reference
KRICT/MIT	2019	n/a	25.2	[14]
ISCAS	2018	ITO/SnO_2/ $(FAPbI_3)_{1-x}(MAPbBr_3)x$/spiro/Au	23.7	[6,14]
KRICT	2017	n/a	22.7	[14]
KRICT	2016	FTO/TiO_2/m-TiO_2/$MAPbI_3$/PTAA/Au	22.1	[87]
EPFL - LPI	2016	FTO/TiO_2/m-TiO_2/ $(FAI)_{0.81}(PbI_2)_{0.85}(MAPbBr_3)_{0.15}$/spiro/Au	21.0	[88]
KRICT	2015	FTO/TiO_2/m-TiO_2/$FAPbI_3$/PTAA/Au	20.1	[89]
UCLA	2014	ITO/Y:TiO_2/$MAPbI_{3-x}Cl_x$/spiro/Au	19.3	[26]
KRICT	2014	FTO/TiO_2/m-TiO_2/ $MAPb(I_{1-x}Br_x)_3$/PTAA/Au	16.2	[90]
School of Materials Science and Engineering, **Georgia Institute of Technology**, Atlanta, USA	2013	FTO/TiO_2/$MAPbI_{3-x}Cl_x$/spiro/Ag	15.4	[62]
EPFL - LPI	2013	FTO/TiO_2/m-TiO_2/$CH_3NH_3PbI_3$/spiro/Au	14.1	[43]
Department of Physics, **University of Oxford**, Clarendon Laboratory	2013	FTO/TiO_2/m-Al_2O_3/$MAPbI_{3-x}Cl_x$/spiro/Ag	12.3	[50]
Department of Physics, **University of Oxford**, Clarendon Laboratory	2012	FTO/TiO_2/m-Al_2O_3/$MAPbI_2Cl$/spiro/Ag	10.9	[13]

Note: EPFL-LPI: École Polytechnique fédérale de Lausanne – Laboratory of Photonics and Interfaces; UCLA – University of CALIFORNIA, Los Angeles; KRICT – Korea Research Institute of Chemical Technology; MIT – Massachusetts Institute of Technology; ISCAS – Institute of Semiconductors, Chinese Academy of Science.

1.3 Stability

In spite of the astonishing progresses reached in the last ten years in terms of power conversion efficiency, PSC devices still present a lack of stability. This low stability is related to the strong sensitivity of the absorber and HEL to environmental factors like oxygen, moisture, temperature and UV light. The fabrication techniques and materials also play an important role in the stability of the devices. The number of publications on long-term stability remains scarce comparatively with number of publications focused on PCE. Besides the long-term stability issues, some PSC systems exhibit hysteresis observed when obtaining the corresponding current-voltage curve, which was assigned mainly to the trapping of charges and voltage-induced ionic migration. This chapter reviews both phenomena.

1.3.1 Presence of moisture

Moisture is assumed to be detrimental to organometal halide perovskite since excess of water can damage the crystallinity of the perovskite structure. Few degradation mechanisms have been proposed; however, this still is a matter of discussion since some authors refer that a certain level of humidity is beneficial for the perovskite formation.[91,92] The perovskite hydrolyzes in the presence of moisture rendering back the two precursors - eq.(1.8). Then, the methylammonium iodide decomposes to produce HI - eq.(1.9), which afterwards degrades in the presence of oxygen - eq.(1.10), or after the exposition to UV light - eq.(1.11).

$$CH_3NH_3PbI_3\ (s) \rightleftarrows PbI_2(s) + CH_3NH_3I\ (aq) \quad (1.8)$$

$$CH_3NH_3I\ (aq) \rightleftarrows CH_3NH_2\ (aq) + HI\ (aq) \quad (1.9)$$

$$4\ HI\ (aq) + O_2\ (g) \rightleftarrows 2\ I_2(s) + 2\ H_2O\ (l) \quad (1.10)$$

$$2\ HI\ (aq) \rightleftarrows H_2(g) + I_2\ (s) \quad (1.11)$$

To avoid the perovskite to hydrolyze, the entire process of fabrication of PSC should be conducted inside a glove box filled with an inert gas (normally N_2).

Leguy *et al*.[93], after investigating the hydration mechanism of $CH_3NH_3PbI_3$, demonstrated that only a long time of exposition can cause the irreversible decomposition of perovskite. The authors observed that when $CH_3NH_3PbI_3$ is exposed to 70 % of relative humidity (RH) at room temperature for 60 h, its band gap increases until 3.1 eV by forming $CH_3NH_3PbI_3.H_2O$ - eq.(1.12) - that could return to the original structure after being exposed to a dry atmosphere. However, when the exposure to water is extended, PbI_2 dehydrate is formed and later on water starts dissolving the ion $CH_3NH_3^+$. The -NH- bonds present in the amine salts show a rapid moisture absorption.[94] According to Habisreutinger *et al*.[95], the irreversible decomposition of dehydrate phase of perovskite could occur under illumination, even without excess of water.

$$4(CH_3NH_3)\,PbI_3 + 4\,H_2O \rightleftarrows 4\,[CH_3NH_3PbI_3.H_2O]$$

$$\rightleftarrows (CH_3NH_3)_4PbI_6.2\,H_2O + 3\,PbI_2 + 2\,H_2O \qquad (1.12)$$

Some protocols have been adopted to overcome this problem. According to Ko *et al*.[96], the high efficiency at higher moisture concentrations can be achieved by pre-heating the substrates before PbI_2 deposition. The PSC device was prepared in a 50 % humidity environment and substrates were pre-heated at 50 °C; a PCE of 15.76 % was reported. The pre-heating step is responsible for a better pore filling and surface coverage of the perovskite in the mesoporous TiO_2 - Figure 1.10.

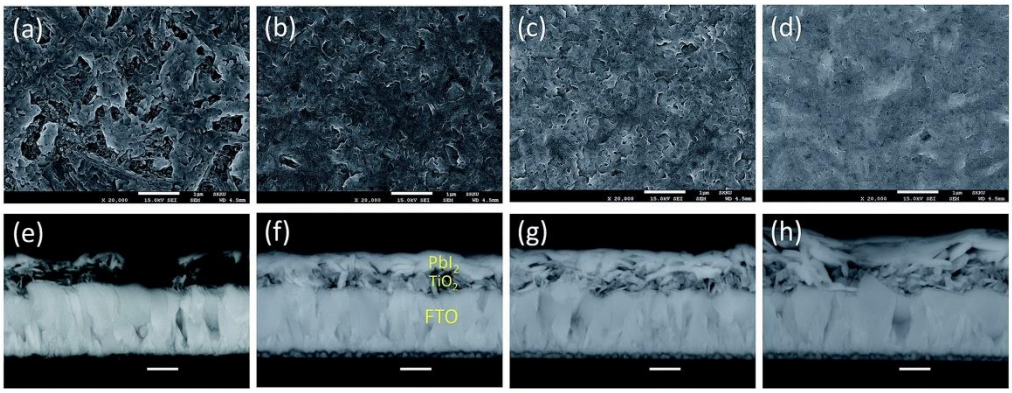

Figure 1.10. Top-view SEM images of the PbI_2 layer deposited on the mesoporous TiO_2 for substrates pre-heated at (a) room temperature, (b) 40 °C, (c) 50 °C and (d) 60 °C and (e-h) corresponding cross-sectional SEM images. Reproduced from [96], with permission of The Royal Society of Chemistry.

Cronin *et al*.[97] found a trade-off between relative humidity and annealing time: for low humidities (0 %, 15 % and 20 %) times of 45 min are required to complete conversion of the perovskite, however for humidities higher than 20 %, the desirable should be less than 30 min. Longer times combined with high humidity values result in chemical degradation of the device. By other side, Throughton *et al*.[98] improved the perovskite deposition method using ethyl acetate as anti-solvent. The ethyl acetate works like a sequester airborne moisture and protect the perovskite intermediate phase, enabling this way the perovskite deposition without stringent atmospheric control. At 75 % of RH the authors produced a $CH_3NH_3PbI_3$ device with 15 % of PCE. The use of oleylammonium polysulfides was also proposed due to its hydrophobic behavior. An ultrathin layer deposited on the perovskite could passivate the surface chemical activity and enhance moisture stability of the devices. This type of approach results in a device, without encapsulation, that retained more than 70 % of its initial PCE after 14 days of exposure to a relative humidity of (40 ± 10) %.[99]

Despite these well-established degradation mechanisms, some authors have a different opinion concerning the role of the humidity during the crystallization of the perovskite. Zhou *et al*.[60] showed that certain levels of humidity, less than

30 % during cell fabrication, improves the morphology of crystal and consequently improves the performance of the device. Moreover, and according to You *et al*.,[92] samples annealed in nitrogen and oxygen dry environment present pinholes and grain boundaries that hampers charge transport, induces recombination and thus lowers the photovoltaic performance - Figure 1.11.

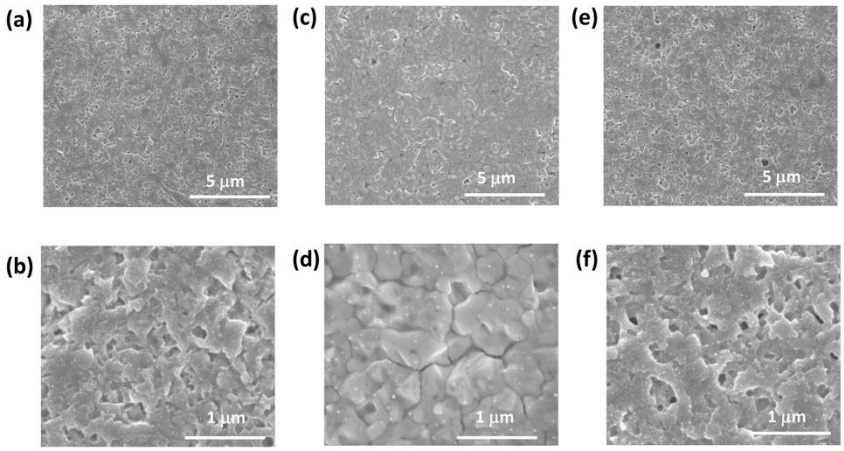

Figure 1.11. Top-view SEM images of the perovskite film annealed under different conditions (a) and (b) in nitrogen; (c) and (d) in ambient air (humidity = (35 ± 5) %); (e) and (f) in oxygen environment. Reprinted from [92], with the permission of AIP Publishing.

Some authors went even further and added substantial quantities of water to the precursor solutions of the perovskite. Liu *et al*.[100] achieved reproducible and high efficiency devices adding 20 vol.% of water to the $CH_3NH_3PbI_{3-x}Cl_x$ perovskite solution. The champion device showed a PCE of 20.1 %, with negligible hysteresis (< 1.5 %). The water helps methylammonium iodide (MAI) to penetrate into the PbI_2 to form a thick film with a pure $MAPbI_3$ phase and slows down the perovskite crystallization rate in order to obtain no defect big and continuous grains.[101] The addition of water also presented a stabilizing effect on long-term device performance, allowing small losses of less than 10 % of the initial PCE for devices prepared with water contents in a range of 6 to 40 days.[102,103,104]

Initially, moisture was thought to affect mostly the perovskite layer. Nevertheless, it was observed that not only the perovskite itself degraded with

moisture, but the commonly used HEL, spiro-OMeTAD, is also affected. Spiro-OMeTAD is hydrophilic due to the Li-TFSI additive, added to increase the hole conductivity. To overcome this limitation, Kwon *et al*.[105] introduced the poly[2,5-bis(2-decyldodecyl)pyrrolo[3,4-c]pyrrole-1,4(2H,5H)-dione-(E)-1, 2-di (2,2′-bithiophen-5-yl) ethene], commonly coded as PDPPDBTE, that due to its excellent hydrophobic properties prevents water to permeate until the perovskite layer. This behavior was confirmed based on the water contact angle with PDPPDBTE and with spiro-OMeTAD, respectively 105° and 70°. The stability tests with spiro-OMeTAD showed a 27.6 % PCE decline after 1000 h of aging time, whereas the device with PDPPDBTE kept the performance; the perovskite solar cells were prepared without encapsulation and stored in air (~20 % of RH) and room temperature. $CuGaO_2$ was also proposed as HEL, after demonstrating a high stability to ambient humidity (30 % - 50 %) when compared to spiro-OMeTAD. The cells presented around 18 % of PCE and maintained more than 90 % of the initial PCE after one month, while on the other hand the spiro-based devices lost more than 80 % with the same exposure time.[106]

1.3.2 Presence of oxygen and UV light effect

UV light has demonstrated to strongly affect PSC performance, especially in devices with TiO_2 mesoporous layer. It is well-known that TiO_2 is a good photocatalyst for oxidizing water and organic compounds[107] and due to its 3.2 eV bandgap it absorbs in the UV spectrum. Thus, several degradation mechanisms have been proposed based on the photoactivity of TiO_2 under UV illumination. Mesoporous TiO_2 incorporates trapping sites and surface defects working as electron-donating sites.[108] Electrons localized in these trapping states bind with oxygen and generate O_2^- - Figure 1.12a. [109] After illumination with UV light an electron-hole pair forms in the TiO_2 and the hole recombines with the electron at the oxygen adsorption site. Then, the oxygen desorbs - Figure 1.12b - leaving an unoccupied site that could serve as a trap state for photo-induced electrons from sensitizers - Figure 1.12c - and holes in HEL may recombine with trapped electrons.

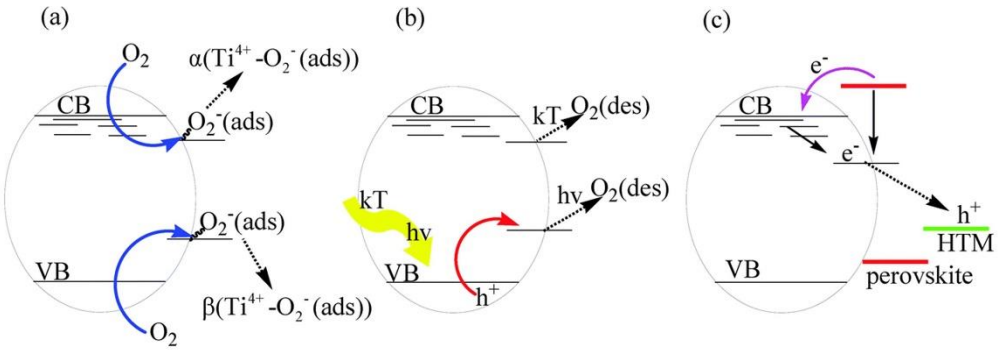

Figure 1.12. O_2 degradation mechanism induced by UV light occurring in the TiO_2. Reproduced from [110], with permission of The Royal Society of Chemistry.

Another degradation mechanism was proposed by Ito *et al*.[111]; these authors assume that the TiO_2 layer may extract electrons from iodide anion forming I_2 at the TiO_2/perovskite interface – eq.(1.13) - and deconstructing the perovskite crystal. Since the reaction presented in eq.(1.14) is reversible, the electron extracted by the TiO_2 may return to the TiO_2 surface giving rise to eq.(1.15) that allows the release of HI. As H^+ is consumed in eq.(1.15), the equilibrium of eq.(1.14) shifts to the right side, releasing CH_3NH_2 due its low boiling point (17 °C).

$$2\,I^- \rightleftarrows I_2 + 2\,e^- \quad (1.13)$$

$$3\,CH_3NH_3^+ \rightleftarrows 3\,CH_3NH_2\,(g) + 3\,H^+ \quad (1.14)$$

$$I^- + I_2 + 3\,H^+ + 2\,e^- \rightleftarrows 3\,HI\,(g) \quad (1.15)$$

To overcome the instability originated by the UV illuminated TiO_2 layer, Chander *et al*.[112] proposed the use of a UV filter. Alternatively, Leijtens et *al*.[38] substituted TiO_2 for an insulating-Al_2O_3 scaffold, which allowed stable photocurrents under continuous full spectrum sunlight for a period of over 1000 h. Bera *et al*.[113] presented Zn_2SnO_4 as electron transporting layer, which improved the crystallization of perovskite layer and prevents the UV-based deactivation; PSC device with Zn_2SnO_4 exhibited a low PCE of 13.3 %, but negligible electrical hysteresis and exceptionally high stability without

encapsulation for over one month. Recently, a strontium oxide (SrO) interlayer was proposed in order to enhance the UV stability of a mesoporous $CH_3NH_3PbI_3$ device. Although, the devices showed a PCE of 17.6 %, the stability increased since devices presented 60 % of the initial PCE, compared to 34 % for devices without interlayer between TiO_2 and perovskite film.[114] However, few studies are found addressing this topic.

1.3.3 Thermal stability

Like moisture, temperature has two type of effects on the degradation of the PSC device: one related to the perovskite material itself and the other related to HEL behavior. Although metal halide perovskite materials have been reported to be stable above 300 °C,[115] some works demonstrated that the decomposition of organic components occurs at temperatures lower than 140 °C.[116] Normally, the perovskite material is annealed at low temperatures, where 80 °C is the minimum temperature for the complete transformation of PbI_2 and CH_3NH_3I in $CH_3NH_3PbI_3$.[117] According to Tan *et al.*,[118] heating up $CH_3NH_3PbI_{3-x}Cl_x$ up to 100 °C (heating rate of 1 °C·min^{-1}) in N_2 atmosphere, the following is observed: 1) the formation of the 3D perovskite structure at 90 °C; and 2) the noticeable degradation of the perovskite at 100 °C - Figure 1.13.

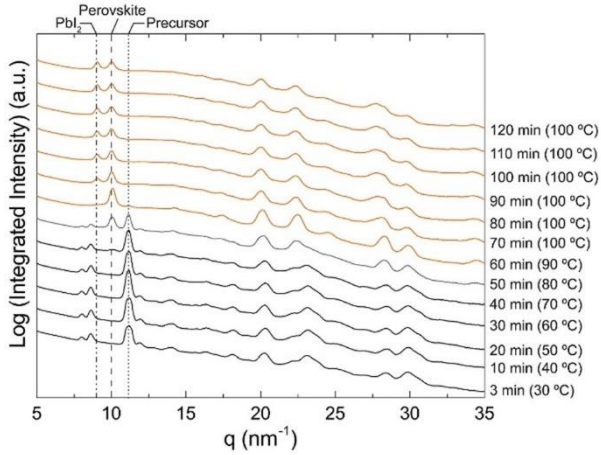

Figure 1.13. Azimuthally integrated plot of Grazing Incidence Wide-Angle X-ray Scattering (GIWAXS) profiles of mesoporous block copolymer-directed alumina

perovskite films in nitrogen at different times and temperatures. Reprinted with permission from [118]. Copyright 2014 American Chemical Society.

For $CH_3NH_3PbI_3$ perovskite, Pisoni *et al*.[119] reported a very low thermal conductivity in both single crystals and polycrystals structure. This means that when heating up the device, the heat is not spread quickly enough and may cause mechanical stress decreasing the lifetime of the PSC device. Misra *et al*.[120] compared two different inorganic precursors for preparing the perovskite material, PbI_2 and $PbBr_2$, and after performing accelerated aging tests in sealed PSCs concluded that $CH_3NH_3PbI_3$ device suffers degradation after 60 min at temperatures between 44 °C - 55 °C, while $CH_3NH_3PbBr_3$ device did not show photo-bleaching or decomposition of the perovskite material. This fact can be explained by the shorter and stronger bonds of Pb-Br compared to Pb-I.[121] Nevertheless, not only the substitution of inorganic precursor increases the thermal stability of the devices, but the use of organic precursors also plays an important role in the stability of the device. Eperon *et al*.[122] and Aharon *et al*.[123] compared PSC devices based on formamidinium (FA) lead trihalide ($HC(NH_2)_2PbI_3$) and based on $CH_3NH_3PbI_3$; both authors obtained the same conclusion: the thermal stability of formamidinium-based devices is higher. The ($HC(NH_2)_2PbI_3$) perovskite just decomposed at 290 °C, while $CH_3NH_3PbI_3$ perovskite started at ~230 °C.[123] The combination of MA/FA proved to be a success, with MA working as a stabilizer of the black phase of FA perovskite. However, traces of yellow phase were always present, even in high efficiency devices, inhibiting charge collection efficiency.[124,125] In order to overcome this problem, Saliba *et al*.[20,126] proposed the incorporation of inorganic materials like Cs and Rb; the incorporation of small amounts of these cations not only increased devices thermal stability, but also increased their robustness to the fluctuating surrounding factors such as temperature, solvent vapours and heating protocols. Very recently, a novel discover of Wang *et al*.[127] caught the attention of the scientific community with the incorporation of caffeine in the $MAPbI_3$ perovskite. The carboxyl groups strongly interact with Pb^{2+} ions slowing down the crystal growth and allowing to obtain a reduced defect density film with better vertical charge transport. The caffeine also interacts with perovskite during

degradation improving its thermal stability. The caffeine-based devices presented a champion PCE of 20.25 % and a stability of over 1300 h at 85 °C (loss < 15 % of initial PCE).

In what concerns HEL thermal stability, Malinaukas *et al.*[128] showed that amorphous polymer spiro-OMeTAD is not stable at temperatures higher than 100 °C since crystallization onsets at this temperature. Large crystals within the amorphous spiro-OMeTAD film cause morphological hole traps and affect the charge transport. According to the authors, even small crystals that remain from the incomplete dissolution of spiro-OMeTAD can induce crystallization during the thermal evaporation of the back contact. Moreover, the crystallization process is accelerated by the additives used for increasing the hole transport, reducing the glass transition temperature of the spiro-OMeTAD. At 80 °C, devices prepared with undoped spiro-OMeTAD thermally degrade slower than lithium doped spiro-OMeTAD devices; Habisreutinger *et al.*[95] attributed this phenomenon to the hygroscopic nature of lithium. Although dopants are very important to increase the conductivity of spiro-OMeTAD, they also play an important role in the thermal degradation of the devices.[129,130,131] Domanski *et al*.[132] reported an interesting study on gold atoms migration when spiro-OMeTAD is used in triple cation PSC devices. Through time-of-flight secondary ion mass spectrometry (ToF-SIMS), the authors observed considerable amounts of gold in the perovskite layer in aged devices at 70 °C - Figure 1.14. So, the temperature observed during the deposition of the gold back contact is enough to cause diffusion of gold into the spiro-OMeTAD layer (red line), which can create deep trap states within the mesoporous TiO_2.[132]

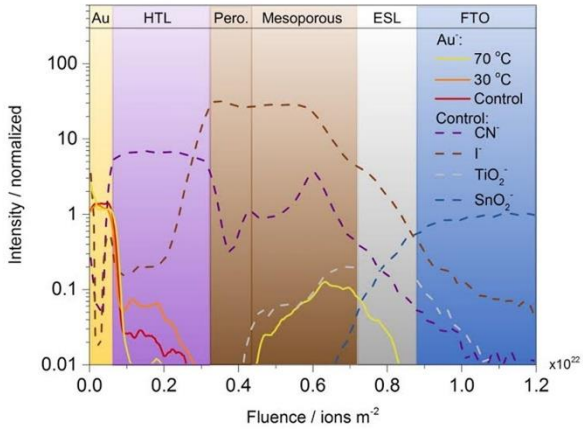

Figure 1.14. ToF-SIMS depth profiles showing the concentration of gold and other selected species across the control and aged devices. Reprinted with permission from [132]. Copyright 2016 American Chemical Society.

Many new organic and inorganic HELs have then been proposed.[53,133,134,135,136] Some of them were able to rival with Spiro-OMeTAD in terms of PCE. Among them are PTAA,[89] 2',7'-bis(bis(4-methoxyphenyl) amino)spiro [cyclopenta[2,1-b:3,4-b']dithiophene-4,9'-fluorene][137] (FDT), CuSCN[138] and copper phthalocyanine[139] (CuPc). Arora *et al*.[138] demonstrated that a deposition of a reduced graphene oxide layer between CuSCN and gold back contact allow to increase the thermal stability of the devices, retaining > 95 % of the initial PCE after 1000 h kept at MPP and under 60 °C. Another surprising result was obtained by Duong *et al*.,[139] which through a thermal treatment at 85 °C of CuPc HEL were able to reduce the migration of Au particles through the HEL cracks, achieving devices with PCE over 20 %, negligible hysteresis and a thermal stability of > 2000 h at 85 °C.

Li *et al*.[140] were even more ambitious testing devices under outdoor conditions. The PSC devices were exposed to real conditions of temperature and UV light in Jeddah (Saudi Arabia) during one week. The devices were made infiltrating the perovskite solution into a mesoporous TiO_2/ZrO_2 scaffold coated with carbon black back-contact and encapsulated with a glass sheet glued by Surlyn® and epoxy resin for avoiding moisture inlet. Figure 1.15 shows the

observed performance; after 7 days the devices remained almost with the same PCE. In this case, the absence of HEL and the use of thermally conductive carbon materials contributed for the exhibited good stability.

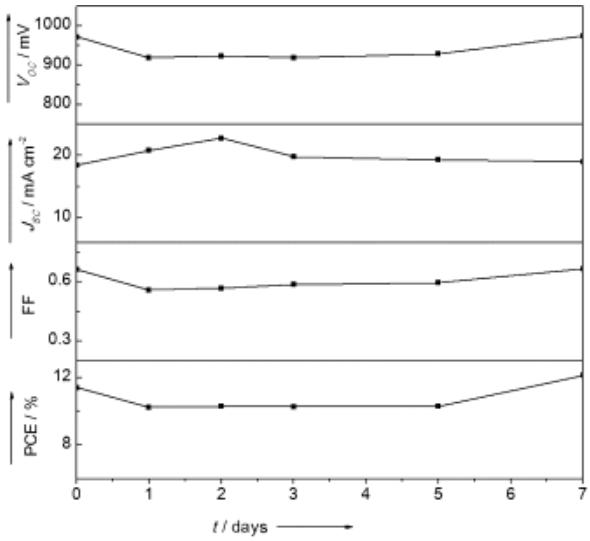

Figure 1.15. Time evolution of the photovoltaic parameters of an encapsulated PSC in Jeddah, Saudi Arabia. Reprinted with permission from [140]. Copyright 2015 WILEY-VCH Verlag GmbH & Co. KGaA, Weinheim.

1.3.4 Perovskite layer deposition method effect

The perovskite deposition method is a key factor for attaining high performances since it determines the surface coverage, crystallinity, thickness and quality of the film responsible for the morphological and transport properties of the perovskite. Several deposition techniques have been proposed; the most used ones can be divided as: (a) solution processed via one-step deposition and (b) two-steps deposition; (c) dual-source vapour deposition (DSVD) and; (d) vapour assisted solution process - Figure 1.16.

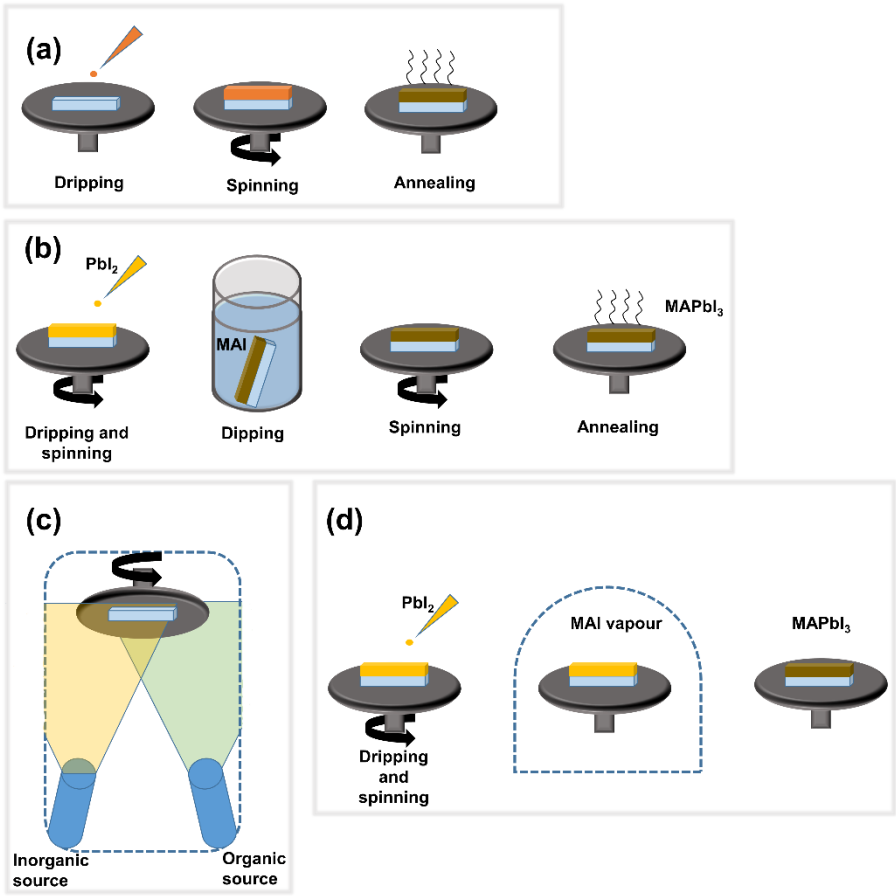

Figure 1.16. Four main methods of perovskite deposition: solution processed (a) via one step deposition; (b) via two steps deposition; (c) vapour deposition; and (d) vapour assisted solution process (MA = $CH_3NH_3^+$).

Solution process methods require normally a spin-coating step. In the case of a one-step deposition, the perovskite solution is dispensed on the substrate at a specific spinning velocity. During the spinning, the excess of perovskite solution is spun off and the perovskite crystallizes upon the evaporation of the solvent. The substrate, precursor solution, processing environment (air or N_2) and application method strongly affect the final morphology of the perovskite. Normally, the solution used in one-step deposition method is a mixture of PbX_2 and CH_3NH_3X (X = Cl, Br or I) from a common solvent such as *γ*-butyrolactone (GBL),[140,141] dimethylformamide (DMF)[142,143] or dimethyl sulfoxide

(DMSO).[144,145] However, the one-step method originates uncontrolled perovskite precipitation producing large and small size crystals, resulting in poor reproducibility of the solar cell performance.[43] To better control the crystal formation and growth, Jeon *et al*.[146] proposed the use of an anti-solvent method. The procedure is similar to the one-step deposition but, during the precursor spinning, an anti-solvent like toluene, is dripped onto the substrate. The toluene retards the rapid reaction between $CH_3NH_3I(Br)$ and $PbI(Br)_2$ enabling the formation of a dense and more uniform surface.[146] Saliba *et al*.[20,126] reported devices with PCE well above 20 % using the anti-solvent method and two different perovskite compositions (triple and quadruple cations). The incorporation of cesium (Cs) in the MA/FA formulation lowers the effective Cs/MA/FA cation radius shifting the tolerance factor towards a cubic lattice structure corresponding to the black phase of perovskite. The yellow phase is suppressed, at room temperature, making the cells less sensitive to small variations of the fabrication process; cells with 20 % of PCE are then more easily obtained. The authors reported Cs/FA/MA cells with 20 % of PCE, which decreased to *ca*. 18 % of PCE after 250 h under full illumination, at room temperature and under nitrogen atmosphere.[126]

The photoactive black phase of perovskites only exists between 0.8 and 1.0 of tolerance factor; however, rubidium (Rb) is smaller than inferior limit. With this in mind, Saliba *et al*.[20] proposed its use in a quadruple cation configuration. It was possible to demonstrate by intensity-modulated photocurrent spectroscopy (IMPS) that the charge transport within the Rb/Cs/MA/FA perovskite layer is substantially faster than in triple cation configuration. The champion cell with these four cations displayed 21.8 % of PCE and a tested cell retained 95 % of the initial PCE after 500 h at 85 °C under full illumination and MPP in a nitrogen glove box.[20] This is a landmark result both in terms of power conversion efficiency and stability.

The two-steps deposition proposed by Burschka *et al*.[43] emerged with the same purpose of controlling the formation and growth of perovskite crystals. PbI_2 solution (*e.g*. in DMF) is first deposited by spin-coating onto the TiO_2 layer and dried. Subsequently, the substrate is dipped into CH_3NH_3I solution (*e.g*. in 2-propanol) for a given time followed by spinning and annealing of the

perovskite. The formation of perovskite crystals occurs from the reaction between PbI_2 and CH_3NH_3I. Compared to the one-step method, the PbI_2 can be deposited at higher concentrations leading to a more compact film with high absorbance and reproducibility. The confinement of PbI_2 within the mesoporous TiO_2 film resulted in a layered PbI_2 crystalline structure, which facilitates the insertion of CH_3NH_3I precursors to yield $CH_3NH_3PbI_3$ nanocrystals.[43] After the publication of this new method by Burschka *et al*.,[43] several variations begun to be explored, like the use of warm substrates to improve the pore filling and surface coverage of the perovskite layer,[96] pre-wetting stage in 2-propanol to improve the conversion of PbI_2 to $CH_3NH_3PbI_3$[147] or even the use of DMSO to create an amorphous layer of PbI_2 that is more stable, uniform and smooth.[145] Zhao *et al.*[148] reported then a three-step deposition method, where after the PbI_2:CH_3NH_3Cl deposition they thermally decompose it to form PbI_2 that is finally converted into $CH_3NH_3PbI_3$ by dipping in a regular 2-propanol solution of CH_3NH_3I at room temperature. This method facilitated the rapid conversion of PbI_2 to perovskite crystals without any residue of PbI_2 in the final perovskite. Another study with similarities to the two-steps deposition method was performed by Xiao *et al*.[149]; they called it inter-diffusion method. Compact $CH_3NH_3PbI_3$ films were prepared by interdiffusion of spin-coated stacking layers of PbI_2 and CH_3NH_3I followed by annealing treatment. This method allows controlling the balance between complete PbI_2 conversion and the peeling off of the film.

In the case of planar structures, the most effective film deposition technique is the vapour deposition because the dipping in CH_3NH_3I solution led to the peeling off/dissolution of the $CH_3NH_3PbI_3$ film, resulting in a poor-quality and non-uniform perovskite film. The DSVD method was described first by Liu *et al.*[62] in 2013. The CH_3NH_3I and $PbCl_2$ are heated until 120 °C and 325 °C, respectively, and then deposited simultaneously onto the TiO_2 under high vacuum.[62] The precursors can be sequentially deposited too. This method allows obtaining an extremely uniform perovskite film without pinholes - Figure 1.17. The perovskite layer in devices prepared by DSVD led to a maximum PCE of 15 %, whereas an equivalent PSC device prepared by the solution method exhibited only 12 %.

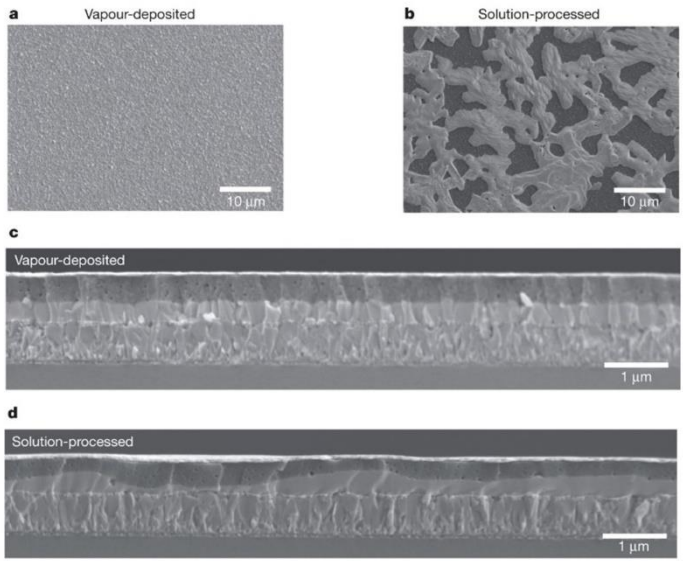

Figure 1.17. SEM top view of a a) DSVD perovskite film and b) a solution processed perovskite film; cross-sectional SEM images under lower magnification of a complete PSC constructed from a c) DSVD perovskite film and d) a solution processed perovskite film. Reprinted by permission from Macmillan Publishers Ltd: Nature [62], copyright 2013.

There is another method combining solvent-based and sublimation techniques, the so-called vapour assisted solution process. It is similar to the two-steps deposition method differing in the second step: instead of dipping in CH_3NH_3I, the PbI_2 film is exposed to a CH_3NH_3I vapour at mild temperatures to induce the intercalation reaction to form $CH_3NH_3PbI_3$ crystals.[61] The advantage of this technique is the low demand in terms of vacuum and temperature. Casaluci *et al.*[58] prepared planar perovskites in ambient air using this deposition method; after the deposition of PbI_2 by spin-coating and its annealing step, the samples were put on a hot plate surrounded by CH_3NH_3I powder, under low vacuum, for the complete formation of the perovskite film. A PCE of 12.7 % was achieved with this planar structure showing good stability in air at 50 % of RH and 20 °C during 14 days (without encapsulation). This technique takes advantage of a kinetically controlled CH_3NH_3I diffusion into the PbI_2 to generate

a more thermodynamically stable compact perovskite film with well-defined grains.[30]

In 2016, Li *et al*.[150] proposed a simple and effective method to suppress the use of toxic anti-solvents and to produce large area cells, called vacuum flash-assisted solution process - Figure 1.18. After depositing the perovskite precursor solution ($FA_{0.81}MA_{0.15}Pb_{2.51}Br_{0.45}$) by spin-coating, the film was immediately placed into a vacuum chamber at 20 Pa for few seconds. This step allows the quick crystallization of the perovskite intermediate phase by removing solvents (GBL and DMF). The intermediate perovskite still has DMSO in its composition, which is later removed raising the temperature up to 100 °C for 30 min, transforming the nanofibrous aggregates of the intermediate film in a smooth and crystalline layer without pinholes. The devices prepared by this method retained 90 % of their initial PCE compared with 70 % by devices prepared with the same perovskite composition but by the anti-solvent method.[150] The great advantage of this method is the possibility of being done outside the glove box. Recently, Cheng *et al*.[151] prepared an air-stable perovskite with $(FAI)_{0.46}(MAI)_{0.40}(MABr)_{0.14}(PbI_2)_{0.86}(PbBr_2)_{0.14}$ (MAI excess) as active layer under more than 50 % of RH, achieving PCE of 18.8 % and small hysteresis effect. The authors believe that the large amount of MA^+ cations interact with *δ*-phase perovskite, facilitating the formation of *α*-phase perovskite.

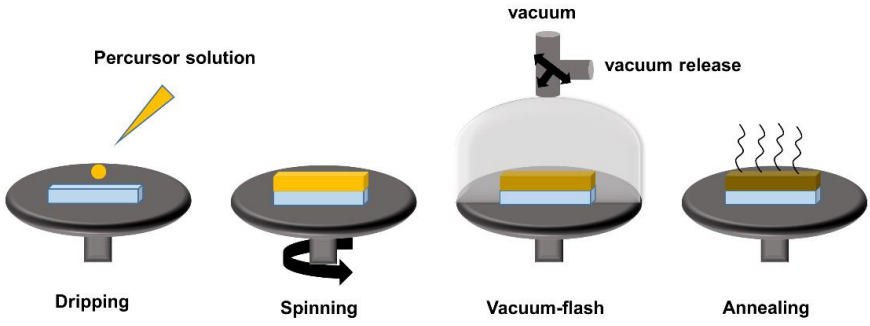

Figure 1.18. Schematic illustration of vacuum flash-assisted solution process steps (adapted from [150]).

Table 3 summarizes the main deposition methods, highlighting the PCE and stability output of representative devices. Ongoing studies on different configurations aim efficiency and stability improvements. Particularly in what concerns accelerated aging tests, it is observed a diversity of results since they are quite dependent on the method used for determining the maximum power point; to obtain accurate comparative results it is critical to standardize this procedure.[152,153]

Table 1.2. Advantages and disadvantages of different perovskite deposition processes with reference to the best PCE obtained and stability reported (*PCE of the first device reported; **Best PCE achieved until the date; ***Two deposition and two sintering steps).

Deposition Process		Advantages	Disadvantages	η / %	Stability
Solution process	One-step deposition	- Easy to perform; - Fast process.	- Wide range of crystal size; - Poor reproducibility.	10.9 % [13]	-
	One-step deposition via anti-solvent method	- Dense and uniform surface of perovskite layer; - Fast process.	- Operator depending technique.	16.2 % *[146] 22.6 % **[154]	- No hysteresis;[20] - Maintained 95 % of its initial PCE for 500 h, at 85 °C and under full illumination and MPP.[20]
	Two-step deposition	- Control in the formation and growth of the crystals.	- Long-time preparation***; - Traces of PbI_2 in the final perovskite; - Peeling off/dissolution of the $CH_3NH_3PbI_3$ film in planar architectures.	15.0 % *[43] 20.2 % **[89]	- Maintained more than 80 % of its initial PCE for 500 h, at 45 °C and 1 sun.[43]
Vapour methods	Dual source vapour deposition	- Uniform perovskite layer; - Less thickness variation than simple solution-processed layers.	- High vacuum and temperature requirements.	15.4 % *[62] 20.1 % **[155]	- No hysteresis;[156] - < 5 % PCE degradation after 1 year under dark.[155]
	Vapour assisted solution process	- Low demand in terms of vacuum and temperature; - Well defined grains.	- Gas-solid reaction requires hours for full conversion.	19.1 % [157]	- No traces of PbI_2 in the device after 14 days (no encapsulation) under air at 50 % of RH and 20 °C.[58]
Vacuum flash-assisted solution process		- Smooth and crystalline layer without pinholes; - Easily scalable; - May be performed at air ambient.	- Vacuum requirement.	19.6 % *[150]	- Maintained 90 % of initial PCE after 100 h of continuous illumination.[150]

Although the majority of the deposition methods referred above allow good performances, they are difficult to implement at large scale mainly due to the use of spin-coating technique. Therefore, other techniques start now to emerge as an option: spray coating, slot-die, doctor-blade and inkjet printing - Table 1.3.

The spray coating deposition consists in the nebulisation of the precursor solution and its deposition by a carrier gas in a hot substrate to evaporate the solvents. Even though this method is easy to implement and to perform, it is needed to optimize several deposition variables at the same time to obtain a perovskite film with high quality. The most important variables are the solvent boiling point, amount of the precursor solution, precursor ratio of organic and lead halide components, substrate temperature, spray speed and droplet size. According to Barrows *et al*.[158], spray solutions with too low boiling point (*e.g*. chlorobenzene) can dry before reaching the substrate inducing pinholes and non-uniform perovskite layer. On the other side, use of solvents with high boiling points (*e.g*. DMSO) results in thickness irregularities in large area substrates due to long drying times. The substrate temperature also plays an important role since low temperatures may cause incomplete $MAPbI_3$ conversion; by optimization of that temperature up to 80 °C and the amount of MAI in the precursor solution, Xia *et al*.[159] achieved a 16.2 % PCE device (J_{sc} = 20.7mA·cm^{-2}, V_{oc} = 1.06 V and FF = 0.740). Until the date, the record belongs to Heo *et al*.[160] that presented a 18.3 % PCE for a small area PSC and 15.5 % for a 40 cm^2 active area module.

Slot-die coating deposition involves the transport of precursor solution from the coating head (containing an ink reservoir) to the substrate forming a continuous solution meniscus. The meniscus liquid edge of precursor solution moves to spread the solution film across the substrate. In some cases only PbI_2 is deposited by this method; after that the substrate is dipped in an anti-solvent solution to complete formation of perovskite.[161] The quality of the perovskite film is dependent of temperature substrate and gas blowing. The major disadvantage of this method compared with spin-coating technique is the drying step and the post thermal annealing. Slot-die deposition involves wet and slow drying under ambient conditions causing uncontrolled crystal growth and pinholes in PbI_2 films. Whitaker *et al*.[162] by the addition of methylamonium chloride to the

perovskite precursor solution achieved high degree of crystallinity and an 8 min processing window time between perovskite deposition and anti-solvent dipping. This time delay is very important in scale-up deposition techniques due to the inherent delay between the coating station and anti-solvent dipping/thermal annealing one. Slot-die coating yielded a PCE of 18 % (J_{sc} = 21.5 mA·cm^{-2}, V_{oc} = 1.1 V and *FF* = 0.760).

Blade coating is a similar method to the slot-die: a blade is used to spread loaded precursor solution along the substrate to form a wet solution film. These two methods, slot-die and blade coating, are normally used as a first step of a two-steps perovskite deposition, being the dipping the second step. Razza *et al*.[163] detected that the optimal dipping time is longer for samples prepared by blade-coating compared to spin-coating since PbI_2 films are more compact taking more time to fully conversion. The PCE record for blade-coating PSC is set on 20.2 % for small areas[164] and 14.6 % for a module with 57.2 cm^2 of active area.[165]

Ink-jet printing uses a nozzle to drop the perovskite precursor solution ink from a piezoelectric-driven inkjet head with a monitorized *xyz* table. This is one of the most versatile deposition techniques since it is possible to manipulate very easily the shape and thickness of the perovskite layer deposited. However, it also presents some disadvantages, being the right wetting behavior of the ink the most important one.[166] The last results obtained with this technique allowed to demonstrate that the technology is becoming competitive with other deposition methods in terms of the quality of the active layer. Abzieher *et al*.[167] and Li *et al*.[168] reached PCEs of 22.7 % and 17.7 % for small devices and 2 cm^2 active area module, respectively.

Table 1.3. Advantages and disadvantages of possible large-scale perovskite deposition processes with reference to the best PCE obtained for small PSC and modules.

Deposition Process		Advantages	Disadvantages	η / %
Spray coating	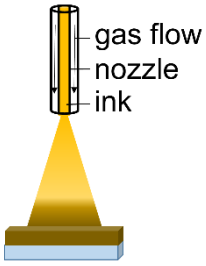	- easily scalable; - low material waste.	- perovskite crystallinity affected by several variables that need optimization.	18.3 %;[160] 15.5 % (module 40 cm^2 active area).[160]
Slot-die and blade coating	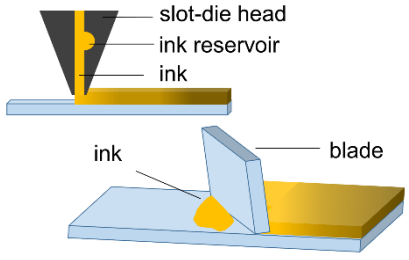	- well-established industrial deposition techniques; - can operate at very high deposition rates; - good to encapsulate; - low investment cost; - flexible.[169]	- wet and slow drying step; - use of gas flow to dry the coated solution.	Slot-die: 18.0 %;[162] 13.8 % (module 144 cm^2 active area).[170] Blade: 20.2 %;[164] 14.6 % (module 57.2 cm^2 active area).[165]
Inkjet printing	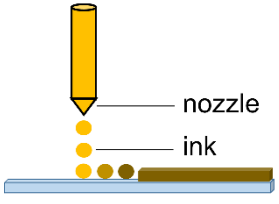	- flexibility of printed shapes and thickness; - substrate independence; - low material waste.	- hard to apply anti-solvent techniques to control crystallization; - printing speed limited by the numbers of nozzles and typically slower than other coating methods.	22.7 %;[167] 17.7 % (module 2 cm^2 active area).[168]

1.3.5 Hysteresis effect

A challenging characteristic of perovskite solar cells is the presence of hysteresis in the *I-V* curve when measured under common voltage sweep rates (usually in the range of 100 - 1 $mV \cdot s^{-1}$).[171] Hysteresis evolves from the irreproducibility of the *I-V* curve depending on the scan direction and scan rate. Usually, a forward scan followed by a backward bias results in an enhanced performance and in a particular larger fill factor. For these cases, the *I-V* characteristic curve is not suitable to provide a reliable value of the PCE and so, understanding the hysteresis source is essential to avoid ambiguities on the PSC devices characterization and to improve the stability of the device.

This phenomenon was first reported by Dualeh *et al*.,[172] who observed a strong hysteresis in the *I-V* curves under illumination of lead iodide PSC. Besides, hysteresis depends also if forward (from short circuit to forward bias) or reverse (from forward bias to short circuit) scan is performed first - Figure 1.19. The forward scan is far more rate dependent than the reverse scan, suggesting that some slow charged carriers are involved in the current and voltage generation.

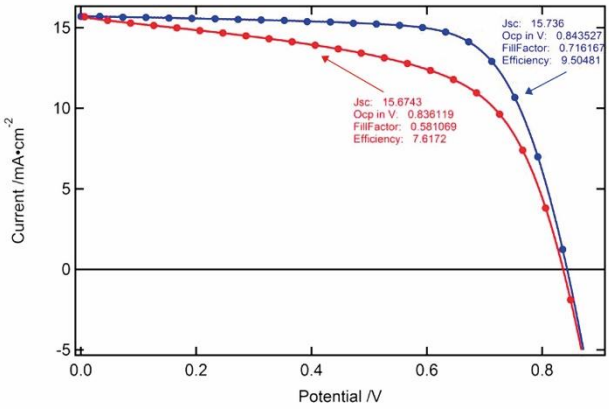

Figure 1.19. *I-V* curve of a standard perovskite solar cell that presents hysteresis: reverse scan - blue dots; forward scan **-** red dots. Reprinted with permission from [172].Copyright 2014 American Chemical Society.

Several investigations on this topic pointed out that the physical origin of hysteresis may be related to: trapping of electronic carriers at the perovskite

interface(s);[173,174] ferroelectric effects;[175,176] ionic displacement[171] or combinations among those.[177]

A theoretical study was performed by van Reenen *et al*.;[177] these authors concluded that a combined effect of ion migration through the perovskite and trapping of charge carriers at the perovskite interfaces is responsible for the hysteresis behaviour. These two effects induce large densities of charges (either electrons and holes) at the perovskite interface. For an unfavorable biasing, the high density of charges induces a severe non-radiative trap-assisted recombination with consequent reduction of photocurrent and PCE of the device. On the other hand, at favorable biasing, a low density of trapped electrons and free holes accumulate at the same interface contributing for a better performance of the cell. This work allows to conclude that, for decreasing the hysteresis effect and enhance the photovoltaic performance of PSCs, the ionic movement and the electronic defects responsible for the trap-assisted recombination should be reduced.

More recently, Meloni *et al*.[178] combined experimental and computational approaches to assess the hysteresis origin. Since it was previously determined that hysteresis phenomenon takes place in a timescale of microseconds to seconds,[179] this long timescale suggests that it is a thermally activated process. Thus, from the dependent-temperature measurements of the current-voltage characteristic curves the activation energy for the hysteretic process was determined and compared to the computational results. The idea of dependence of hysteresis phenomenon with the processing and measurement conditions was excluded since the activation energy values do not suffer a significant change when processing parameters and the measurements conditions are changed. Furthermore, the computationally calculated activation energy of the migration of vacancies of the various ionic species showed that the lowest value is for halides, which matches with the experimental observations. Therefore, it was possible to conclude that the migration of the halide species is the cause of the hysteretic behavior in the PSC devices.[178] This conclusion is also supported by Zhang *et al*.,[180] who refers that the reduction and/or stabilization of the mobile halide ion species could improve the stabilization of PCE of devices.

Tress *et al*.[181] studied experimentally the hysteresis origin, extending the conventional studies of $CH_3NH_3PbI_3$ to mixed cation/halide perovskite systems. It was shown that *I-V* hysteresis results from an interplay between charge transport in the perovskite layer, charge extraction at the contacts and a slow field-induced process in the perovskite and at electrodes interfaces; the latter attributed to ion migration. However, it was also observed an "inverted" hysteresis in the mixed cation/halide perovskite devices, *i.e*. a reduced device performance when a forward bias is followed by a backward scan - Figure 1.20. Since this behavior was also observed in devices with TiO_2 mesoporous covered by a thin insulating alumina shell, the authors attributed the inverted hysteresis to an energetic extraction barrier at the TiO_2 interface.

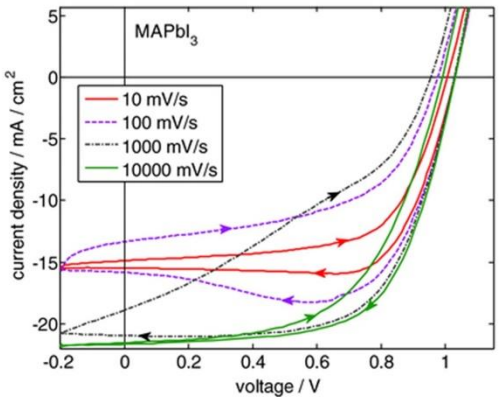

Figure 1.20. "Inverted" hysteresis in mixed perovskite. Reprinted with permission from [181]. Copyright 2016 WILEY-VCH Verlag GmbH & Co. KGaA, Weinheim.

In 2017, Domanski *et al*.[182] studied the effect of the electric field-induced ionic defect migration on the long-term performance of several perovskite systems. It was experimentally validated that ion vacancies migrate and accumulate at the perovskite/charge selective contacts. Moreover, it was also proposed that cation vacancies can migrate to the electron contact on longer timescales than the ones usually observed (above 10^3 s), playing then an important role in the long-term stability of devices. This cation accumulation is responsible for a performance loss of about 10-15 % over several hours operating at maximum power point. Nevertheless, the initial PCE can be totally restored after leaving the cells under dark. This was observed for several cycles

of dark/illumination, simulating the night/day phases that cells will be submitted under real outdoor conditions.

The elimination of the hysteresis in perovskite solar cells will not only allow a more correct characterisation of the devices, but it will allow to fabricate long-term stable PSC devices. Yoon *et al*.[183] prepared a hysteresis-free planar perovskite with 19 % of PCE, using C_{60} as electron transport layer deposited by a room-temperature vacuum-process. This result was achieved optimizing the C_{60} layer thickness to 35 nm, which passivates the grain boundaries of the perovskite and enhances the charge transport properties. The preparation of perovskite large size crystal grains also emerged as a possibility to reduce the hysteretic behavior of the devices.[184] Besides a better charge transfer at the interfaces, larger crystals present less defects (source of ions) and less grain boundaries (fast channel of ionic migration).[185]

1.4 Lead-free perovskites

The most used metal cation in PSCs is lead, but the environmental impact of its usage due to its toxicity is becoming an important issue for PSC commercialisation. $CH_3NH_3PbI_3$ in contact with polar solvents such as water can convert to PbI_2, a carcinogen compound that is moderately water-soluble and whose use was banned in many countries. Nevertheless, studies demonstrated that even in the event of the total destruction of a large solar electrical power plant, the amount of lead added to the environment through rainwater is small in comparison to the natural occurrence of lead.[186] Despite, researchers addressed the use of other metal cations besides lead. The first material identified as promising for this substitution was tin (Sn). A partial substitution of lead by tin was reported by Zuo *et al*. [187] reaching a PCE of 10.1 %, with the proportion of 15 % Sn and 85 % Pb. The increase of Sn concentration reduces the band gap of perovskite responsible for the enhancement in solar light absorption[188] - Figure 1.21 - but the presence of Pb is essential for retarding the oxidation of Sn^{2+} to Sn^{4+}.[189]

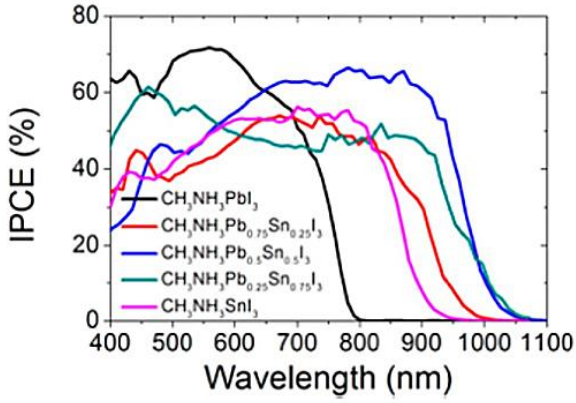

Figure 1.21. IPCE spectra of devices based on $CH_3NH_3Sn_{1-x}Pb_xI_3$ perovskites. Reprinted with permission from [188].Copyright 2014 American Chemical Society.

The complete substitution of Pb in perovskite devices is difficult because tin-based materials are extremely reactive. In particular, Sn^{2+} oxidation state is chemically unstable and easily oxidizes to Sn^{4+} that may act as a p-type dopant within the material. The Sn^{4+} destroys the charge neutrality of the perovskite structure with consequent formation of oxides/hydroxides of Sn and methylammonium iodide; this results in limited diffusion lengths for the photoexcited carriers.[190] Indeed, the efficiencies achieved until now by completely lead-free perovskite devices are very low. The first Sn-based perovskite was reported by Noel *et al*.[191] $CH_3NH_3SnI_3$ perovskite solar cell displayed a maximum PCE of 6.4 %, corresponding to a V_{oc} of 0.88 V, J_{sc} of 16.8 $mA \cdot cm^{-2}$ and *FF* of 0.42. It is important to emphasize the low reproducibility and reduced long-term stability of the assembled devices. Another lead-free light harvester material based on $CH_3NH_3SnI_3$ perovskite semiconductor was reported by Hao *et al*.[192] This material exhibits an optical bandgap of 1.3 eV, but through bandgap engineering by chemical substitution in the form of $CH_3NH_3SnI_{3-x}Br_x$, the spectral absorption in the visible region can be enhanced, which allowed to prepare a lead-free solar cell with a PCE of 5.73 % for the proportion $x = 2$. To stabilize the Sn-based perovskite absorbers, Liao *et al*.[193] incorporated 20 % of phenylethylammonium (PEA) into $FASnI_3$ perovskite achieving 5.93 % of PCE and stability up to 1000 h. This value was further increased up to 9 % after optimization of the PEA amount (0.08 M), which

allowed highly homogeneous growth, high crystallinity and oriented $FASnI_3$ grains at relatively low temperature. The number of grain boundaries was reduced along with reduction of Sn^{2+} vacancies. The devices displayed negligible hysteresis, as they benefit from very low trap-assisted recombination, low shunt losses and more efficient charge collection.

Recently, methylammonium bismuth iodide - $(CH_3NH_3)_3Bi_2I_9$ - emerged as another possible substitute for toxic lead and unstable tin-based perovskites, due to its advantages of non-toxicity, ambient stability and low-temperature solution processability. Applied by spin-coater and followed by a heating step, the precursor solution leads to a reddish film that allows to prepare a PSC with a PCE of less than 1 % with a V_{oc} of ~0.51 V in a planar arrangement.[194] Besides the very low performance of the device, the authors believe that reducing the background carrier concentration and optical band gap, bismuth-based organic-inorganic materials could lead to a new era of light absorbers for PSC.[195,196] In fact, the substitution of MA^+ cation by silver (Ag) allowed Kim *et al*.[197] to prepare devices based in bismuth with a PCE of 1.22 % and excellent stability under ambient conditions. The films were prepared from silver and bismuth precursor solutions in n-butylamine by spin coating. After that, they were annealed in N_2 atmosphere, forming $AgBi_2I_7$ perovskite film with high crystallinity and good surface morphology. On the other side, Jain *et al*.[198] focused on the deposition method of the $(CH_3NH_3)_3Bi_2I_9$ perovskite and by a vapour-assisted solution process achieved a device with a V_{oc} of 1.01 V and a PCE value of 3.17 %. The best until the date, for a ternary bismuth-based PSC.

In 2015, Prochowicz *et al*.[199] introduced the mechanosynthesis as an easy and fast method to produce highly crystalline $CH_3NH_3PbI_3$ perovskite. The method is based on the chemical reactions that occur in a ball-mill induced by high pressures and temperatures that come from the impact of the balls. According to the authors, at the end of the reactions no precursor materials (CH_3NH_3I and PbI_2) are present in the produced material - Figure 1.22. The final perovskite when applied in a device, by one step deposition, allows obtaining 9.1 % of PCE. Since it works with $CH_3NH_3PbI_3$ composition, it could be a good approach to easily prepare new and more complex lead-free perovskites.

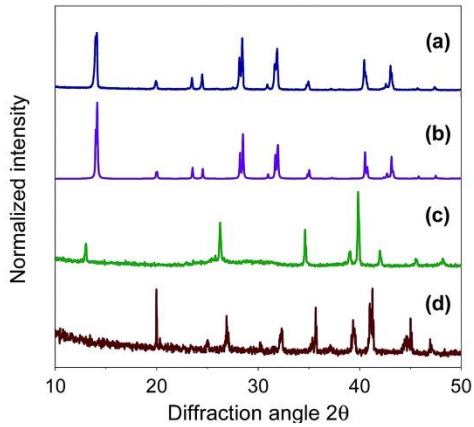

Figure 1.22. Powder x-ray diffraction patterns of: (a) simulated $CH_3NH_3PbI_3$; (b) mechanosynthesis perovskite; (c) PbI_2, and (d) MAI. Reproduced from [199] with permission of The Royal Society of Chemistry.

Until now, the preferable substitute of lead is tin; however, tin is also classified as a harmful chemical. According to several studies the Sn-based devices do not present more economical nor environmental advantages compared with Pb-based devices: 1) tin metal is 9 times more expensive than lead;[200] 2) it is the third most critical metal in strategic energy technologies; 3) its production is fairly concentrated on high political risk countries;[201] and 4) terrestrial eco-toxicity warning contribution impacts are greater than lead by up to 10 times.[202]

1.5 Encapsulation solutions for long-term lifetime

Efficiency, stability and cost are the three main pillars to accelerate an effective industrial exploitation of a given PV technology. Perovskite solar cells have demonstrated high power conversion efficiencies with cost-effective materials and fabrication processes, but stability is still a major issue that needs to be addressed. The poor stability of the perovskite solar cells under ambient conditions has challenging the research community to develop good sealing materials to avoid degradation mechanisms, mainly related to oxygen and moisture exposure under outdoor operation.

Standard protocols, either for characterising the solar cells performance and stability have been already established for conventional photovoltaic technologies, while no protocols have been established for PSCs. However, it is very important to standardize the characterization tests to allow direct comparison of the obtained results among different research groups and producers. Some authors reported a list of recommendations that should be considered during the performance tests of PSC.[203,204] Some of them are very easy to implement and they have demonstrated to have a large impact in photovoltaic parameters measured: use of a light mask with known active area during the characterisation; record forward and reverse *I-V* curves at various scan rates; and measurement of the steady-state photocurrent at several voltages near to the maximum power point. In what concerns stability, no specific recommendations have been proposed but using an appropriate encapsulation process may significantly contribute to stabilise the device under operation conditions and thus eliminating the degradation effect due to moisture and oxygen.

Typical encapsulation processes used consider a top glass substrate spaced from the device by means of traditional Surlyn® sealant (DuPont, United States). The sandwiched device is then protected around with a polymeric resin for avoiding moisture and oxygen intake;[140,205] however, this polymeric encapsulation was good only for few days. Recently, Matteocci *et al*.[206] reported a comparative study between different types of sealing procedures based in thermal plastics and light curable resins. After sealing, the devices were exposed to accelerated life time tests like damp-heat, light-soaking and temperature stress and their PCE decay was analysed - Table 1.4. The best sealing procedure used an adhesive (Kapton®, DuPont, United States) followed by a light-curable glue (Henkel, Germany) and a UV curable glue (ThreeBond, United States) as edge sealant. The devices presented only a 2 % PCE decrease after 170 h; this reduction was mainly related to thermal degradation of spiro-OMeTAD, as well as UV-degradation of sensitive inner-components. However, an important conclusion of this study was that, besides the sealing materials, the sealing procedure itself may induce a net loss of PCE. Actually, encapsulation processes normally use temperature, UV curing and pressure that can affect the

PCE stability.[206] For example, in the case of sealing a PSC device with Surlyn foil by hot-press, it demonstrated a higher loss of efficiency compared with the unsealed blank device.

Table 1.4. Sealing procedures for the encapsulation of PSC and their effect on the PCE value after 170 h of shelf-life (dark, 30 % of RH).[206]

Sealing procedure	Sealing materials	Relative PCE decrease at 170 h
Hot press 100 ºC, 0.4 bar, 40 s	Thermo-plastic foil (Surlyn 60)	58 %
UV lamp exposure, 40 s	UV curable glue	21 %
Xenon lamp (AM 1.5G) exposure, 10 s	Light curable glue (Henkel)	21 %
Xenon lamp (AM 1.5G) exposure, 10 s	Adhesive (Kapton) + light curable glue	< 5 %
Xenon lamp (AM 1.5G) exposure, 10 s + UV masking the active area	Adhesive (Kapton) + light curable glue (Henkel) + UV curable glue as edge sealant (ThreeBond)	< 5 %
Unsealed	-	33 %

In flexible PSC devices the most common encapsulation is plastic barrier films. Weerasinghe *et al*.[207] reported two types of encapsulation, partial and complete, both using a commercial plastic barrier encapsulant adhesive (Viewbarrier®, Mitsubishi Plastic, Inc., Japan) that was laminated at 100 °C onto the flexible device back contact. Researchers are also using conductive tapes back contact. Shao et *al*.[208] demonstrated that a commercial carbon conductive tape could be laminated above the perovskite layers with good adhesion and playing two important roles: being simultaneously back contact and encapsulant, which reduces the fabrication costs of the device.

Polymeric based encapsulating approaches, although effective for accelerated lifetime tests, will hardly survive to 20 years of lifetime demanded to the commercial devices; the best option would be then to use glass

encapsulation using glass frits. For dye-sensitized solar cells, Ribeiro *et al*.[209] reported a laser assisted glass sealing process using a low melting point glass frit. The sealed cells showed to be leak-free to helium gas. Moreover, the photovoltaic performance of laser-sealed DSCs was assessed, presenting almost no performance decrease after 1000 h of aging tests (765 $mW \cdot cm^{-2}$ and 0.6 V), whereas devices sealed by the conventional method (Surlyn®) presented almost 34 % PCE decrease.[210] In 2014, this technique was successfully up-scaled to large areas by pre-heating the substrates to *ca*. 250 °C. The required sealing temperature is needed for dissipating the tensions related to the thermal expansion owing to the laser firing.[211] However, PSCs cannot withstand to temperatures above 100 °C - 120 °C. New sealing frits and laser-assisted procedures were developed by the same group to address this requirement. In 2017, Emami *et al*.[212] reported laser assisted glass sealed cells at room temperature of circular shape with a diameter of 3.5 cm. The sealed samples were exposed to 11 humidity-freeze cycles and 50 thermal cycles (standard IEC-61646) presenting values of helium leaks below the reject limit of 5×10^{-8} $atm \cdot cm^3 \cdot s^{-1}$ (standard MIL-STD-883H). Recently, the authors up-scaled the process for larger devices with 7×7 cm^2, presenting a leak rate value lower than 1×10^{-7} $atm \cdot cm^3 \cdot s^{-1}$ after 5 humidity-freeze cycles.[213] FTO substrate with TiO_2 blocking layer and scribing was successfully sealed to another FTO substrate, showing that the developed encapsulation method is compatible with perovskite solar cells configuration.

1.6 Scope of the thesis

In the last few years, research on PSC technology has been growing quite fast and remarkable power conversion efficiencies have been achieved. However, their long-term stability and manufacturing protocols are also critical to the large scale-up, enabling its emergence in the PV-market. The work developed in this thesis aims to contribute to the study of PSC major drawbacks, not only in terms of stability, namely temperature, oxygen and relative humidity sensitivity, but also in terms of simplifying manufacturing protocols aiming reduction of costs.

This work is divided in 5 chapters. In **Chapter 1**, solar energy is discussed as one of the most promising renewable sources to answer to the energy demand of the world population in the future. Particular emphasis is given to PSC technology, explaining its operation principles and presenting pros and cons of the different types of architectures and materials used so far. It is also presented the state-of-the-art concerning PSC stability, referencing the different factors that influence their long-term operation. In this chapter, attention is also given to lead-free PSC and encapsulation methods, not only to protect the cells from the environmental factors, but also to avoid natural lead leakage.

Chapter 2 focuses in a step-by-step analysis of the technical problems of each layer of the PSC and their impact on the device performance is addressed. This chapter provides a useful detailed protocol to obtain PSC with reproducible ~15 % of power conversion efficiency. This chapter allows also to have a summary of the experimental protocols followed during the different studies developed within this thesis.

Chapter 3 studies the effect of temperature on the PSC under operation. Temperature is one of the most important environmental factor related to PSC stability since it is the only one that cannot be controlled by encapsulation. This work aims at mimicking as closely as possible real operating conditions, exposing the cells, with different HELs, to temperatures between -5 °C to 80 °C and sealed under ambient conditions of oxygen and humidity. These results allowed to understand the role of temperature in the devices degradation mechanism under real outdoor operation.

The following chapter, **Chapter 4** aims at understanding the role of other two environmental factors that may affect PSC performance and stability: oxygen and relative humidity. These results allowed to understand that the restricted conditions of dry and inert conditions reported in the literature to prepare the perovskite and hole extraction layers are overrated. The best performing device was prepared with a triple-cation perovskite layer prepared in dry atmospheric air, presenting a power conversion efficiency of 16.7 %.

Finally, **Chapter 5** presents the main conclusions of the work developed in the scope of this thesis, along with future work suggestions and guidelines.

References

[1] BP Statistical Review of World Energy 2017, June, 2017.

[2] N.L. Panwar, S.C. Kaushik, S. Kothari, *Role of renewable energy sources in environmental protection: A review*, Renewable and Sustainable Energy Reviews **15** (2011), p:1513-1524.

[3] N. Kannan, D. Vakeesan, *Solar energy for future world: - A review*, Renewable and Sustainable Energy Reviews **62** (2016), p:1092-1105.

[4] SunPower, www.us.sunpower.com/solar-panels-technology/facts/, 2019.

[5] Fraunhofer - Photovoltaics report, www.ise.fraunhofer.de/content/dam/ise/de/documents/publications/studies/Photovoltaics-Report.pdf, 2019.

[6] M.A. Green, Y. Hishikawa, E.D. Dunlop, D.H. Levi, J. Hohl-Ebinger, M. Yoshita, A.W.Y. Ho-Baillie, *Solar cell efficiency tables (Version 53)*, Progress in Photovoltaics: Research and Applications **27** (2019), p:3-12.

[7] D. Mulvaney, *Hazardous Materials Used In Silicon PV Cell Production: A Primer*, Solar Industry, September 2013.

[8] K. Kakiage, Y. Aoyama, T. Yano, K. Oya, J.I. Fujisawa, M. Hanaya, *Highly-efficient dye-sensitized solar cells with collaborative sensitization by silyl-anchor and carboxy-anchor dyes*, Chemical Communications **51** (2015) p:15894-15897.

[9] A. Kojima, K. Teshima, Y. Shirai, T. Miyasaka, *Organometal halide perovskites as visible-light sensitizers for photovoltaic cells*, Journal of the American Chemical Society **131** (2009), p:6050-6051.

[10] I. Chung, B. Lee, J. He, R.P.H. Chang, M.G. Kanatzidis, *All-solid-state dye-sensitized solar cells with high efficiency*, Nature **485** (2012), p:486-489.

[11] S.P. Singh, P. Nagarjuna, *Organometal halide perovskites as useful materials in sensitized solar cells*, Dalton Transactions **43** (2014), p:5247-5251.

[12] L. Etgar, P. Gao, Z. Xue, Q. Peng, A.K. Chandiran, B. Liu, M.K. Nazeeruddin, M. Grätzel, *Mesoscopic $CH_3NH_3PbI_3/TiO_2$ heterojunction solar cells*, Journal of the American Chemical Society **134** (2012), p:17396-17399.

[13] M.M. Lee, J. Teuscher, T. Miyasaka, T.N. Murakami, H.J. Snaith, *Efficient hybrid solar cells based on meso-superstructured organometal halide perovskites*, Science **338** (2012), p:643-647.

[14] National Renewable Energy Laboratory, https://www.nrel.gov/pv/cell-efficiency.html, 2019.

[15] D. Cui, Z. Yang, D. Yang, X. Ren, Y. Liu, Q. Wei, H. Fan, J. Zeng, S. Liu, *Color-Tuned Perovskite Films Prepared for Efficient Solar Cell Applications*, The Journal of Physical Chemistry C **120** (2016), p:42-47.

[16] Y. Deng, Q. Wang, Y. Yuan, J. Huang, *Vividly colorful hybrid perovskite solar cells by doctor-blade coating with perovskite photonic nanostructures*, Materials Horizons **2** (2015), p:578-583.

[17] G.E. Eperon, V.M. Burlakov, A. Goriely, H.J. Snaith, *Neutral Color Semitransparent Microstructured Perovskite Solar Cells*, ACS Nano **8** (2014), p:591-598.

[18] E.H. Jung, N.J. Jeon, E.Y. Park, C.S. Moon, T.J. Shin, T.-Y. Yang, J.H. Noh, J. Seo, *Efficient, stable and scalable perovskite solar cells using poly(3-hexylthiophene)*, Nature **567** (2019), p:511-515.

[19] G. Grancini, C. Roldán-Carmona, I. Zimmermann, E. Mosconi, X. Lee, D. Martineau, S. Narbey, F. Oswald, F. De Angelis, M. Graetzel, M.K. Nazeeruddin, *One-Year stable perovskite solar cells by 2D/3D interface engineering*, Nature Communications **8** (2017), 15684.

[20] M. Saliba, T. Matsui, K. Domanski, J.-Y. Seo, A. Ummadisingu, S.M. Zakeeruddin, J.-P. Correa-Baena, W.R. Tress, A. Abate, A. Hagfeldt, M. Grätzel, *Incorporation of rubidium cations into perovskite solar cells improves photovoltaic performance*, Science **354** (2016), p: 206-209.

[21] D. Yang, X. Zhou, R. Yang, Z. Yang, W. Yu, X. Wang, C. Li, S. Liu, R.P.H. Chang, *Surface optimization to eliminate hysteresis for record efficiency planar perovskite solar cells*, Energy & Environmental Science **9** (2016), p:3071-3078.

[22] K.T. Cho, S. Paek, G. Grancini, C. Roldan-Carmona, P. Gao, Y. Lee, M.K. Nazeeruddin, *Highly efficient perovskite solar cells with a compositionally engineered perovskite/hole transporting material interface*, Energy & Environmental Science **10** (2017), p:621-627.

[23] H.J. Snaith, *Perovskites: The emergence of a new era for low-cost, high-efficiency solar cells*, Journal of Physical Chemistry Letters **4** (2013), p:3623-3630.

[24] M. He, D. Zheng, M. Wang, C. Lin, Z. Lin, *High efficiency perovskite solar cells: From complex nanostructure to planar heterojunction*, Journal of Materials Chemistry A **2** (2014), p: 5994-6003.

[25] J.S. Yun, A. Ho-Baillie, S. Huang, S.H. Woo, Y. Heo, J. Seidel, F. Huang, Y.-B. Cheng, M.A. Green, *Benefit of Grain Boundaries in Organic–Inorganic Halide Planar Perovskite Solar Cells*, The Journal of Physical Chemistry Letters **6** (2015), p:875-880.

[26] Y. Yang, *Small Molecule, Polymer and Perovskite Photovoltaic Cells with Very High Performance*, Hybrid and Organic Photovoltaics Lausanne - Switzerland, 2014.

[27] S. Brittman, G.W.P. Adhyaksa, E.C. Garnett, *The expanding world of hybrid perovskites: materials properties and emerging applications*, MRS Communications **5** (2015), p:7-26.

[28] W.F. Mohammed, O. Daoud, M. Al-Tikriti, *Power Conversion Enhancement of CdS/CdTe Solar Cell Interconnected with Tunnel Diode, Circuits and Systems* Vol.03 No.03 (2012), p:230-237.

[29] C.-S. Jiang, M. Yang, Y. Zhou, B. To, S.U. Nanayakkara, J.M. Luther, W. Zhou, J.J. Berry, J. van de Lagemaat, N.P. Padture, K. Zhu, M.M. Al-Jassim, *Carrier separation and transport in perovskite solar cells studied by nanometre-scale profiling of electrical potential*, Nature Communications **6** (2015), 8397.

[30] T. Salim, S. Sun, Y. Abe, A. Krishna, A.C. Grimsdale, Y.M. Lam, *Perovskite-based solar cells: impact of morphology and device architecture on device performance*, Journal of Materials Chemistry A **3** (2015), p:8943-8969.

[31] J.-H. Im, C.-R. Lee, J.-W. Lee, S.-W. Park, N.-G. Park, *6.5% efficient perovskite quantum-dot-sensitized solar cell*, Nanoscale **3** (2011), p:4088-4093.

[32] E. Olsen, G. Hagen, S. Eric Lindquist, *Dissolution of platinum in methoxy propionitrile containing LiI/I_2*, Solar Energy Materials and Solar Cells **63** (2000), p:267-273.

[33] H.S. Kim, C.R. Lee, J.H. Im, K.B. Lee, T. Moehl, A. Marchioro, S.J. Moon, R. Humphry-Baker, J.H. Yum, J.E. Moser, M. Grätzel, N.G. Park, *Lead iodide perovskite sensitized all-solid-state submicron thin film mesoscopic solar cell with efficiency exceeding 9%*, Scientific Reports **2** (2012), 591.

[34] U. Bach, D. Lupo, P. Comte, J.E. Moser, F. Weissörtel, J. Salbeck, H. Spreitzer, M. Grätzel, *Solid-state dye-sensitized mesoporous TiO_2 solar cells with high photon-to-electron conversion efficiencies*, Nature 395 (1998), p:583-585.

[35] H.M. Upadhyaya, S. Senthilarasu, M.H. Hsu, D.K. Kumar, *Recent progress and the status of dye-sensitised solar cell (DSSC) technology with state-of-the-art conversion efficiencies*, Solar Energy Materials and Solar Cells **119** (2013), p:291-295.

[36] J. Xiao, J. Shi, D. Li, Q. Meng, *Perovskite thin-film solar cell: Excitation in photovoltaic science*, Science China Chemistry **58** (2015), p:221-238.

[37] N. Elumalai, M. Mahmud, D. Wang, A. Uddin, *Perovskite Solar Cells: Progress and Advancements*, Energies **9** (2016), 861.

[38] T. Leijtens, G.E. Eperon, S. Pathak, A. Abate, M.M. Lee, H.J. Snaith, *Overcoming ultraviolet light instability of sensitized TiO_2 with meso-superstructured organometal tri-halide perovskite solar cells*, Nature Communications **4** (2013), 2885.

[39] P. Cui, D. Wei, J. Ji, H. Huang, E. Jia, S. Dou, T. Wang, W. Wang, M. Li, *Planar p–n homojunction perovskite solar cells with efficiency exceeding 21.3%*, Nature Energy **4** (2019), p:150-159.

[40] K. Kalyanasundaram, M. Grätzel, *Applications of functionalized transition metal complexes in photonic and optoelectronic devices*, Coordination Chemistry Reviews **177** (1998), p:347-414.

[41] X. Xin, M. Scheiner, M. Ye, Z. Lin, *Surface-treated TiO_2 nanoparticles for dye-sensitized solar cells with remarkably enhanced performance*, Langmuir **27** (2011), p:14594-14598.

[42] T. Leijtens, B. Lauber, G.E. Eperon, S.D. Stranks, H.J. Snaith, *The importance of perovskite pore filling in organometal mixed halide sensitized TiO_2-based solar cells*, Journal of Physical Chemistry Letters **5** (2014), p:1096-1102.

[43] J. Burschka, N. Pellet, S.-J. Moon, R. Humphry-Baker, P. Gao, M.K. Nazeeruddin, M. Gratzel, *Sequential deposition as a route to high-performance perovskite-sensitized solar cells*, Nature **499** (2013), p:316--319.

[44] D. Zheng, G. Wang, W. Huang, B. Wang, W. Ke, J.L. Logsdon, H. Wang, Z. Wang, W. Zhu, J. Yu, M.R. Wasielewski, M.G. Kanatzidis, T.J. Marks, A. Facchetti, *Combustion Synthesized Zinc Oxide Electron-Transport Layers for Efficient and Stable Perovskite Solar Cells*, Advanced Functional Materials **29** (2019), 1900265.

[45] D. Bi, G. Boschloo, S. Schwarzmüller, L. Yang, E.M.J. Johansson, A. Hagfeldt, *Efficient and stable $CH_3NH_3PbI_3$-sensitized ZnO nanorod array solid-state solar cells*, Nanoscale **5** (2013), p:11686-11691.

[46] D.Y. Son, J.H. Im, H.S. Kim, N.G. Park, *11% efficient perovskite solar cell based on ZnO nanorods: An effective charge collection system*, Journal of Physical Chemistry C **118** (2014), p:16567-16573.

[47] L. Zuo, Z. Gu, T. Ye, W. Fu, G. Wu, H. Li, H. Chen, *Enhanced Photovoltaic Performance of CH3NH3PbI3 Perovskite Solar Cells through Interfacial Engineering Using Self-Assembling Monolayer*, Journal of the American Chemical Society **137** (2015), p:2674-2679.

[48] D. Shen, W. Zhang, F. Xie, Y. Li, A. Abate, M. Wei, *Graphene quantum dots decorated TiO2 mesoporous film as an efficient electron transport layer for high-performance perovskite solar cells*, Journal of Power Sources **402** (2018), p:320-326.

[49] J.M. Ball, M.M. Lee, A. Hey, H.J. Snaith, *Low-temperature processed meso-superstructured to thin-film perovskite solar cells*, Energy and Environmental Science **6** (2013), p:1739-1743.

[50] J.M. Ball, M.M. Lee, A. Hey, H.J. Snaith, *Low-temperature processed meso-superstructured to thin-film perovskite solar cells*, Energy & Environmental Science **6** (2013), p:1739-1743.

[51] K. Wojciechowski, M. Saliba, T. Leijtens, A. Abate, H.J. Snaith, *Sub-150 °C processed meso-superstructured perovskite solar cells with enhanced efficiency*, Energy and Environmental Science **7** (2014), p:1142-1147.

[52] G. Niu, X. Guo, L. Wang, *Review of recent progress in chemical stability of perovskite solar cells*, Journal of Materials Chemistry A **3** (2015), p:8970-8980.

[53] J.A. Christians, R.C.M. Fung, P.V. Kamat, *An inorganic hole conductor for Organo-lead halide perovskite solar cells - improved hole conductivity with copper iodide*, Journal of the American Chemical Society **136** (2014), p:758-764.

[54] P. Qin, S. Tanaka, S. Ito, N. Tetreault, K. Manabe, H. Nishino, M.K. Nazeeruddin, M. Gratzel, *Inorganic hole conductor-based lead halide perovskite solar cells with 12.4% conversion efficiency*, Nat Commun **5** (2014), 3834.

[55] N.J. Jeon, J.H. Noh, W.S. Yang, Y.C. Kim, S. Ryu, J. Seo, S.I. Seok, *Compositional engineering of perovskite materials for high-performance solar cells*, Nature **517** (2015), p:476-480.

[56] T. Leijtens, S.D. Stranks, G.E. Eperon, R. Lindblad, E.M.J. Johansson, I.J. McPherson, H. Rensmo, J.M. Ball, M.M. Lee, H.J. Snaith, *Electronic properties of meso-superstructured and planar organometal halide perovskite films: Charge trapping, photodoping, and carrier mobility*, ACS Nano **8** (2014), p:7147-7155.

[57] Y. Zhao, K. Zhu, *Solution chemistry engineering toward high-efficiency perovskite solar cells*, Journal of Physical Chemistry Letters **5** (2014), p:4175-4186.

[58] S. Casaluci, L. Cinà, A. Pockett, P.S. Kubiak, R.G. Niemann, A. Reale, A. Di Carlo, P.J. Cameron, *A simple approach for the fabrication of perovskite solar cells in air*, Journal of Power Sources **297** (2015), p:504-510.

[59] M. Lyu, J.-H. Yun, R. Ahmed, D. Elkington, Q. Wang, M. Zhang, H. Wang, P. Dastoor, L. Wang, *Bias-dependent effects in planar perovskite solar cells based on $CH_3NH_3PbI_{3-x}Cl_x$ films*, Journal of Colloid and Interface Science **453** (2015), p:9-14.

[60] H. Zhou, Q. Chen, G. Li, S. Luo, T.B. Song, H.S. Duan, Z. Hong, J. You, Y. Liu, Y. Yang, *Interface engineering of highly efficient perovskite solar cells*, Science **345** (2014), p:542-546.

[61] Q. Chen, H. Zhou, Z. Hong, S. Luo, H.S. Duan, H.H. Wang, Y. Liu, G. Li, Y. Yang, *Planar heterojunction perovskite solar cells via vapor-assisted solution process*, Journal of the American Chemical Society **136** (2014), p:622-625.

[62] M. Liu, M.B. Johnston, H.J. Snaith, *Efficient planar heterojunction perovskite solar cells by vapour deposition*, Nature **501** (2013), p:395-398.

[63] M.I. Dar, F. Javier Ramos, Z. Xue, B. Liu, S. Ahmad, S.A. Shivashankar, M.K. Nazeeruddin, M. Grätzel, *Photoanode based on (001)-oriented anatase nanoplatelets for organic-inorganic lead iodide perovskite solar cell*, Chemistry of Materials **26** (2014), p:4675-4678.

[64] D. Liu, T.L. Kelly, *Perovskite solar cells with a planar heterojunction structure prepared using room-temperature solution processing techniques*, Nature Photonics **8** (2014), p:133-138.

[65] L. Wang, W. Fu, Z. Gu, C. Fan, X. Yang, H. Li, H. Chen, *Low temperature solution processed planar heterojunction perovskite solar cells with a CdSe nanocrystal as an electron transport/extraction layer*, Journal of Materials Chemistry C **2** (2014), p:9087-9090.

[66] E.H. Anaraki, A. Kermanpur, L. Steier, K. Domanski, T. Matsui, W. Tress, M. Saliba, A. Abate, M. Grätzel, A. Hagfeldt, J.-P. Correa-Baena, *Highly efficient and stable planar perovskite solar cells by solution-processed tin oxide*, Energy & Environmental Science **9** (2016), p:3128-3134.

[67] J. Kim, G. Kim, T.K. Kim, S. Kwon, H. Back, J. Lee, S.H. Lee, H. Kang, K. Lee, *Efficient planar-heterojunction perovskite solar cells achieved via interfacial modification of a sol-gel ZnO electron collection layer*, Journal of Materials Chemistry A **2** (2014), p:17291-17296.

[68] Y. Guo, C. Liu, K. Inoue, K. Harano, H. Tanaka, E. Nakamura, *Enhancement in the efficiency of an organic-inorganic hybrid solar cell with a doped P3HT hole-transporting layer on a void-free perovskite active layer,* Journal of Materials Chemistry A **2** (2014), p:13827-13830.

[69] B. Xu, D. Bi, Y. Hua, P. Liu, M. Cheng, M. Gratzel, L. Kloo, A. Hagfeldt, L. Sun, *A low-cost spiro[fluorene-9,9[prime or minute]-xanthene]-based hole transport material for highly efficient solid-state dye-sensitized solar cells and perovskite solar cells*, Energy & Environmental Science **9** (2016), p:873-877.

[70] A. Mei, X. Li, L. Liu, Z. Ku, T. Liu, Y. Rong, M. Xu, M. Hu, J. Chen, Y. Yang, M. Grätzel, H. Han, *A hole-conductor-free, fully printable mesoscopic perovskite solar cell with high stability*, Science **345** (2014), p:295-298.

[71] X. Zhou, C. Bao, F. Li, H. Gao, T. Yu, J. Yang, W. Zhu, Z. Zou, *Hole-transport-material-free perovskite solar cells based on nanoporous gold back electrode*, RSC Advances **5** (2015), p:58543-58548.

[72] Z. Liu, T. Shi, Z. Tang, B. Sun, G. Liao, *Using a low-temperature carbon electrode for preparing hole-conductor-free perovskite heterojunction solar cells under high relative humidity*, Nanoscale **8** (2016), p:7017-7023.

[73] H. Zhang, H. Wang, S.T. Williams, D. Xiong, W. Zhang, C.-C. Chueh, W. Chen, A.K.-Y. Jen, *$SrCl_2$ Derived Perovskite Facilitating a High Efficiency of 16% in Hole-Conductor-Free Fully Printable Mesoscopic Perovskite Solar Cells*, Advanced Materials **29** (2017), 1606608.

[74] M. Xiao, F. Huang, W. Huang, Y. Dkhissi, Y. Zhu, J. Etheridge, A. Gray-Weale, U. Bach, Y.B. Cheng, L. Spiccia, *A fast deposition-crystallization procedure for highly efficient lead iodide perovskite thin-film solar cells*, Angewandte Chemie - International Edition **53** (2014), p:9898-9903.

[75] Z. Ku, Y. Rong, M. Xu, T. Liu, H. Han, *Full printable processed mesoscopic $CH_3NH_3PbI_3/TiO_2$ heterojunction solar cells with carbon counter electrode*, Scientific Reports **3** (2013), 3132.

[76] A. Mei, X. Li, L. Liu, Z. Ku, T. Liu, Y. Rong, M. Xu, M. Hu, J. Chen, Y. Yang, M. Grätzel, H. Han, *A hole-conductor–free, fully printable mesoscopic perovskite solar cell with high stability*, Science **345** (2014), p:295-298.

[77] C. Tian, A. Mei, S. Zhang, H. Tian, S. Liu, F. Qin, Y. Xiong, Y. Rong, Y. Hu, Y. Zhou, S. Xie, H. Han, *Oxygen management in carbon electrode for high-performance printable perovskite solar cells*, Nano Energy **53** (2018), p:160-167.

[78] X. Jiang, Z. Yu, Y. Zhang, J. Lai, J. Li, G.G. Gurzadyan, X. Yang, L. Sun, *High-Performance Regular Perovskite Solar Cells Employing Low-Cost Poly(ethylenedioxythiophene) as a Hole-Transporting Material*, Scientific Reports **7** (2017), 42564.

[79] J.-Y. Jeng, Y.-F. Chiang, M.-H. Lee, S.-R. Peng, T.-F. Guo, P. Chen, T.-C. Wen, *$CH_3NH_3PbI_3$ Perovskite/Fullerene Planar-Heterojunction Hybrid Solar Cells*, Advanced Materials **25** (2013), p:3727-3732.

[80] C.-H. Chiang, Z.-L. Tseng, C.-G. Wu, *Planar heterojunction perovskite/PC71BM solar cells with enhanced open-circuit voltage via a (2/1)-step spin-coating process*, Journal of Materials Chemistry A **2** (2014), p:15897-15903.

[81] P. Docampo, J.M. Ball, M. Darwich, G.E. Eperon, H.J. Snaith, *Efficient organometal trihalide perovskite planar-heterojunction solar cells on flexible polymer substrates*, Nature Communications **4** (2013), 2761.

[82] L. Hu, J. Peng, W. Wang, Z. Xia, J. Yuan, J. Lu, X. Huang, W. Ma, H. Song, W. Chen, Y.-B. Cheng, J. Tang, *Sequential Deposition of $CH_3NH_3PbI_3$ on Planar NiO Film for Efficient Planar Perovskite Solar Cells*, ACS Photonics **1** (2014), p:547-553.

[83] J.-Y. Jeng, K.-C. Chen, T.-Y. Chiang, P.-Y. Lin, T.-D. Tsai, Y.-C. Chang, T.-F. Guo, P. Chen, T.-C. Wen, Y.-J. Hsu, *Nickel Oxide Electrode Interlayer in $CH_3NH_3PbI_3$ Perovskite/PCBM Planar-Heterojunction Hybrid Solar Cells*, Advanced Materials **26** (2014), p:4107-4113.

[84] W. Chen, Y. Wu, Y. Yue, J. Liu, W. Zhang, X. Yang, H. Chen, E. Bi, I. Ashraful, M. Grätzel, L. Han, *Efficient and stable large-area perovskite solar cells with inorganic charge extraction layers*, Science **350** (2015), p:944-948.

[85] D. Yang, T. Sano, Y. Yaguchi, H. Sun, H. Sasabe, J. Kido, *Achieving 20% Efficiency for Low-Temperature-Processed Inverted Perovskite Solar Cells*, Advanced Functional Materials **29** (2019), 1807556.

[86] F. Matebese, R. Taziwa, D. Mutukwa, *Progress on the Synthesis and Application of CuSCN Inorganic Hole Transport Material in Perovskite Solar Cells*, Materials (Basel, Switzerland) **11** (2018), 2592.

[87] S.S. Shin, E.J. Yeom, W.S. Yang, S. Hur, M.G. Kim, J. Im, J. Seo, J.H. Noh, S.I. Seok, *Colloidally prepared La-doped $BaSnO_3$ electrodes for efficient, photostable perovskite solar cells*, Science **356** (2017), p:167-171.

[88] D. Bi, C. Yi, J. Luo, J.-D. Décoppet, F. Zhang, Shaik M. Zakeeruddin, X. Li, A. Hagfeldt, M. Grätzel, *Polymer-templated nucleation and crystal growth of perovskite films for solar cells with efficiency greater than 21%*, Nature Energy **1** (2016), 16142.

[89] W.S. Yang, J.H. Noh, N.J. Jeon, Y.C. Kim, S. Ryu, J. Seo, S.I. Seok, *High-performance photovoltaic perovskite layers fabricated through intramolecular exchange*, Science **348** (2015), p:1234-1237.

[90] N.J. Jeon, J.H. Noh, Y.C. Kim, W.S. Yang, S. Ryu, S.I. Seok, *Solvent engineering for high-performance inorganic–organic hybrid perovskite solar cells*, Nature Materials **13** (2014), 897.

[91] H. Zhou, Q. Chen, G. Li, S. Luo, T.-b. Song, H.-S. Duan, Z. Hong, J. You, Y. Liu, Y. Yang, *Interface engineering of highly efficient perovskite solar cells*, Science **345** (2014), p:542-546.

[92] J. You, Y. Yang, Z. Hong, T.-B. Song, L. Meng, Y. Liu, C. Jiang, H. Zhou, W.-H. Chang, G. Li, Y. Yang, *Moisture assisted perovskite film growth for high performance solar cells*, Applied Physics Letters **105** (2014), 183902.

[93] A.M.A. Leguy, Y. Hu, M. Campoy-Quiles, M.I. Alonso, O.J. Weber, P. Azarhoosh, M. Van Schilfgaarde, M.T. Weller, T. Bein, J. Nelson, P. Docampo, P.R.F. Barnes, *Reversible hydration of $CH_3NH_3PbI_3$ in films, single crystals, and solar cells*, Chemistry of Materials **27** (2015), p:3397-3407.

[94] M. Petrović, V. Chellappan, S. Ramakrishna, Perovskites: *Solar cells & engineering applications – materials and device developments*, Solar Energy **122** (2015), p:678-699.

[95] S.N. Habisreutinger, T. Leijtens, G.E. Eperon, S.D. Stranks, R.J. Nicholas, H.J. Snaith, *Carbon Nanotube/Polymer Composites as a Highly Stable Hole Collection Layer in Perovskite Solar Cells*, Nano Letters **14** (2014), p:5561-5568.

[96] H.S. Ko, J.W. Lee, N.G. Park, *15.76% efficiency perovskite solar cells prepared under high relative humidity: Importance of PbI_2 morphology in two-step deposition of $CH_3NH_3PbI_3$*, Journal of Materials Chemistry A **3** (2015), p:8808-8815.

[97] H.M. Cronin, K.D.G.I. Jayawardena, Z. Stoeva, M. Shkunov, S.R.P. Silva, *Effects of ambient humidity on the optimum annealing time of mixed-halide Perovskite solar cells*, Nanotechnology **28** (2017), 114004.

[98] J. Troughton, K. Hooper, T.M. Watson, *Humidity resistant fabrication of CH3NH3PbI3 perovskite solar cells and modules*, Nano Energy **39** (2017), p:60-68.

[99] Y. Hou, Z.R. Zhou, T.Y. Wen, H.W. Qiao, Z.Q. Lin, B. Ge, H.G. Yang, *Enhanced moisture stability of metal halide perovskite solar cells based on sulfur–oleylamine surface modification*, Nanoscale Horizons **4** (2019), p:208-213.

[100] D. Liu, C.J. Traverse, P. Chen, M. Elinski, C. Yang, L. Wang, M. Young, R.R. Lunt, *Aqueous-Containing Precursor Solutions for Efficient Perovskite Solar Cells*, Advanced Science **5** (2018), 1700484.

[101] C.-H. Chiang, M.K. Nazeeruddin, M. Grätzel, C.-G. Wu, *The synergistic effect of H_2O and DMF towards stable and 20% efficiency inverted perovskite solar cells*, Energy & Environmental Science **10** (2017), p:808-817.

[102] C. Clegg, I.G. Hill, *Systematic study on the impact of water on the performance and stability of perovskite solar cells*, RSC Advances **6** (2016), p:52448-52458.

[103] C.-G. Wu, C.-H. Chiang, Z.-L. Tseng, M.K. Nazeeruddin, A. Hagfeldt, M. Grätzel, *High efficiency stable inverted perovskite solar cells without current hysteresis*, Energy & Environmental Science **8** (2015), p:2725-2733.

[104] X. Gong, M. Li, X.-B. Shi, H. Ma, Z.-K. Wang, L.-S. Liao, *Controllable Perovskite Crystallization by Water Additive for High-Performance Solar Cells*, Advanced Functional Materials **25** (2015), p:6671-6678.

[105] Y.S. Kwon, J. Lim, H.J. Yun, Y.H. Kim, T. Park, *A diketopyrrolopyrrole-containing hole transporting conjugated polymer for use in efficient stable*

organic-inorganic hybrid solar cells based on a perovskite, Energy and Environmental Science **7** (2014), p:1454-1460.

[106] H. Zhang, H. Wang, W. Chen, A.K.-Y. Jen, *$CuGaO_2$: A Promising Inorganic Hole-Transporting Material for Highly Efficient and Stable Perovskite Solar Cells*, Advanced Materials **29** (2017), 1604984.

[107] A. Fujishima, T.N. Rao, D.A. Tryk, *Titanium dioxide photocatalysis*, Journal of Photochemistry and Photobiology C: Photochemistry Reviews **1** (2000), p:1-21.

[108] K. Schwanitz, E. Mankel, R. Hunger, T. Mayer, W. Jaegermann, *Photoelectron spectroscopy at the solid-liquid interface of dye-sensitized solar cells: Unique experiments with the solid-liquid interface analysis system SoLiAS at BESSY*, Chimia **61** (2007), p:796-800.

[109] N. Aristidou, I. Sanchez-Molina, T. Chotchuangchutchaval, M. Brown, L. Martinez, T. Rath, S.A. Haque, *The Role of Oxygen in the Degradation of Methylammonium Lead Trihalide Perovskite Photoactive Layers*, Angewandte Chemie - International Edition **54** (2015), p:8208-8212.

[110] T.A. Berhe, W.-N. Su, C.-H. Chen, C.-J. Pan, J.-H. Cheng, H.-M. Chen, M.-C. Tsai, L.-Y. Chen, A.A. Dubale, B.-J. Hwang, *Organometal halide perovskite solar cells: degradation and stability*, Energy & Environmental Science **9** (2016), p:323-356.

[111] S. Ito, S. Tanaka, K. Manabe, H. Nishino, *Effects of surface blocking layer of Sb2S3 on nanocrystalline TiO_2 for $CH_3NH_3PbI_3$ perovskite solar cells*, Journal of Physical Chemistry C **118** (2014), p:16995-17000.

[112] N. Chander, A.F. Khan, P.S. Chandrasekhar, E. Thouti, S.K. Swami, V. Dutta, V.K. Komarala, *Reduced ultraviolet light induced degradation and enhanced light harvesting using $YVO_4:Eu^{3+}$ down-shifting nano-phosphor layer in organometal halide perovskite solar cells*, Applied Physics Letters **105** (2014), 033904.

[113] A. Bera, A.D. Sheikh, M.A. Haque, R. Bose, E. Alarousu, O.F. Mohammed, T. Wu, *Fast Crystallization and Improved Stability of Perovskite Solar Cells with Zn_2SnO4 Electron Transporting Layer: Interface Matters*, ACS Applied Materials & Interfaces **7** (2015), p:28404-28411.

[114] Y. Sun, X. Fang, Z. Ma, L. Xu, Y. Lu, Q. Yu, N. Yuan, J. Ding, *Enhanced UV-light stability of organometal halide perovskite solar cells with interface modification and a UV absorption layer*, Journal of Materials Chemistry C **5** (2017), p:8682-8687.

[115] J.H. Heo, S.H. Im, J.H. Noh, T.N. Mandal, C.S. Lim, J.A. Chang, Y.H. Lee, H.J. Kim, A. Sarkar, M.K. Nazeeruddin, M. Grätzel, S.I. Seok, *Efficient inorganic-organic hybrid heterojunction solar cells containing perovskite compound and polymeric hole conductors*, Nature Photonics **7** (2013) p:486-491.

[116] A. Dualeh, N. Tétreault, T. Moehl, P. Gao, M.K. Nazeeruddin, M. Grätzel, *Effect of annealing temperature on film morphology of organic-inorganic hybrid pervoskite solid-state solar cells*, Advanced Functional Materials **24** (2014), p:3250-3258.

[117] A. Dualeh, N. Tétreault, T. Moehl, P. Gao, M.K. Nazeeruddin, M. Grätzel, *Effect of Annealing Temperature on Film Morphology of Organic–Inorganic Hybrid Pervoskite Solid-State Solar Cells*, Advanced Functional Materials **24** (2014), p:3250-3258.

[118] K.W. Tan, D.T. Moore, M. Saliba, H. Sai, L.A. Estroff, T. Hanrath, H.J. Snaith, U. Wiesner, *Thermally induced structural evolution and performance of mesoporous block copolymer-directed alumina perovskite solar cells*, ACS Nano **8** (2014), p:4730-4739.

[119] A. Pisoni, J. Jaćimović, O.S. Barišić, M. Spina, R. Gaál, L. Forró, E. Horváth, *Ultra-low thermal conductivity in organic-inorganic hybrid perovskite $CH_3NH_3PbI_3$*, Journal of Physical Chemistry Letters **5** (2014), p:2488-2492.

[120] R.K. Misra, S. Aharon, B. Li, D. Mogilyansky, I. Visoly-Fisher, L. Etgar, E.A. Katz, Temperature- and Component-Dependent Degradation of Perovskite Photovoltaic Materials under Concentrated Sunlight, The Journal of Physical Chemistry Letters **6** (2015), p:326-330.

[121] M. Benavides-Garcia, K. Balasubramanian, *Bond energies, ionization potentials, and the singlet-triplet energy separations of $SnCl_2$, $SnBr_2$, SnI_2, $PbCl_2$, $PbBr_2$, PbI_2, and their positive ions*, The Journal of Chemical Physics **100** (1994), p:2821-2830.

[122] G.E. Eperon, S.D. Stranks, C. Menelaou, M.B. Johnston, L.M. Herz, H.J. Snaith, *Formamidinium lead trihalide: A broadly tunable perovskite for efficient planar heterojunction solar cells*, Energy and Environmental Science **7** (2014), p:982-988.

[123] S. Aharon, A. Dymshits, A. Rotem, L. Etgar, *Temperature dependence of hole conductor free formamidinium lead iodide perovskite based solar cells*, Journal of Materials Chemistry A **3** (2015), p:9171-9178.

[124] N. Pellet, P. Gao, G. Gregori, T.-Y. Yang, M.K. Nazeeruddin, J. Maier, M. Grätzel, *Mixed-Organic-Cation Perovskite Photovoltaics for Enhanced Solar-Light Harvesting*, Angewandte Chemie International Edition **53** (2014), p:3151-3157.

[125] N.J. Jeon, J.H. Noh, W.S. Yang, Y.C. Kim, S. Ryu, J. Seo, S.I. Seok, *Compositional engineering of perovskite materials for high-performance solar cells*, Nature **517** (2015), 476.

[126] M. Saliba, T. Matsui, J.-Y. Seo, K. Domanski, J.-P. Correa-Baena, M.K. Nazeeruddin, S.M. Zakeeruddin, W. Tress, A. Abate, A. Hagfeldt, M. Gratzel, *Cesium-containing triple cation perovskite solar cells: improved stability, reproducibility and high efficiency*, Energy & Environmental Science **9** (2016), p:1989-1997.

[127] R. Wang, J. Xue, L. Meng, J.-W. Lee, Z. Zhao, P. Sun, L. Cai, T. Huang, Z. Wang, Z.-K. Wang, Y. Duan, J.L. Yang, S. Tan, Y. Yuan, Y. Huang, Y. Yang, *Caffeine Improves the Performance and Thermal Stability of Perovskite Solar Cells*, Joule **6** (2019), p:1464-1477.

[128] T. Malinauskas, D. Tomkute-Luksiene, R. Sens, M. Daskeviciene, R. Send, H. Wonneberger, V. Jankauskas, I. Bruder, V. Getautis, *Enhancing Thermal Stability and Lifetime of Solid-State Dye-Sensitized Solar Cells via Molecular Engineering of the Hole-Transporting Material Spiro-OMeTAD*, ACS Applied Materials & Interfaces **7** (2015), p:11107-11116.

[129] H. Zheng, G. Liu, C. Zhang, L. Zhu, A. Alsaedi, T. Hayat, X. Pan, S. Dai, *The influence of perovskite layer and hole transport material on the temperature stability about perovskite solar cells*, Solar Energy **159** (2018), p:914-919.

[130] A. Magomedov, E. Kasparavičius, K. Rakstys, S. Paek, N. Gasilova, K. Genevičius, G. Juška, T. Malinauskas, M.K. Nazeeruddin, V. Getautis, *Pyridination of hole transporting material in perovskite solar cells questions the long-term stabilit*y, Journal of Materials Chemistry C **6** (2018), p:8874-8878.

[131] E. Kasparavicius, A. Magomedov, T. Malinauskas, V. Getautis, *Long-Term Stability of the Oxidized Hole-Transporting Materials used in Perovskite Solar Cells*, Chemistry – A European Journal **24** (2018), p:9910-9918.

[132] K. Domanski, J.-P. Correa-Baena, N. Mine, M.K. Nazeeruddin, A. Abate, M. Saliba, W. Tress, A. Hagfeldt, M. Grätzel, *Not All That Glitters Is Gold: Metal-Migration-Induced Degradation in Perovskite Solar Cells*, ACS Nano **10** (2016), p:6306-6314.

[133] Y. Zhang, W. Liu, F. Tan, Y. Gu, *The essential role of the poly(3-hexylthiophene) hole transport layer in perovskite solar cells*, Journal of Power Sources **274** (2015), p:1224-1230.

[134] S. Ye, W. Sun, Y. Li, W. Yan, H. Peng, Z. Bian, Z. Liu, C. Huang, *CuSCN-Based Inverted Planar Perovskite Solar Cell with an Average PCE of 15.6%*, Nano Letters **15** (2015), p:3723-3728.

[135] J. Liu, Y. Wu, C. Qin, X. Yang, T. Yasuda, A. Islam, K. Zhang, W. Peng, W. Chen, L. Han, *A dopant-free hole-transporting material for efficient and stable perovskite solar cells*, Energy and Environmental Science **7** (2014), p:2963-2967.

[136] Y. Du, H. Cai, J. Ni, J. Li, H. Yu, X. Sun, Y. Wu, H. Wen, J. Zhang, *Air-processed, efficient $CH_3NH_3PbI_{3-x}Cl_x$ perovskite solar cells with organic polymer PTB7 as a hole-transport layer*, RSC Advances **5** (2015), p:66981-66987.

[137] M. Saliba, S. Orlandi, T. Matsui, S. Aghazada, M. Cavazzini, J.-P. Correa-Baena, P. Gao, R. Scopelliti, E. Mosconi, K.-H. Dahmen, F. De Angelis, A. Abate, A. Hagfeldt, G. Pozzi, M. Graetzel, M.K. Nazeeruddin, *A molecularly engineered hole-transporting material for efficient perovskite solar cells*, Nature Energy **1** (2016), 15017.

[138] N. Arora, M.I. Dar, A. Hinderhofer, N. Pellet, F. Schreiber, S.M. Zakeeruddin, M. Grätzel, *Perovskite solar cells with CuSCN hole*

extraction layers yield stabilized efficiencies greater than 20%, Science **358** (2017), p:768-771.

[139] T. Duong, J. Peng, D. Walter, J. Xiang, H. Shen, D. Chugh, M. Lockrey, D. Zhong, J. Li, K. Weber, T.P. White, K.R. Catchpole, *Perovskite Solar Cells Employing Copper Phthalocyanine Hole-Transport Material with an Efficiency over 20% and Excellent Thermal Stability*, ACS Energy Letters **3** (2018), p:2441-2448.

[140] X. Li, M. Tschumi, H. Han, S.S. Babkair, R.A. Alzubaydi, A.A. Ansari, S.S. Habib, M.K. Nazeeruddin, S.M. Zakeeruddin, M. Grätzel, *Outdoor Performance and Stability under Elevated Temperatures and Long-Term Light Soaking of Triple-Layer Mesoporous Perovskite Photovoltaics*, Energy Technology **3** (2015), p:551-555.

[141] B. Conings, L. Baeten, C. De Dobbelaere, J. D'Haen, J. Manca, H.G. Boyen, *Perovskite-based hybrid solar cells exceeding 10% efficiency with high reproducibility using a thin film sandwich approach*, Advanced Materials **26** (2014), p:2041-2046.

[142] H.J. Snaith, A. Abate, J.M. Ball, G.E. Eperon, T. Leijtens, N.K. Noel, S.D. Stranks, J.T.W. Wang, K. Wojciechowski, W. Zhang, *Anomalous hysteresis in perovskite solar cells*, Journal of Physical Chemistry Letters **5** (2014), p:1511-1515.

[143] Y.-J. Jeon, S. Lee, R. Kang, J.-E. Kim, J.-S. Yeo, S.-H. Lee, S.-S. Kim, J.-M. Yun, D.-Y. Kim, *Planar heterojunction perovskite solar cells with superior reproducibility*, Scientific Reports **4** (2014), 6953.

[144] S. Bae, S.J. Han, T.J. Shin, W.H. Jo, *Two different mechanisms of $CH_3NH_3PbI_3$ film formation in one-step deposition and its effect on photovoltaic properties of OPV-type perovskite solar cells*, Journal of Materials Chemistry A **3** (2015), p:23964-23972.

[145] Y. Wu, A. Islam, X. Yang, C. Qin, J. Liu, K. Zhang, W. Peng, L. Han, *Retarding the crystallization of PbI_2 for highly reproducible planar-structured perovskite solar cells via sequential deposition*, Energy & Environmental Science **7** (2014), p:2934-2938.

[146] N.J. Jeon, J.H. Noh, Y.C. Kim, W.S. Yang, S. Ryu, S.I. Seok, *Solvent engineering for high-performance inorganic–organic hybrid perovskite solar cells*, Nat Mater **13** (2014), p:897-903.

[147] C.-C. Chung, C.S. Lee, E. Jokar, J.H. Kim, E.W.-G. Diau, *Well-Organized Mesoporous TiO_2 Photoanode by Using Amphiphilic Graft Copolymer for Efficient Perovskite Solar Cells*, The Journal of Physical Chemistry C **120** (2016), p:9619-9627.

[148] Y. Zhao, K. Zhu, Three-step sequential solution deposition of PbI_2-free $CH_3NH_3PbI_3$ perovskite, Journal of Materials Chemistry A **3** (2015), p:9086-9091.

[149] Z. Xiao, C. Bi, Y. Shao, Q. Dong, Q. Wang, Y. Yuan, C. Wang, Y. Gao, J. Huang, *Efficient, high yield perovskite photovoltaic devices grown by interdiffusion of solution-processed precursor stacking layers*, Energy & Environmental Science **7** (2014), p:2619-2623.

[150] X. Li, D. Bi, C. Yi, J.-D. Décoppet, J. Luo, S.M. Zakeeruddin, A. Hagfeldt, M. Grätzel, *A vacuum flash–assisted solution process for high-efficiency large-area perovskite solar cells*, Science **353** (2016), p:58-62.

[151] L. Chen, H. Cao, S. Wang, Y. Luo, T. Tao, J. Sun, M. Zhang, *Efficient air-stable perovskite solar cells with a $(FAI)_{0.46}(MAI)_{0.40}(MABr)_{0.14}(PbI_2)_{0.86}(PbBr_2)_{0.14}$ active layer fabricated via a vacuum flash-assisted method under RH > 50%*, RSC Advances **9** (2019), p:10148-10154.

[152] E. Zimmermann, K.K. Wong, M. Müller, H. Hu, P. Ehrenreich, M. Kohlstädt, U. Würfel, S. Mastroianni, G. Mathiazhagan, A. Hinsch, T.P. Gujar, M. Thelakkat, T. Pfadler, L. Schmidt-Mende, *Characterization of perovskite solar cells: Towards a reliable measurement protocol*, APL Materials **4** (2016), 091901.

[153] N. Pellet, F. Giordano, M. Ibrahim Dar, G. Gregori, S.M. Zakeeruddin, J. Maier, M. Grätzel, *Hill climbing hysteresis of perovskite-based solar cells: a maximum power point tracking investigation*, Progress in Photovoltaics: Research and Applications **25** (2017), p:942-950.

[154] N.J. Jeon, H. Na, E.H. Jung, T.-Y. Yang, Y.G. Lee, G. Kim, H.-W. Shin, S. Il Seok, J. Lee, J. Seo, *A fluorene-terminated hole-transporting material*

for highly efficient and stable perovskite solar cells, Nature Energy **3** (2018), p:682-689.

[155] X. Zhu, D. Yang, R. Yang, B. Yang, Z. Yang, X. Ren, J. Zhang, J. Niu, J. Feng, S. Liu, *Superior stability for perovskite solar cells with 20% efficiency using vacuum co-evaporation*, Nanoscale **9** (2017), p:12316-12323.

[156] Q. Lin, A. Armin, R.C.R. Nagiri, P.L. Burn, P. Meredith, *Electro-optics of perovskite solar cells*, Nat Photon **9** (2015), p:106-112.

[157] M.-H. Li, H.-H. Yeh, Y.-H. Chiang, U.-S. Jeng, C.-J. Su, H.-W. Shiu, Y.-J. Hsu, N. Kosugi, T. Ohigashi, Y.-A. Chen, P.-S. Shen, P. Chen, T.-F. Guo, *Highly Efficient 2D/3D Hybrid Perovskite Solar Cells via Low-Pressure Vapor-Assisted Solution Process*, Advanced Materials **30** (2018), 1801401.

[158] A.T. Barrows, A.J. Pearson, C.K. Kwak, A.D.F. Dunbar, A.R. Buckley, D.G. Lidzey, *Efficient planar heterojunction mixed-halide perovskite solar cells deposited via spray-deposition*, Energy & Environmental Science **7** (2014), p:2944-2950.

[159] X. Xia, H. Li, W. Wu, Y. Li, D. Fei, C. Gao, X. Liu, *Efficient Light Harvester Layer Prepared by Solid/Mist Interface Reaction for Perovskite Solar Cells*, ACS Applied Materials & Interfaces **7** (2015), p:16907-16912.

[160] J.H. Heo, M.H. Lee, M.H. Jang, S.H. Im, *Highly efficient $CH_3NH_3PbI_{3-x}Cl_x$ mixed halide perovskite solar cells prepared by re-dissolution and crystal grain growth via spray coating*, Journal of Materials Chemistry A **4** (2016), p:17636-17642.

[161] M. Jung, S.-G. Ji, G. Kim, S.I. Seok, *Perovskite precursor solution chemistry: from fundamentals to photovoltaic applications*, Chemical Society Reviews **48** (2019), p:2011-2038.

[162] J.B. Whitaker, D.H. Kim, Bryon W. Larson, F. Zhang, J.J. Berry, M.F.A.M. van Hest, K. Zhu, *Scalable slot-die coating of high performance perovskite solar cells*, Sustainable Energy & Fuels **2** (2018), p:2442-2449.

[163] S. Razza, F. Di Giacomo, F. Matteocci, L. Cinà, A.L. Palma, S. Casaluci, P. Cameron, A. D'Epifanio, S. Licoccia, A. Reale, T.M. Brown, A. Di

Carlo, *Perovskite solar cells and large area modules (100 cm^2) based on an air flow-assisted PbI_2 blade coating deposition process*, Journal of Power Sources **277** (2015), p:286-291.

[164] W.-Q. Wu, Q. Wang, Y. Fang, Y. Shao, S. Tang, Y. Deng, H. Lu, Y. Liu, T. Li, Z. Yang, A. Gruverman, J. Huang, *Molecular doping enabled scalable blading of efficient hole-transport-layer-free perovskite solar cells*, Nature Communications **9** (2018), 1625.

[165] Y. Deng, X. Zheng, Y. Bai, Q. Wang, J. Zhao, J. Huang, *Surfactant-controlled ink drying enables high-speed deposition of perovskite films for efficient photovoltaic modules*, Nature Energy **3** (2018), p:560-566.

[166] I.A. Howard, T. Abzieher, I.M. Hossain, H. Eggers, F. Schackmar, S. Ternes, B.S. Richards, U. Lemmer, U.W. Paetzold, *Coated and Printed Perovskites for Photovoltaic Applications*, Advanced Materials, 1806702.

[167] T. Abzieher, S. Moghadamzadeh, F. Schackmar, H. Eggers, F. Sutterlüti, A. Farooq, D. Kojda, K. Habicht, R. Schmager, A. Mertens, R. Azmi, L. Klohr, J.A. Schwenzer, M. Hetterich, U. Lemmer, B.S. Richards, M. Powalla, U.W. Paetzold, *Electron-Beam-Evaporated Nickel Oxide Hole Transport Layers for Perovskite-Based Photovoltaics*, Advanced Energy Materials **9** (2019), 1802995.

[168] P. Li, C. Liang, B. Bao, Y. Li, X. Hu, Y. Wang, Y. Zhang, F. Li, G. Shao, Y. Song, *Inkjet manipulated homogeneous large size perovskite grains for efficient and large-area perovskite solar cells*, Nano Energy **46** (2018), p:203-211.

[169] T.M. Schmidt, T.T. Larsen-Olsen, J.E. Carlé, D. Angmo, F.C. Krebs, *Upscaling of Perovskite Solar Cells: Fully Ambient Roll Processing of Flexible Perovskite Solar Cells with Printed Back Electrodes*, Advanced Energy Materials **5** (2015), 1500569.

[170] PV-Magazine, *Solliance achieves 14.5% cell efficiency on perovskite module*, https://www.pv-magazine.com/2018/04/09/solliance-achieves-14-5-cell-efficiency-on-perovskite-module/, May 2019.

[171] W. Tress, N. Marinova, T. Moehl, S.M. Zakeeruddin, M.K. Nazeeruddin, M. Gratzel, *Understanding the rate-dependent J-V hysteresis, slow time component, and aging in $CH_3NH_3PbI_3$ perovskite solar cells: the role of*

a compensated electric field, Energy & Environmental Science **8** (2015) p:995-1004.

[172] A. Dualeh, T. Moehl, N. Tétreault, J. Teuscher, P. Gao, M.K. Nazeeruddin, M. Grätzel, I*mpedance spectroscopic analysis of lead iodide perovskite-sensitized solid-state solar cells*, ACS Nano **8** (2014), p:362-373.

[173] Y. Shao, Z. Xiao, C. Bi, Y. Yuan, J. Huang, *Origin and elimination of photocurrent hysteresis by fullerene passivation in $CH_3NH_3PbI_3$ planar heterojunction solar cells*, Nature Communications **5** (2014), 5784.

[174] J. Xu, A. Buin, A.H. Ip, W. Li, O. Voznyy, R. Comin, M. Yuan, S. Jeon, Z. Ning, J.J. McDowell, P. Kanjanaboos, J.-P. Sun, X. Lan, L.N. Quan, D.H. Kim, I.G. Hill, P. Maksymovych, E.H. Sargent, *Perovskite–fullerene hybrid materials suppress hysteresis in planar diodes*, Nature Communications **6** (2015), 7081.

[175] J. Wei, Y. Zhao, H. Li, G. Li, J. Pan, D. Xu, Q. Zhao, D. Yu, *Hysteresis Analysis Based on the Ferroelectric Effect in Hybrid Perovskite Solar Cells*, The Journal of Physical Chemistry Letters **5** (2014), p:3937-3945.

[176] J.M. Frost, K.T. Butler, A. Walsh, *Molecular ferroelectric contributions to anomalous hysteresis in hybrid perovskite solar cells*, APL Materials **2** (2014), 081506.

[177] S. van Reenen, M. Kemerink, H.J. Snaith, *Modeling Anomalous Hysteresis in Perovskite Solar Cells*, The Journal of Physical Chemistry Letters **6** (2015), p:3808-3814.

[178] S. Meloni, T. Moehl, W. Tress, M. Franckevicius, M. Saliba, Y.H. Lee, P. Gao, M.K. Nazeeruddin, S.M. Zakeeruddin, U. Rothlisberger, M. Graetzel, *Ionic polarization-induced current-voltage hysteresis in $CH_3NH_3PbX_3$ perovskite solar cells*, Nat Commun **7** (2016), 10334.

[179] Y. Zhao, C. Liang, H. Zhang, D. Li, D. Tian, G. Li, X. Jing, W. Zhang, W. Xiao, Q. Liu, F. Zhang, Z. He, *Anomalously large interface charge in polarity-switchable photovoltaic devices: an indication of mobile ions in organic-inorganic halide perovskites*, Energy & Environmental Science **8** (2015), p:1256-1260.

[180] T. Zhang, H. Chen, Y. Bai, S. Xiao, L. Zhu, C. Hu, Q. Xue, S. Yang, *Understanding the relationship between ion migration and the*

anomalous hysteresis in high-efficiency perovskite solar cells: A fresh perspective from halide substitution, Nano Energy **26** (2016), p:620-630.

[181] W. Tress, J.P. Correa Baena, M. Saliba, A. Abate, M. Graetzel, *Inverted Current–Voltage Hysteresis in Mixed Perovskite Solar Cells: Polarization, Energy Barriers, and Defect Recombination*, Advanced Energy Materials **6** (2016), 1600396.

[182] K. Domanski, B. Roose, T. Matsui, M. Saliba, S.-H. Turren-Cruz, J.-P. Correa-Baena, C. Roldan Carmona, G. Richardson, J. Foster, F. De Angelis, J. Ball, a. petrozza, N. Mine, M.K. Nazeeruddin, W. Tress, M. Gratzel, U. Steiner, A. Hagfeldt, A. Abate, *Migration of cations induces reversible performance losses over day/night cycling in perovskite solar cells*, Energy & Environmental Science **10** (2017), p:604-613.

[183] H. Yoon, S.M. Kang, J.-K. Lee, M. Choi, *Hysteresis-free low-temperature-processed planar perovskite solar cells with 19.1% efficiency*, Energy & Environmental Science **9** (2016), p:2262-2266.

[184] D. Gedamu, I.M. Asuo, D. Benetti, M. Basti, I. Ka, S.G. Cloutier, F. Rosei, R. Nechache, *Solvent-Antisolvent Ambient Processed Large Grain Size Perovskite Thin Films for High-Performance Solar Cells*, Scientific Reports **8** (2018), 12885.

[185] C. Li, A. Guerrero, Y. Zhong, S. Huettner, *Origins and mechanisms of hysteresis in organometal halide perovskites*, Journal of Physics: Condensed Matter **29** (2017), 193001.

[186] B. Hailegnaw, S. Kirmayer, E. Edri, G. Hodes, D. Cahen, *Rain on Methylammonium Lead Iodide Based Perovskites: Possible Environmental Effects of Perovskite Solar Cells*, The Journal of Physical Chemistry Letters **6** (2015), p:1543-1547.

[187] F. Zuo, S.T. Williams, P.-W. Liang, C.-C. Chueh, C.-Y. Liao, A.K.Y. Jen, *Binary-Metal Perovskites Toward High-Performance Planar-Heterojunction Hybrid Solar Cells*, Advanced Materials **26** (2014), p:6454-6460.

[188] F. Hao, C.C. Stoumpos, R.P.H. Chang, M.G. Kanatzidis, *Anomalous Band Gap Behavior in Mixed Sn and Pb Perovskites Enables Broadening of*

Absorption Spectrum in Solar Cells, Journal of the American Chemical Society **136** (2014), p:8094-8099.

[189] Y. Ogomi, A. Morita, S. Tsukamoto, T. Saitho, N. Fujikawa, Q. Shen, T. Toyoda, K. Yoshino, S.S. Pandey, T. Ma, S. Hayase, *$CH_3NH_3Sn_xPb_{(1-x)}I_3$ Perovskite Solar Cells Covering up to 1060 nm*, The Journal of Physical Chemistry Letters **5** (2014), p:1004-1011.

[190] F. Hao, C.C. Stoumpos, P. Guo, N. Zhou, T.J. Marks, R.P.H. Chang, M.G. Kanatzidis, *Solvent-Mediated Crystallization of $CH_3NH_3SnI_3$ Films for Heterojunction Depleted Perovskite Solar Cells*, Journal of the American Chemical Society **137** (2015), p:11445-11452.

[191] N.K. Noel, S.D. Stranks, A. Abate, C. Wehrenfennig, S. Guarnera, A.A. Haghighirad, A. Sadhanala, G.E. Eperon, S.K. Pathak, M.B. Johnston, A. Petrozza, L.M. Herz, H.J. Snaith, *Lead-free organic-inorganic tin halide perovskites for photovoltaic applications*, Energy and Environmental Science **7** (2014), p:3061-3068.

[192] F. Hao, C.C. Stoumpos, D.H. Cao, R.P.H. Chang, M.G. Kanatzidis, *Lead-free solid-state organic-inorganic halide perovskite solar cells*, Nat Photon **8** (2014), p:489-494.

[193] S. Shao, J. Liu, G. Portale, H.-H. Fang, G.R. Blake, G.H. ten Brink, L.J.A. Koster, M.A. Loi, *Highly Reproducible Sn-Based Hybrid Perovskite Solar Cells with 9% Efficiency*, Advanced Energy Materials **8** (2018), 1702019.

[194] M. Lyu, J.-H. Yun, M. Cai, Y. Jiao, P.V. Bernhardt, M. Zhang, Q. Wang, A. Du, H. Wang, G. Liu, L. Wang, *Organic–inorganic bismuth (III)-based material: A lead-free, air-stable and solution-processable light-absorber beyond organolead perovskites*, Nano Research 9 (2016), p:1-11.

[195] C. Hrizi, N. Chaari, Y. Abid, N. Chniba-Boudjada, S. Chaabouni, *Structural characterization, vibrational and optical properties of a novel one-dimensional organic–inorganic hybrid based-iodobismuthate(III) material, $[C_{10}H_7NH_3]BiI_4$*, Polyhedron **46** (2012), p:41-46.

[196] D.B. Mitzi, P. Brock, *Structure and Optical Properties of Several Organic−Inorganic Hybrids Containing Corner-Sharing Chains of Bismuth Iodide Octahedra*, Inorganic Chemistry **40** (2001), p:2096-2104.

[197] Y. Kim, Z. Yang, A. Jain, O. Voznyy, G.-H. Kim, M. Liu, L.N. Quan, F.P. García de Arquer, R. Comin, J.Z. Fan, E.H. Sargent, *Pure Cubic-Phase Hybrid Iodobismuthates $AgBi_2I_7$ for Thin-Film Photovoltaics*, Angewandte Chemie International Edition **55** (2016), p:9586-9590.

[198] S.M. Jain, D. Phuyal, M.L. Davies, M. Li, B. Philippe, C. De Castro, Z. Qiu, J. Kim, T. Watson, W.C. Tsoi, O. Karis, H. Rensmo, G. Boschloo, T. Edvinsson, J.R. Durrant, *An effective approach of vapour assisted morphological tailoring for reducing metal defect sites in lead-free, $(CH_3NH_3)_3Bi_2I_9$ bismuth-based perovskite solar cells for improved performance and long-term stability*, Nano Energy **49** (2018), p:614-624.

[199] D. Prochowicz, M. Franckevicius, A.M. Cieslak, S.M. Zakeeruddin, M. Gratzel, J. Lewinski, *Mechanosynthesis of the hybrid perovskite $CH_3NH_3PbI_3$: characterization and the corresponding solar cell efficiency*, Journal of Materials Chemistry A **3** (2015), p:20772-20777.

[200] London Metal Exchange, Available from: http://www.lme.com/, January, 2017.

[201] E.T. R.L.Moss, H.Kara, P.Willis and J.Kooroshy, *Critical Metals in Strategic Energy Technologies: Assessing Rare Metals as SupplyChain Bottlenecks in Low-Carbon Energy Technologies,* European Comition, Luxembourg, 2011.

[202] E.S. van der Voet, Reijo ; Eckelman, Matthew ; Norgate, Terry ; Mudd, Gavin ; Hisschier, Roland ; Spijker, Job ; Vijver, Martina ; Selinus, Olle ; Posthuma, Leo ; de Zwart, Dick ; van de Meent, Dik; Reuter, Markus ; Tikana, Ladji ; Valdivia, Sonia ; Wäger, Patrick ; Hauschild, Michael Zwicky; de Koning, Arjan, *Environmental challenges of anthropogenic metals flows and cycles*, United Nations Environment Programme, 2013.

[203] J.A. Christians, J.S. Manser, P.V. Kamat, *Best Practices in Perovskite Solar Cell Efficiency Measurements. Avoiding the Error of Making Bad Cells Look Good*, The Journal of Physical Chemistry Letters **6** (2015), p:852-857.

[204] E.L. Unger, E.T. Hoke, C.D. Bailie, W.H. Nguyen, A.R. Bowring, T. Heumuller, M.G. Christoforo, M.D. McGehee, *Hysteresis and transient*

behavior in current-voltage measurements of hybrid-perovskite absorber solar cells, Energy & Environmental Science **7** (2014), p:3690-3698.

[205] F.J. Ramos, D. Cortes, A. Aguirre, F.J. Castano, S. Ahmad, *Fabrication and encapsulation of perovskites sensitized solid state solar cells*, 2014 IEEE 40th Photovoltaic Specialist Conference, PVSC 2014, p:2584-2587.

[206] F. Matteocci, L. Cinà, E. Lamanna, S. Cacovich, G. Divitini, P.A. Midgley, C. Ducati, A. Di Carlo, *Encapsulation for long-term stability enhancement of perovskite solar cells*, Nano Energy **30** (2016), p:162-172.

[207] H.C. Weerasinghe, Y. Dkhissi, A.D. Scully, R.A. Caruso, Y.-B. Cheng, *Encapsulation for improving the lifetime of flexible perovskite solar cells*, Nano Energy **18** (2015), p:118-125.

[208] Y. Shao, Q. Wang, Q. Dong, Y. Yuan, J. Huang, *Vacuum-free laminated top electrode with conductive tapes for scalable manufacturing of efficient perovskite solar cells*, Nano Energy **16** (2015), p:47-53.

[209] F. Ribeiro, J. MaçAira, R. Cruz, J. Gabriel, L. Andrade, A. Mendes, *Laser assisted glass frit sealing of dye-sensitized solar cells*, Solar Energy Materials and Solar Cells **96** (2012), p:43-49.

[210] J. Maçaira, L. Andrade, A. Mendes, *Laser sealed dye-sensitized solar cells: Efficiency and long term stability*, Solar Energy Materials and Solar Cells **157** (2016), p:134-138.

[211] F. Ribeiro, J. Maçaira, I. Mesquita, J. Gabriel, L. Andrade, A. Mendes, *Laser assisted dye-sensitized solar cell sealing: From small to large cells areas*, Journal of Renewable and Sustainable Energy **6** (2014), 011208.

[212] S. Emami, J. Martins, L. Andrade, J. Mendes, A. Mendes, *Low temperature hermetic laser-assisted glass frit encapsulation of soda-lime glass substrates*, Optics and Lasers in Engineering **96** (2017), p:107-116.

[213] S. Emami, J. Martins, R. Madureira, D. Hernandez, G. Bernardo, J. Mendes, A. Mendes, *Development of hermetic glass frit encapsulation for perovskite solar cells*, Journal of Physics D: Applied Physics **52** (2018), 074005.

CHAPTER 2

INSIGHTS IN PEROVSKITE SOLAR CELL FABRICATION: UNRAVELLING THE HIDDEN CHALLENGES OF EACH LAYER

Adapted from the peer-reviewed article

Stockhausen, V., Mesquita, I., Andrade, L., Mendes, A., *Insights in Perovskite Solar Cell Fabrication: Unraveling the Hidden Challenges of Each Layer*, IEEE Journal of Photovoltaics **8** (2018), p:1029-1038.

In this work I. Mesquita performed the following studies: carrier gas effect in the blocking layer deposition, presence of humidity and oxygen during the perovskite layer, gold deposition technique and stability of different hole extraction materials. I. Mesquita also contributed to the writing and submission of the paper. This work followed the preparation procedures implemented by I. Mesquita, for the first time, in the host-laboratory.

2

INSIGHTS IN PEROVSKITE SOLAR CELL FABRICATION: UNRAVELLING THE HIDDEN CHALLENGES OF EACH LAYER

Abstract

Perovskite solar cells (PSC) are undoubtedly the most active research area in photovoltaics at this moment. Actually, since 2009 this emerging technology passed from 3.8 % to the present > 25 % of energy conversion efficiency. Along with that, a huge amount of sometimes contradicting and incomplete information about how to prepare and characterise PSC is provided, which makes it difficult to not get lost. This chapter aims to give orientation for PSC fabrication protocols that are quickly implementable and that lead to reliable and moderate efficiencies. Therefore, a step-by-step analysis of each layer is provided and, within this scope, several fabrication techniques are compared in terms of efficiency optimization. Furthermore, a new and versatile alternative to laser-assisted scribing for substrate patterning is presented. Electrochemical characterisation of dummy cells as an easy and versatile tool for blocking layer characterisation is demonstrated for TiO_2 layers. After optimization of each layer, PSCs with an average efficiency of (14.8 ± 1.0) % was obtained.

2.1 Introduction

In only few years, perovskite solar cells (PSCs) have emerged as a new member of the 3rd generation family of photovoltaic devices presenting a surprising power conversion efficiency (PCE) evolution from 3.8 % in 2009 to 25.2 % in 2019.[1] This type of solar cells is a very promising alternative to conventional photovoltaic panels of silicon or GaAs, that use harmful chemicals and complex purification processes,[2] due to their exceptional optoelectronic properties. Although the astonishing PCE evolution, these devices still present some practical drawbacks in terms of stability to the most common environmental factors like UV light, oxygen, moisture and temperature. Attempting to address high efficiencies and stabilities a huge variety of chemical formulations and device architectures has been published. It includes planar devices[3] using an inverted p-i-n architecture[4] and PSC employing a mesoporous structure that can either actively participate in the electron transfer[5] (active mesoporous layer) or merely serve as scaffold structure[6] (passive mesoporous layer). Within perovskites, chemical engineering has originated a huge quantity of complex perovskite compositions, mixing multiple cations, anions and metals.[7,8,9,10] Many scientific groups have been deciding to direct research efforts in scope of new high efficient and stable materials, however some reported protocols, showing outstanding results, are hard to reproduce, even for very experienced groups in the area. The unmentioned technical details and the barely explained procedures are the biggest lacks, that slows down the progress and may lead to contradictory results between groups. Thus, small fabrication errors within each layer of the PSCs will sum up and lead to an overall efficiency drop.

In this chapter, it is presented a comprehensive protocol that yield reproducible ~15 % PSCs for the mesoporous single-junction architecture, the most used among the scientific community. We also focus our efforts to present a step-by-step analysis of the technical problems of each layer of a PSC; and a possible impact of their modification on the device performance was assessed. In the end, the characterisation of the entire device was discussed. The understanding of the operation and preparation of this type of

solar cells due in large part to the past work done in dye-sensitized solar cells.[11,12,13]

2.2 Materials and Methods

Figure 2.1 shows a schematic representation of a mesoporous conductive semiconductor PSC. On top of a transparent conductive oxide (TCO) substrate that was scribed in order to divide photo from counter-electrode (grey line), a dense TiO_2 layer is deposited, followed by a mesoporous layer. The adjacent perovskite layer partially infiltrates into the mesoporous structure and forms a capping layer. It is followed by a hole extraction layer; finally, a nanometric metallic layer serves as current collector.

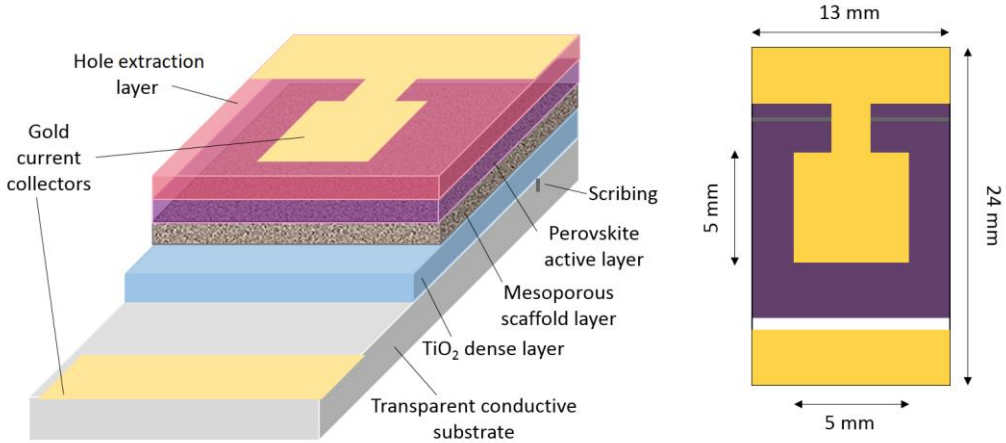

Figure 2.1. Schematic representation of a mesoporous conductive semiconductor PSC in cross-section (left) and top-view (right).

In the following, layer fabrication details and, when applicable, alternative fabrication methods are presented. Furthermore, it will be discussed what equipment is required for device fabrication and which equipment acquisition can be postponed thanks to alternative fabrication protocols.

2.2.1 Substrate preparation

Fluoride-doped tin oxide (FTO) substrates (2.2 mm thickness, TEC7, Solaronix) were patterned via VersaLaser (VLS 2.30, Universal Laser Systems, USA) to create two separate charge collection areas on the FTO substrate - method (A). As an alternative to laser scribing, which requires the availability of such an equipment, an electrochemical reductive treatment can be performed to remove selectively the conductive layer - method (B). Keep into consideration that the chemicals used for that purpose are highly corrosive, which requires adequate protection and care. In order to do so, the substrate area for TCO removal was delimited by Kapton® tape and exposed to a 3 M HCl solution. A constant potential of -2.4 V was applied until cathodic current decrease started to flatten. Meanwhile, the tin oxide of the FTO turned grey and started to peel off; samples were removed from the solution and rinsed with water. With a cotton swab dipped in a diluted nitric acid solution (0.5 M), remaining tin residues were cleaned off. Then, Kapton® tape was removed and samples were abundantly rinsed with water.

In a next step, samples were mechanically cleaned, using a toothbrush and a 10 % Hellmanex III solution (Hellma GmbH, Germany). Subsequently, substrates were abundantly rinsed with water and sonicated in ethanolic KOH solution for 5 minutes. The substrates were again abundantly rinsed with water and sonicated in water for 5 minutes, before being rinsed with acetone and dried in nitrogen flux. Prior to blocking layer deposition, substrates were additionally cleaned during 20 minutes by an ozone cleaner (UVO-Cleaner, Jelight Company Inc., USA). Alternatively to an ozone cleaner, plasma treatment can be applied,[14] among other efficient methods.

2.2.2 Electron Blocking and Mesoporous Layer preparation

TiO_2 blocking layer was deposited by two different methods. Method (A) was done by spin-coating of a commercial solution (Ti-Nanoxide BL/SC, Solaronix, Switzerland) (5000 rpm, 30 s, 2000 rpm·s^{-1}). Before film deposition, the area of photoanode contact was protected by adhesive tape (Scotch® Magic™ Tape,

3M) - Figure 2.2a - and the films were subsequently calcined at 550 °C during 1 h, under application of a stepwise temperature increase of 100 °C each 10 minutes. Method (B) employed spray pyrolysis of a precursor solution containing 0.56 M acetylacetone (Sigma-Aldrich, 99.6 %) and 0.18 M titanium diisopropoxide bis(acetylacetonate) (Sigma-Aldrich, 75 wt.% in isopropanol) in 7 mL 2-propanol (Sigma-Aldrich, anhydrous, 99.5 %) that was sufficient for 64 samples. Here, substrates were pre-heated at 450 °C and the photoanode area was protected with a glass stripe - Figure 2.2b - before applying the spray via an atomizer, using either air or oxygen as carrier gas - Figure 2.2c. Afterwards, samples were left for more 45 minutes at that temperature. For application of mesoporous TiO_2, a commercial paste (generally 30-NR-D, Dyesol, Australia, unless otherwise stated) was diluted in pure ethanol (1:6 w/w) and applied on the substrates via spin-coating (5000 rpm, 10 s, 2000 rpm·s^{-1}). Prior to deposition, photoanode contact had been protected with adhesive tape. Samples were then immediately transferred to a hot plate at 100 °C for pre-drying before being calcined in an oven at 500 °C during 30 min. Subsequently, samples were transferred to oxygen-free and dry conditions (glove box) before allowing to cool below 100 °C.

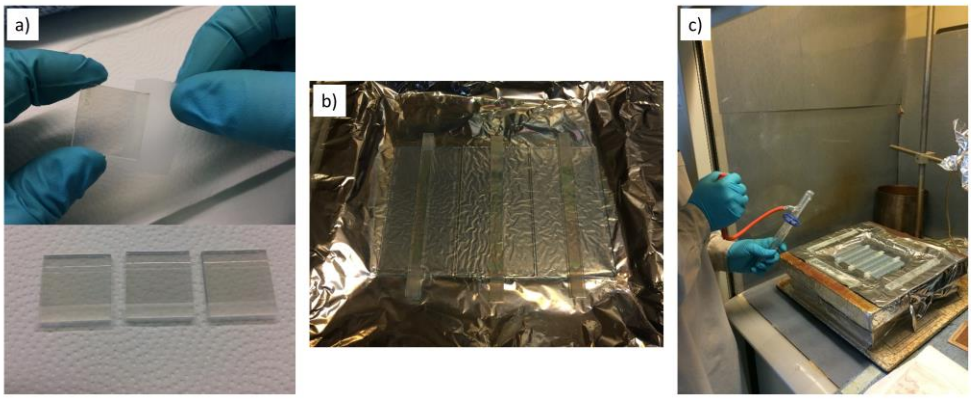

Figure 2.2. Principal steps of blocking layer deposition: a) protection of photoanode contact with adhesive tape before spinning – Method (A); b) protection of photoanode contact with glass strips before spray – Method (B); and c) atomizer and hot plate used for spray pyrolysis.

2.2.3 Perovskite Active Layer preparation

The perovskite precursor solution was prepared according to the following conditions published by Saliba *et al.*:[8] 1.1 M lead iodide (PbI_2, Sigma-Aldrich, 99.999 % trace metal basis), 0.2 M lead bromide ($PbBr_2$, Sigma-Aldrich, 99.999 % trace metal basis), 0.2 M methylammonium bromide (MABr, Dyesol) and 1.0 M formamidinium iodide (FAI, Dyesol) were dissolved in 1 mL of a N,N-dimethylformamide (DMF) / dimethyl sulfoxide mixture (DMSO) (8:2 v/v, both from Sigma-Aldrich, 99.8 % and ≥ 99.9 %, respectively). From this solution, 0.95 mL were added to 0.05 mL of a 1.5 M CsI stock solution in DMSO (Sigma-Aldrich, 99.999 % trace metals basis). This final solution was deposited on the substrates by applying a two-step spin-coating program (step 1: 1000 rpm, 10 s, 200 rpm·s^{-1}, step 2: 6000 rpm, 30 s, 2000 rpm·s^{-1}). After 25 s, 100 μL of chlorobenzene was poured onto the spinning substrate; a procedure which is known as anti-solvent technique. Careful adjustment of dripping speed and tip-to-sample distance had to be trained to fabricate reproductive samples. Samples showed a brownish tone immediately after spin-coating and were subsequently sintered at 100 °C for 40 minutes before being allowed to cool down - Figure 2.3. After each deposition, the interior of the spin coater was cleaned with a cloth to remove the condensed chemicals.

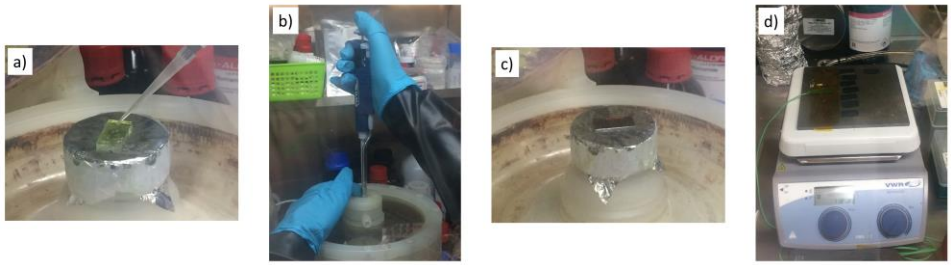

Figure 2.3. Principal steps of perovskite layer deposition: a) perovskite precursor solution deposition on the substrate; b) chlorobenzene deposition; c) substrate with perovskite layer immediately after the spinning; and d) substrates with perovskite layer on the hot plate at 100 °C.

2.2.4 Hole Extraction Layer (HEL) and Current Collector

Two different hole extraction materials were tested. Method (A): spiro-OMeTAD solution contained 75 mM spiro-OMeTAD (Chemborun, 99.7 % sublimed grade), 0.24 M 4-*tert*-butylpyridine (*t*-BP, Sigma-Aldrich, 96 %), 41 mM lithium bistrifluoromethane sulfonimidate (Li-TFSI, Acros Organics) that was obtained from a 1.8 M stock solution in acetonitrile (Sigma-Aldrich, 99.999 % electronic grade) and 27 mM FK209 Co(III) TFSI salt (Dyesol) that was obtained from a 0.27 M stock solution in acetonitrile. The solution was deposited via spin-coating (4000 rpm, 20 s, 2000 rpm·s^{-1}). Method (B): P3HT (Poly(3-hexylthiophene-2,5-diyl)) solution was fabricated from 15 mg/mL P3HT (Chemborun China), 23 mM *t*-BP and 0.7 mM Li-TFSI. It was deposited by spin-coating (3000 rpm, 30 s, 2000 rpm·s^{-1}). Afterwards, photoanode contacts covered with perovskite and hole conductor were mechanically cleaned with a scalpel and cotton swabs dipped in acetonitrile - Figure 2.4.

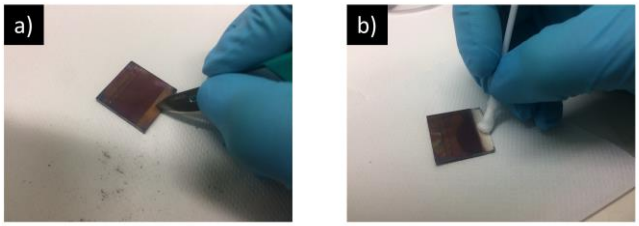

Figure 2.4. Cleaning step of the photoanode contact: a) with a scalpel; and b) cotton swab soaked in acetonitrile.

Finally, a 60 nm thick gold layer as current collector was applied through a stainless steel mask by two different methods: 1) by thermal evaporation on a VaporStation 4 (Oxford Vacuum Science, U.K.), applying a deposition rate of 0.01 nm·s^{-1} for the first 4 nm, followed by 0.1 nm·s^{-1} for the remaining thickness; and 2) by sputtering using a Leica EM ACE200 (Leica Microsystems, Germany) and applying a current of 60 mA and a deposition duration of 360 s - Figure 2.5. A mask of adhesive black tape with an active

area of 0.2 cm^2 was applied on the glass side of the device prior to photoelectrochemical characterisation.

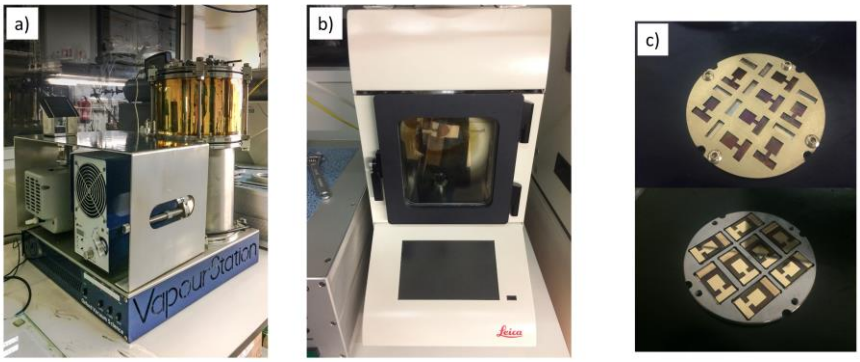

Figure 2.5. Photograph of a) thermal evaporator VaporStation 4; b) gold sputtering Leica EM ACE200; and c) substrates in the sample holder before (top) and after (bottom) gold deposition.

2.2.5 Dummy Cell preparation

The preparation was analogous to PSC, however applying merely blocking layer, hole extraction layer and gold layer by thermal evaporation.

2.2.6 Characterisation

For photoelectrochemical characterisation, a 150 W Oriel class A solar simulator, (Newport, USA) using a 1.5 air mass filter (Newport, USA) was employed. The effective irradiation intensity was measured with a single crystal Si photodiode (Newport, USA). *I-V* curves were recorded with a potentiostat (Zennium, Zahner-Elektrik GmbH, Germany) at a scan rate of 10 $mV \cdot s^{-1}$, sweeping from open-circuit to short-circuit potential (backward scan). Before each measurement, the open-circuit potential (V_{oc}) was allowed to stabilise under irradiation, which generally took less than one minute. Care was taken that starting potentials were chosen to be not more than 20 mV superior to V_{oc} in order to protect the cell.[15] Scanning electron microscopy (SEM) images were recorded with a Quanta 400 FEG (FEI, USA).

2.3 Results and discussion

FTO on glass is usually employed as transparent conductive substrate, due to its stability towards elevated temperatures. Several sheet resistances are available on the market and generally FTO with a sheet resistance of 7 - 10 $\Omega \cdot \square^{-1}$ is used in solar cells technologies, as it is a good compromise in terms of conductivity versus transparency. A thorough substrate cleaning is an essential step and often underrated; however, it plays an important role as the perovskite solar cell is constituted by several layers that are all within the nanometer scale and any contamination of the substrate will thus lead to film defects that lower overall device efficiency. The scribing of the substrate locally removes the TCO layer and prevents the electric short-circuit between photoanode and the cathode. It is often obtained by laser ablation of the conductive layer, but not every laboratory possesses a suitable equipment. A low-cost alternative is chemical etching of the conductive layer,[16] though it leads to rather inhomogeneous FTO removal. A very versatile, innovative and low-cost strategy is the electrochemical reductive treatment of the FTO, which leads to a clean and complete FTO removal on the exposed areas.[17]

The compact n-type titanium dioxide film acts as electron-selective layer and thus prevents recombination of excitons at the TCO surface. If this layer is absent, not dense enough or possesses pinholes, the fabricated cells will show decreased efficiencies due to recombination. At the same time, it has to be thin enough to provide efficient electron transport by minimizing charge accumulation and therefore recombination. The so-called blocking layer can be fabricated by several ways, including chemical bath deposition,[18] spin-coating,[19,20] spray pyrolysis,[8,21,22] sputtering,[23,24] electron-beam evaporation[25] and atomic layer deposition[26,27]. It was decided to compare TiO_2 blocking layers obtained by spray pyrolysis and spin-coating of a commercial solution (Ti-Nanoxide BL/SC, Solaronix, Switzerland). An easy way to check if the electrochemical behaviour of the blocking layer follows a diode-like behaviour is to fabricate dummy cells. Such cells are composed by a compact TiO_2 layer on top of the TCO substrate, a HEL like spiro-OMeTAD and a gold contact; similar to a perovskite cell, however without any

photoactive layer. Cyclic voltammetry (CV) has been performed on dummy cells with different blocking layers and the results are shown in Figure 2.6.

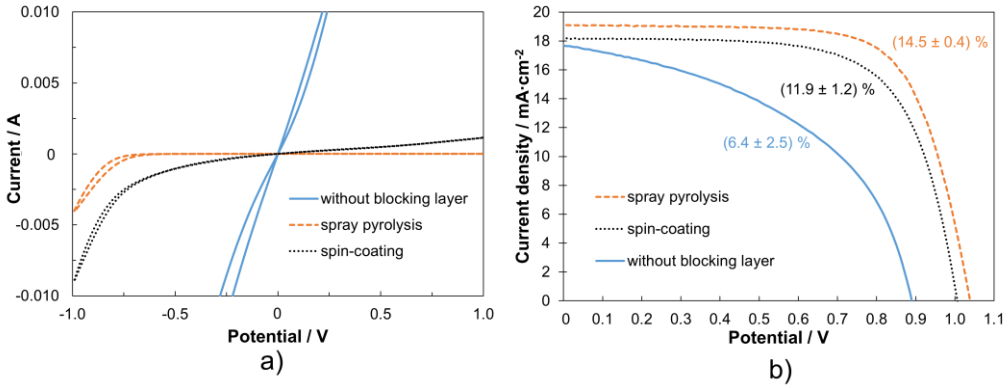

Figure 2.6. Blocking layer study: a) CV of dummy cells; and b) *I-V* curves of PSC at 0.95 sun without blocking layer (blue line), with blocking layer made by spin-coating (black dotted line) and by spray pyrolysis (orange dashed line).

In the case of a blocking layer made by spray pyrolysis, the CV shows zero anodic current and a steep increase of the cathodic current, which suggests a dense and pinhole-free layer with high electronic conductivity. In case of the blocking layer formed by spin coating, the CV shows, in addition to the cathodic current increase at lower potential, a sluggish cathodic and anodic current evolution across the entire potential window, which is an indication for pinholes. For comparison, the CV of a dummy cell without any blocking layer demonstrates a typical ohmic behavior, proving the absence of any blocking effect at positive potential. The PSC corresponding to the blocking layer fabrication methods show *I-V* curves that underline the extremely important role of the blocking layer. The cell with the blocking layer made by spray pyrolysis shows best power conversion efficiency (PCE), whereas cells made by spin-coated blocking layer perform worse. The cell without any blocking layer shows the lowest PCE that, however, are not zero. The reason is that the perovskite layer itself is an electron transporter[20] as well as it is capable to transport holes.[28,29] This renders the TCO-perovskite interface into a non-selective contact that promotes recombination and therefore leads to decreased PCE.

Images of the different blocking layers recorded by SEM show some fundamental differences - Figure 2.7. The layer deposited by spray pyrolysis is rather thin and homogeneous whereas the layer deposited by spin coating is thicker and shows cracks - Figure 2.7c. It can be concluded that PSC with a blocking layer fabricated by spray pyrolysis show superior PCE and therefore, this fabrication method might be recommended. The influence of the carrier gas was further tested but it came out that pure oxygen did not improve cell PCE - Table 2.1. Due to lack of deposition control, blocking layer thickness may vary between 30 nm to 80 nm, as SEM cross-sections showed (not presented). However, no correlated impact on PSC power conversion efficiency was verified.

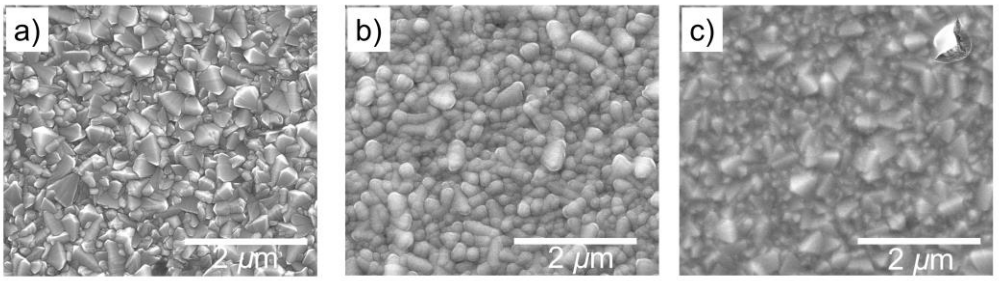

Figure 2.7. Scanning electron microscopy images (top-view) of: a) a bare TCO substrate; b) TiO_2 compact layer deposited by spray pyrolysis; and c) spin-coating of a commercial solution.

Table 2.1. Photovoltaic parameters of PSC with TiO_2 compact layer deposited by spray pyrolysis using different carrier gases.

Spray pyrolysis carrier gas	J_{sc} / mA·cm^{-2}	V_{oc} / V	*FF*	η / %
Air (best cell)	18.6	1.09	0.76	15.8
Air (average)				15.5 ± 0.4
O_2 (best cell)	19.0	0.98	0.77	14.8
O_2 (average)				14.0 ± 0.7

Mesoporous titanium dioxide layer has been employed in dye-sensitized solar cells (DSC), with the function to increase active surface area and

transport electrons under light excitation.[30] As the initial perovskite solar cells were thought as a continuity of DSC, a mesoporous titanium dioxide film was also applied, even if the extinction coefficient of perovskites such as $(CH_3NH_3)PbI_3$ (known as MAPI) is about ten times higher than that of N719 dye.[31] As a consequence, the increase of active surface is turned obsolete. Thus, PSC without mesoporous layer, so-called planar devices, have been developed, reaching already PCE values very close to the mesoporous PSC.[32] Besides higher power conversion efficiencies, some PSC with a mesoporous layer show reduced efficiency deviation between forward and backward scan, a phenomenon described as hysteresis.[22,33,34] When Snaith *et al*.[35] demonstrated that even with mesoporous layers of alumina high efficiencies of 15.9 % could be obtained, it was deduced that the mesoporous layer mainly fulfills a structural role for crystal growth and geometry determination, even if efficient electron injection from the perovskite into the TiO_2 mesoporous layer was reported.[36] However, latest results demonstrate that ionic migration at the perovskite/TiO_2 blocking layer interface, which is responsible for charge accumulation and therefore recombination events, is reduced or even suppressed in presence of the TiO_2 mesoporous layer.[37] As hysteresis also depends on ionic migration,[38,39,40,41] its reduction in the presence of mesoporous TiO_2 is the consequence. Concluding, best results have been achieved so far using a thin TiO_2 mesoporous layer and a perovskite capping layer that prevents recombination between TiO_2 and the HEL.[36,37]

There exist several commercial pastes with different sizes of TiO_2 particles and therefore, it was decided to compare two different particle sizes, namely one with 20 nm (18 NR-T, GreatCell Solar Ltd.) and other with 30 nm (30 NR-D, GreatCell Solar Ltd.) average particle diameter. The same paste dilution ratio in pure ethanol (1:6) as well as the same deposition and sintering conditions were applied. Figure 2.8 shows that both mesoporous layers lead to very comparable cell PCE that are within the error scale. This points a higher tolerance towards the mesoporous layer architecture, as long as the particle size remains similar.

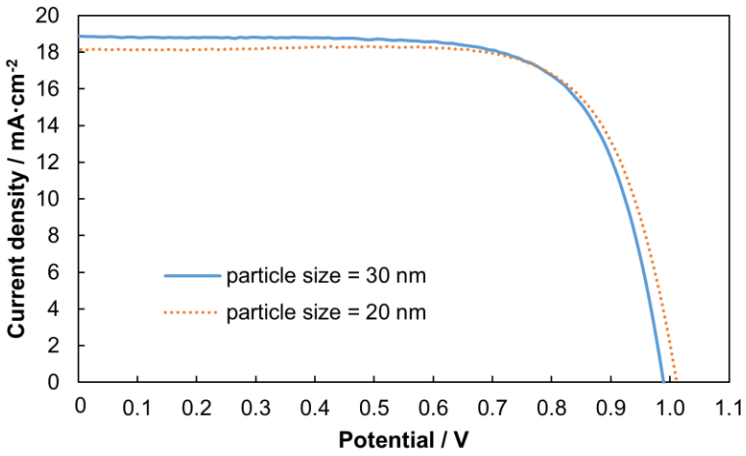

Figure 2.8. *I-V* curves of devices with a TiO_2 mesoporous layer made from 30 NR-D paste (average particle size of 30 nm, blue line) and from 18 NR-T paste (average particle size of 20 nm, dotted orange line) at 0.94 sun. Both pastes were purchased from GreatCell Solar Ltd.

Within perovskite materials, a huge variety of recipes and deposition techniques are available, which are well summarized in the book by Park *et al*.[42] and in the review by Song *et al*.[43] It might be not an easy task to decide for the suitable perovskite type and fabrication process. The name perovskite refers to a crystalline structure of the type ABX_3, A and B being cations and X an anion. The perovskite class suitable for solar cells is an organic lead halide, with A being generally an organic cation, B being the lead ion and X being a halogen, usually bromine, iodine, chlorine and mixtures. Lead substitution by tin and germanium analogues leads to perovskites with severe stability problems[35,44,45] and therefore will not be addressed here. Our focus was to determine a perovskite formulation easy to implement and that results in reproducible perovskite layers with enhanced stability. Many results have been published with monocationic perovskites, however with some inherent limitations that are briefly exposed here: MAPI has been intensively studied[46] but has some drawbacks such as weak stability towards moisture[47,48] and temperature.[49] Formamidinium (FA) was proposed as alternative cation,

however its perovskite analogue $FAPbI_3$ crystallises in the photoinactive phase below 60 °C,[50] such as the inorganic cation analogue $CsPbI_3$.[51] Whereas several groups observed improved stability of the photoactive phase upon using binary mixed cation perovskites [52,53,54,55,56], Saliba *et al.*[8] decided to combine the three cations in a perovskite and achieved high efficiencies (> 20 %) on a very reproducible basis.

Several methods exist for solution-processed film fabrication, the most common being simple spreading of the perovskite precursor solution on the substrate, also known as one-step deposition. However, films with poor surface control and therefore huge efficiency variations generally emerge.[46] A more sophisticated approach is the two-steps deposition, where the metal halide is first deposited and annealed before being brought in contact with the ammonium salt as vapour or in solution.[46,57] Nevertheless, several drawbacks of this deposition method were experienced in our group, such as incomplete conversion of the metal halide or partial dissolution of the perovskite during the subsequent washing step. Furthermore, it is more time-consuming as it requires two sintering steps. The anti-solvent technique was introduced in 2014 by the group of S. Seok[22] and since then, it has been the method of choice for subsequently published record PCE.[58] It is quite simple to implement and requires only one precursor solution, whereas the crystallisation of the perovskite is initiated by adding a so-called anti-solvent. This anti-solvent is chosen not to dissolve the perovskite on the one side and to displace the solvent of the latter on the other side. The main drawback of this deposition method is its artisanal aspect, requiring a certain degree of training before reaching enhanced reproducibility. However, smooth perovskite films with homogeneous composition and large grain boundaries are obtained after a short training time. Figure 2.9 shows a cross-section of a PSC with the perovskite capping layer on top of the mesoporous TiO_2 layer with grains growing from the bottom to the top and which are thought to enhance charge transport, according to Saliba *et al*.[8] The top view of the perovskite layer - Figure 2.9b - shows grains with diameters between 200 nm and 500 nm, which is in good agreement with the original report.[8]

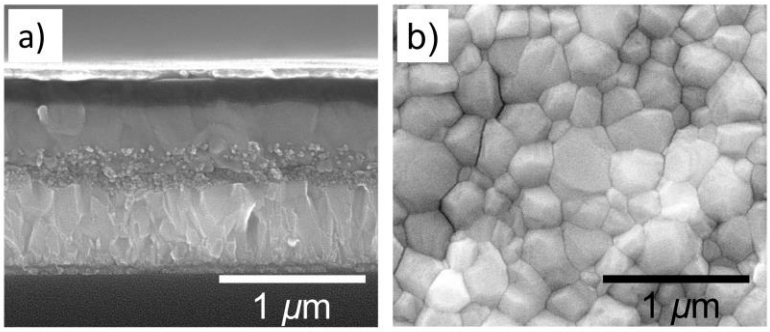

Figure 2.9. SEM images: a) cross-section of a PSC device showing the TiO_2 compact layer (*ca*. 80 nm), followed by the TiO_2 mesoporous layer of 150-200 nm (granulated layer). The adjacent perovskite layer partially infiltrates into the mesoporous structure and its capping layer has a thickness of 200-300 nm (grey layer). The spiro-OMeTAD hole extraction layer (black layer) has a thickness of 130-190 nm, followed by a 60 nm-thick gold layer as current collector (shining layer); b) top-view of the perovskite layer, showing grains with *ca*. 200-500 nm diameter.

One of the biggest detrimental factors for perovskite fabrication and stability is atmospheric humidity, together with oxygen, which will be detailed assessed in the next chapters.[59] PSC that are meant to exhibit prolonged stability require fabrication and storage in inert atmosphere or device encapsulation after fabrication.[60,61] Therefore, PSC are generally fabricated in glove boxes with dry and oxygen-free atmosphere. And not only that, also the substrates should be absolutely moisture-free. After sintering the mesoporous layer, substrates should thus be handled only in dry atmosphere or transferred to dry atmosphere such as a glove box before cooling below 150 °C. Within the degradation mechanism of perovskite structures, oxygen only interferes subsequently to hydration[61] and can therefore be considered less critical if moisture is absent or very low. Laboratories that are newcomers in this area of research might not possess a glove box infrastructure. Low atmospheric humidity levels are assumed to be less critical to perovskite fabrication but these conditions depend strongly on the geographic localization, the season and some more inherent factors. To demonstrate the effect of moisture and oxygen atmosphere on perovskite formation, a comparative test of PSC

devices, that were fabricated inside and outside the glove box (relative humidity (RH) outside the glove box: 58 %), was performed. The results are presented in Figure 2.10 and Table 2.2 and it can be observed that in case of perovskite being fabricated in ambient atmosphere, the active layer showed a lighter color and the corresponding PSC showed lower V_{oc} and J_{sc} (short-circuit density). As a strategy to minimize water uptake by the substrate, samples were heated to 100 °C immediately before the perovskite precursor solution was deposited. Corresponding PSC showed an improved V_{oc} and J_{sc}, however the fill factor decreased. This is likely due to inhomogeneous crystal growth, induced by the elevated temperature of the substrate. For the best cells obtained, a little improvement can be stated when hot substrates were used, though average PSC came out to be very similar to those without heat treatment.

This study shows that it is highly recommended to work with a glove box, providing very low humidity (< 0.002 % of RH) and oxygen levels; however, in the next Chapter 4 is possible to observe that is not true for all the types of atmospheres. Another possible strategy might be the use of a perovskite formulation that is optimized towards enhanced resistance at elevated humidity levels.[62]

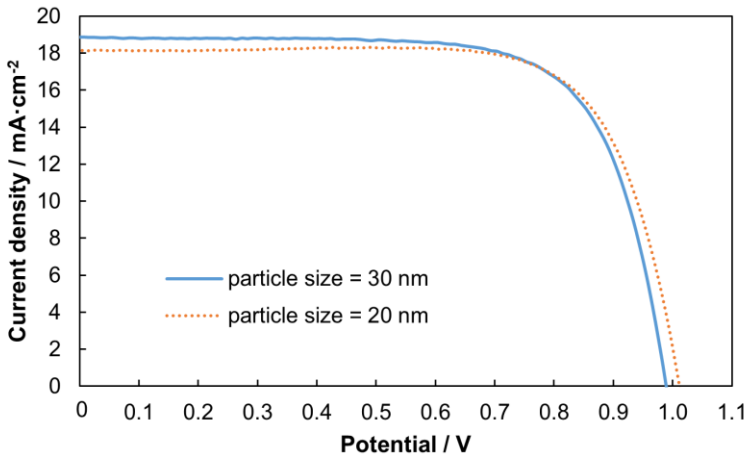

Figure 2.10. *I-V* curves of PSC fabricated in a glove box with 0 % of RH at 25 °C (blue line), at ambient humidity (58 % of RH) at 25 °C (orange dashed line), and at ambient

humidity with pre-heated substrates at 100 °C (grey dotted line). Inset photograph of samples prepared inside (left) and outside (right) the glove box at 25 °C.

Table 2.2. Best and average PCE of PSC devices with a perovskite layer prepared within different conditions.

Perovskite fabrication condition	J_{sc} / mA cm^{-2}	V_{oc} / V	*FF*	η / %
0 % of RH, 25 °C	18.5	1.06	0.72	15.1 (best) 14.7 ± 0.3 (average)
58 % of RH 25 °C	16.3	0.83	0.67	9.9 (best) 7.4 ± 2.4 (average)
58 % of RH, 100 °C	17.6	1.02	0.57	10.8 (best) 7.4 ± 2.6 (average)

Atop the photoactive layer, the HEL selectively transports the holes to the current collector and therefore fulfils the complementary role to the TiO_2 layer. It has to be pinhole-free to inhibit contact of the current collector with the perovskite layer, for the same reasons that were already stressed out concerning the electron conducting layer. Generally, a formulation using spiro-OMeTAD is used and contains, among others, the ionic liquid Li-TFSI to increase hole conductivity. However, both Li-TFSI and spiro-OMeTAD have hydrophilic properties[63] and promote humidity ingestion, leading to poor humidity stability of the entire device. Two different HELs were compared towards their stability, namely spiro-OMeTAD as molecular HEL and P3HT as polymeric HEL.

It turns out that spiro-OMeTAD leads to better PCE - Figure 2.11a - showing better current density, open circuit potential and fill factor all together. The advantage lies in an enhanced stability (at least during 2 months) despite lower efficiency when P3HT is employed - Figure 2.11b.

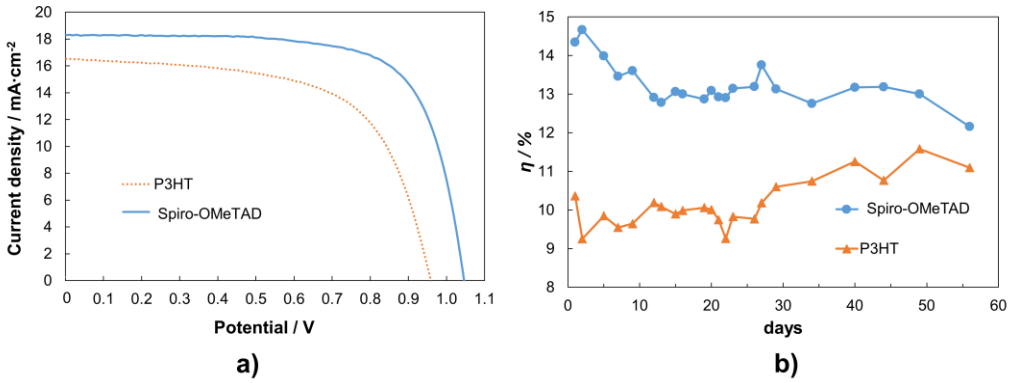

Figure 2.11. HEL study: a) *I-V* curves of PSC devices using spiro-OMeTAD (blue line) and P3HT (dotted orange line) as HEL; and b) stability of PCE of PSC devices using spiro-OMeTAD (blue circles) and P3HT (orange triangles).

Generally, current collectors are made of gold despite its higher cost, as alternative metals such as silver and aluminium have been demonstrating weak stabilities.[64,65,66] Among gold deposition methods, one of the most common ones are sputtering and thermal evaporation. However, almost all published works use thermal evaporation. We decided therefore to compare gold films with similar thickness that were fabricated by these two techniques. Indeed, thermal evaporation leads to a better overall cell performance - Figure 2.12.

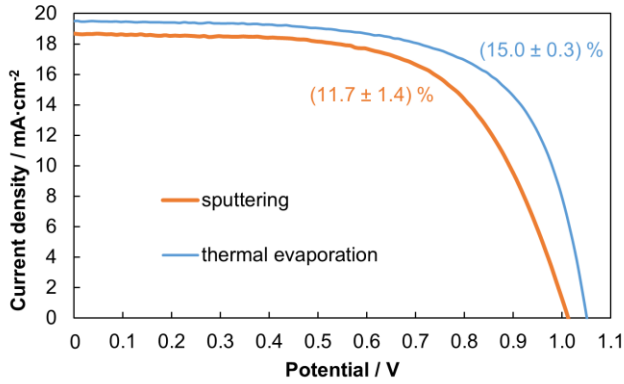

Figure 2.12. *I-V* curves of PSC with gold current collector deposited by thermal evaporation (blue line) and by sputtering (dashed orange line).

The reason for the worse performance of PSC with sputtered current collector was evidenced by doing a test with scotch tape. Whereas in case of thermal evaporation, the gold layer could be easily stripped off, in case of sputtering deposition, the gold remained stuck into HEL. Even after dissolving the layer, gold traces were still detected with the naked eye in the perovskite layer. This means that during the gold layer deposition, the plasma used in the sputtered technique is so strong that allows a deeper penetration of gold into the device structure, creating recombination centers. Thus, a thermal evaporator is needed for efficient PSC fabrication, even if this step increases considerably the energy payback time of device.[67]

Following all the layer fabrication steps mentioned before, it was possible to prepare a PSC with an average PCE of (14.8 ± 1.0) % for a set of 49 cells - Figure 2.13 (left).

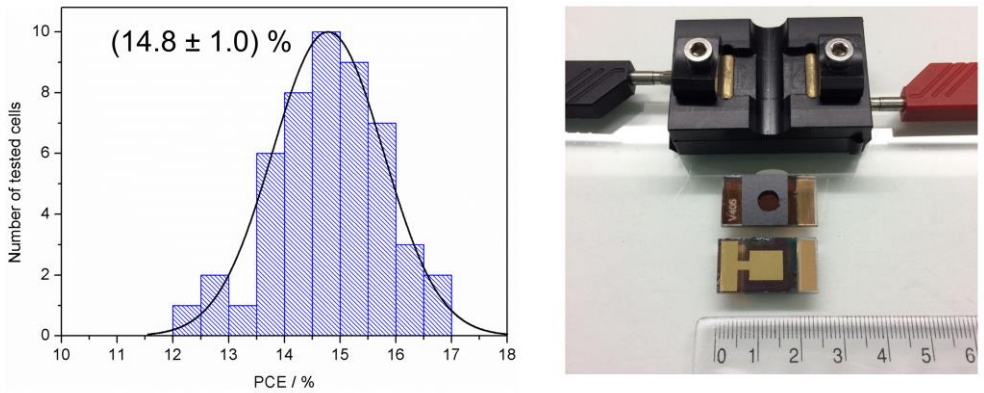

Figure 2.13. Power conversion efficiency distribution of all the cells prepared in standard conditions (left) and a PSC device with testing holder that allows reproducible testing conditions (right).

In laboratory conditions, cell efficiencies are generally measured for cell active areas inferior to 1 cm^2. The cell area delimited by the deposition of the current collector should be only slightly superior to the active cell area (delimited by a mask) to avoid recombination events. Instead of using crocodile clamps arbitrarily connected to the cell, a suitable sample holder is preferable for maximal reproducibility - Figure 2.13 (right). Among all factors that describe

the performance of the cell, the maximum power point (MPP) is the most valuable information in terms of applicability in solar devices as it describes best the operating parameters of the cell.[15,58,68] The MPP is obtained via mathematic extraction from *I-V* curves and its tracking is an obligatory factor in publications in photovoltaic area. *I-V* curves are generally obtained by dynamic scanning of external loads, though care must be taken that the scan rate does not overpass the dynamic electrochemical events inside the PSC. An example is given in Figure 2.14, where a PSC was measured at three different scan rates. If merely the *I-V* curve is considered for PCE determination, best results are obtained with a scan rate of 1 $V \cdot s^{-1}$. But if *I-V* curve of the same cell is recorded at 10 $mV \cdot s^{-1}$ and at 1 $V \cdot s^{-1}$, a striking difference is observed concerning the hysteresis - Figure 2.15. Whereas hysteresis is rather low in the former case, it considerably increases in the latter case. This means that if the *I-V* curve is recorded in backward scan in such conditions, the obtained results do not reflect the real behaviour of the cell and therefore lead to overestimation of the cell performance.[15,58] Lacking so far easily implementable measurement protocols for MPP tracking, conditions for *I-V* curve recording should be carefully chosen, with the goal to not overestimate real cell photovoltaic characteristics.

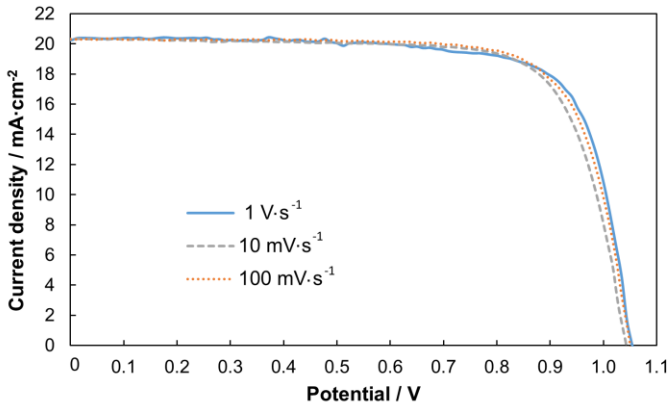

Figure 2.14. *I-V* curves of a PSC recorded at different scan rates: 1 $V \cdot s^{-1}$ (blue line); 10 $mV \cdot s^{-1}$ (grey dashed line); and 100 $mV \cdot s^{-1}$ (orange dotted line).

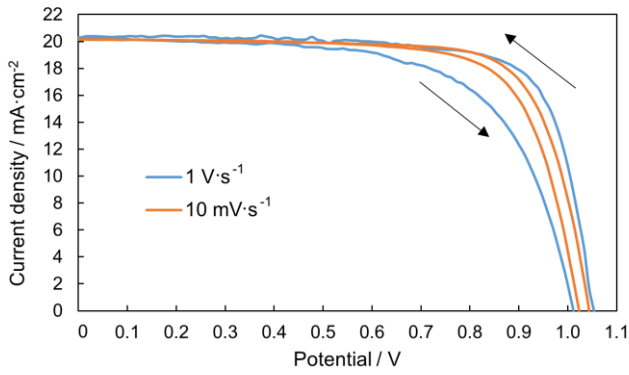

Figure 2.15. Hysteresis of a PSC recorded at a scan rate of 10 $mV \cdot s^{-1}$ (orange line) and 1 $V \cdot s^{-1}$ (blue line).

2.3 Conclusions

PSCs represent a very attractive photovoltaic technology as innumerous publications have demonstrated. PSCs are made of several thin layers and not only each layer, but also each interface, plays an important role for the manufacturing of efficient devices. It was evidenced that besides the usual equipment for thin film preparation (hot plate, spin-coater, programmable oven etc.) and photoelectrochemical characterization (potentiostat or variable external load, solar simulator), a glove box and a thermal evaporator for the deposition of the gold current collector are strongly advised. The goal of this work is to analyse and optimise each layer and, as a consequence, demonstrate their influence on the entire PSC device.

It was evidenced by experiments that for PSC performing best, blocking layer has to be deposited via spray pyrolysis, whereas comparable results were obtained when pure oxygen or air was used as carrier gas. For the mesoporous layer, no difference could be stated for both particle sizes used (20 nm and 30 nm), however it is likely that a bigger difference in size may be of matter. Our experience showed that best results for perovskite films were obtained by applying the anti-solvent technique with a triple cation formulation. It was demonstrated that concerning the adjacent HEL, spiro-OMeTAD was

resulting in cells with superior efficiency compared to the polymeric analogue P3HT. Finally, two techniques for the fabrication of gold current collector were presented and it was demonstrated that thermal evaporation lead to better PSC than sputtering. In sputtering case, the plasma allows a deeper penetration of gold into the device structure until the perovskite active layer, creating recombination centers. Incorporating all the discussed optimizations, PSC with an average efficiency of (14.8 ± 1.0) % were fabricated. Furthermore, an innovative, versatile and quick method for electrochemical substrate etching was applied in PSC, making laser-assisted scribing and therefore the necessity of such an equipment obsolete. Dummy cells as selective electrochemical characterisation method for single layers were introduced and yielded versatile results for the qualitative comparison of TiO_2 blocking layers. It is believed that this work contributes to a faster implementation of PSC fabrication in research groups with few experience in this area, thanks to a deeper understanding of fabrication details and useful analysis tools that are easily available.

Acknowledgements

I. Mesquita is grateful to FCT (Fundação para a Ciência e a Tecnologia) for her PhD fellow (ref.: PD/PB/105985/2014). L. Andrade also acknowledges the FCT for funding (IF/01331/2015). This work was supported by: European Union's Horizon 2020 Programme, through a FET Open research and innovation action under grant agreement No 687008 and European Commission through the Seventh Framework Program, the Specific Program "Ideas" of the European Research Council for research and technological development as part of an Advanced Grant under Grant Agreement No. 321315 (BI-DSC). The authors also acknowledge the Projects: i) POCI-01-0145-FEDER-006939 (LEPABE - Laboratory for Process Engineering, Environment, Biotechnology and Energy – UID/EQU/00511/2013), funded by the European Regional Development Fund (ERDF), through COMPETE2020 – Programa Operacional Competitividade e Internacionalização (POCI) and by nationals funds through FCT and ii) NORTE-01-0145-FEDER-000005 – LEPABE-2-ECO-INNOVATION, supported by North Portugal Regional Operational Programme (Norte 2020), under the Portugal 2020 Partnership Agreement, through the European Regional Development Fund (ERDF). The authors thank M. Grätzel for hosting I. Mesquita at EPFL to deepen the knowledge about PSC fabrication and O. Bellon from Greatcellsolar Ltd. for fruitful discussions.

References

[1] National Renewable Energy Laboratory, *www.nrel.gov/pv/cell-efficiency.html*, 2019.

[2] D. Mulvaney, *Hazardous Materials Used In Silicon PV Cell Production: A Primer*, Solar Industry, September 2013.

[3] Q. Jiang, Z. Chu, P. Wang, X. Yang, H. Liu, Y. Wang, Z. Yin, J. Wu, X. Zhang, J. You, *Planar-Structure Perovskite Solar Cells with Efficiency beyond 21%*, Advanced Materials **29** (2017), 1703852.

[4] E. Nouri, M.R. Mohammadi, P. Lianos, *Improving the stability of inverted perovskite solar cells under ambient conditions with graphene-based inorganic charge transporting layers*, Carbon **126** (2018), p:208-214.

[5] P. Zhang, F. Yang, M.A. Kamarudin, C.H. Ng, G. Kapil, T. Ma, S. Hayase, *Performance Enhancement of Mesoporous TiO_2-Based Perovskite Solar Cells by SbI_3 Interfacial Modification Layer*, ACS Applied Materials & Interfaces **10** (2018), p:29630-29637.

[6] D. Ramirez, K. Schutt, J.F. Montoya, S. Mesa, J. Lim, H.J. Snaith, F. Jaramillo, *Meso-Superstructured Perovskite Solar Cells: Revealing the Role of the Mesoporous Layer*, The Journal of Physical Chemistry C **122** (2018), p:21239-21247.

[7] M. Saliba, T. Matsui, K. Domanski, J.-Y. Seo, A. Ummadisingu, S.M. Zakeeruddin, J.-P. Correa-Baena, W.R. Tress, A. Abate, A. Hagfeldt, M. Grätzel, *Incorporation of rubidium cations into perovskite solar cells improves photovoltaic performance*, Science **354** (2016), p:206-209.

[8] M. Saliba, T. Matsui, J.-Y. Seo, K. Domanski, J.-P. Correa-Baena, M.K. Nazeeruddin, S.M. Zakeeruddin, W. Tress, A. Abate, A. Hagfeldt, M. Gratzel, *Cesium-containing triple cation perovskite solar cells: improved stability, reproducibility and high efficiency*, Energy & Environmental Science **9** (2016), p:1989-1997.

[9] Q. Zhang, H. Ting, S. Wei, D. Huang, C. Wu, W. Sun, B. Qu, S. Wang, Z. Chen, L. Xiao, *Recent progress in lead-free perovskite (-like) solar cells*, Materials Today Energy **8** (2018), p:157-165.

[10] H.-S. Kim, A. Hagfeldt, N.-G. Park, *Morphological and compositional progress in halide perovskite solar cells*, Chemical Communications **55** (2019), p:1192-1200.

[11] S.S.M. Fernandes, M.C.R. Castro, I. Mesquita, L. Andrade, A. Mendes, M.M.M. Raposo, *Synthesis and characterization of novel thieno[3,2-b]thiophene based metal-free organic dyes with different heteroaromatic donor moieties as sensitizers for dye-sensitized solar cells*, Dyes and Pigments **136** (2017), p:46-53.

[12] S.S.M. Fernandes, I. Mesquita, L. Andrade, A. Mendes, L.L.G. Justino, H.D. Burrows, M.M.M. Raposo, *Synthesis and characterization of push-*

pull bithiophene and thieno[3,2-b]thiophene derivatives bearing an ethyne linker as sensitizers for dye-sensitized solar cells, Organic Electronics **49** (2017), p:194-205.

[13] J. Macaira, I. Mesquita, L. Andrade, A. Mendes, Role of temperature in the recombination reaction on dye-sensitized solar cells, Physical Chemistry Chemical Physics **17** (2015), p:22699-22710.

[14] C.C. Wu, C.I. Wu, J.C. Sturm, A. Kahn, *Surface modification of indium tin oxide by plasma treatment: An effective method to improve the efficiency, brightness, and reliability of organic light emitting devices*, Applied Physics Letters **70** (1997), p:1348-1350.

[15] J.A. Christians, J.S. Manser, P.V. Kamat, *Best Practices in Perovskite Solar Cell Efficiency Measurements. Avoiding the Error of Making Bad Cells Look Good*, The Journal of Physical Chemistry Letters **6** (2015), p:852-857.

[16] H.-R. Xia, J. Li, W.-T. Sun, L.-M. Peng, *Organohalide lead perovskite based photodetectors with much enhanced performance*, Chemical Communications **50** (2014), p:13695-13697.

[17] S.P. Koiry, P. Jha, P. Veerender, C. Sridevi, A.K. Debnath, A.K. Chauhan, K.P. Muthe, S.C. Gadkari, *An Electrochemical Method for Fast and Controlled Etching of Fluorine-Doped Tin Oxide Coated Glass Substrates*, Journal of The Electrochemical Society **164** (2017), E1-E4.

[18] G. Yin, J. Ma, H. Jiang, J. Li, D. Yang, F. Gao, J. Zeng, Z. Liu, S.F. Liu, *Enhancing Efficiency and Stability of Perovskite Solar Cells through Nb-Doping of TiO_2 at Low Temperature,* ACS Applied Materials & Interfaces **9** (2017), p:10752-10758.

[19] H.-S. Kim, C.-R. Lee, J.-H. Im, K.-B. Lee, T. Moehl, A. Marchioro, S.-J. Moon, R. Humphry-Baker, J.-H. Yum, J.E. Moser, M. Grätzel, N.-G. Park, *Lead Iodide Perovskite Sensitized All-Solid-State Submicron Thin Film Mesoscopic Solar Cell with Efficiency Exceeding 9%*, Scientific Reports **2** (2012), 591.

[20] M. Liu, M.B. Johnston, H.J. Snaith, *Efficient planar heterojunction perovskite solar cells by vapour deposition*, Nature **501** (2013), p:395-398.

[21] D. Bi, C. Yi, J. Luo, J.-D. Décoppet, F. Zhang, Shaik M. Zakeeruddin, X. Li, A. Hagfeldt, M. Grätzel, *Polymer-templated nucleation and crystal growth of perovskite films for solar cells with efficiency greater than 21%*, Nature Energy **1** (2016), 16142.

[22] N.J. Jeon, J.H. Noh, Y.C. Kim, W.S. Yang, S. Ryu, S.I. Seok, *Solvent engineering for high-performance inorganic–organic hybrid perovskite solar cells*, Nat Mater **13** (2014), p:897-903.

[23] D. Yang, Z. Yang, W. Qin, Y. Zhang, S. Liu, C. Li, *Alternating precursor layer deposition for highly stable perovskite films towards efficient solar cells using vacuum deposition*, Journal of Materials Chemistry A **3** (2015), p:9401-9405.

[24] D. Yang, X. Zhou, R. Yang, Z. Yang, W. Yu, X. Wang, C. Li, S. Liu, R.P.H. Chang, *Surface optimization to eliminate hysteresis for record efficiency planar perovskite solar cells*, Energy & Environmental Science **9** (2016), p:3071-3078.

[25] K. Wang, W. Zhao, J. Liu, J. Niu, Y. Liu, X. Ren, J. Feng, Z. Liu, J. Sun, D. Wang, S.F. Liu, *CO_2 Plasma-Treated TiO_2 Film as an Effective Electron Transport Layer for High-Performance Planar Perovskite Solar Cells*, ACS Applied Materials & Interfaces **9** (2017), p:33989-33996.

[26] W. Yongzhen, Y. Xudong, C. Han, Z. Kun, Q. Chuanjiang, L. Jian, P. Wenqin, I. Ashraful, B. Enbing, Y. Fei, Y. Maoshu, Z. Peng, H. Liyuan, *Highly compact TiO_2 layer for efficient hole-blocking in perovskite solar cells*, Applied Physics Express **7** (2014), 052301.

[27] H. Hu, B. Dong, H. Hu, F. Chen, M. Kong, Q. Zhang, T. Luo, L. Zhao, Z. Guo, J. Li, Z. Xu, S. Wang, D. Eder, L. Wan, *Atomic Layer Deposition of TiO_2 for a High-Efficiency Hole-Blocking Layer in Hole-Conductor-Free Perovskite Solar Cells Processed in Ambient Air*, ACS Applied Materials & Interfaces **8** (2016), p:17999-18007.

[28] L. Etgar, *Hole Transport Material (HTM) Free Perovskite Solar Cell, Hole Conductor Free Perovskite-based Solar Cells*, Springer International Publishing, Cham, 2016, p:9-24.

[29] L. Etgar, P. Gao, Z. Xue, Q. Peng, A.K. Chandiran, B. Liu, M.K. Nazeeruddin, M. Grätzel, *Mesoscopic $CH_3NH_3PbI_3/TiO_2$ Heterojunction*

Solar Cells, Journal of the American Chemical Society **134** (2012), p:17396-17399.

[30] A. Hagfeldt, G. Boschloo, L. Sun, L. Kloo, H. Pettersson, *Dye-Sensitized Solar Cells*, Chemical Reviews **110** (2010), p:6595-6663.

[31] J.-H. Im, C.-R. Lee, J.-W. Lee, S.-W. Park, N.-G. Park, *6.5% efficient perovskite quantum-dot-sensitized solar cell*, Nanoscale **3** (2011), p:4088-4093.

[32] P. Cui, D. Wei, J. Ji, H. Huang, E. Jia, S. Dou, T. Wang, W. Wang, M. Li, *Planar p–n homojunction perovskite solar cells with efficiency exceeding 21.3%*, Nature Energy **4** (2019), p:150-159.

[33] H.J. Snaith, A. Abate, J.M. Ball, G.E. Eperon, T. Leijtens, N.K. Noel, S.D. Stranks, J.T.-W. Wang, K. Wojciechowski, W. Zhang, *Anomalous Hysteresis in Perovskite Solar Cells*, The Journal of Physical Chemistry Letters **5** (2014), p:1511-1515.

[34] B. Chen, M. Yang, S. Priya, K. Zhu, *Origin of J–V Hysteresis in Perovskite Solar Cells*, The Journal of Physical Chemistry Letters **7** (2016), p:905-917.

[35] K. Wojciechowski, M. Saliba, T. Leijtens, A. Abate, H.J. Snaith, *Sub-150 ºC processed meso-superstructured perovskite solar cells with enhanced efficiency*, Energy & Environmental Science **7** (2014), p:1142-1147.

[36] T. Leijtens, B. Lauber, G.E. Eperon, S.D. Stranks, H.J. Snaith, *The Importance of Perovskite Pore Filling in Organometal Mixed Halide Sensitized TiO_2-Based Solar Cells*, The Journal of Physical Chemistry Letters **5** (2014), p:1096-1102.

[37] M. Anaya, W. Zhang, B.C. Hames, Y. Li, F. Fabregat-Santiago, M.E. Calvo, H.J. Snaith, H. Miguez, I. Mora-Sero, *Electron injection and scaffold effects in perovskite solar cells*, Journal of Materials Chemistry C **5** (2017), p:634-644.

[38] E.L. Unger, E.T. Hoke, C.D. Bailie, W.H. Nguyen, A.R. Bowring, T. Heumuller, M.G. Christoforo, M.D. McGehee, *Hysteresis and transient behavior in current-voltage measurements of hybrid-perovskite*

absorber solar cells, Energy & Environmental Science **7** (2014), p:3690-3698.

[39] W. Tress, N. Marinova, T. Moehl, S.M. Zakeeruddin, M.K. Nazeeruddin, M. Gratzel, *Understanding the rate-dependent J-V hysteresis, slow time component, and aging in $CH_3NH_3PbI_3$ perovskite solar cells: the role of a compensated electric field*, Energy & Environmental Science **8** (2015), p:995-1004.

[40] S. Meloni, T. Moehl, W. Tress, M. Franckevičius, M. Saliba, Y.H. Lee, P. Gao, M.K. Nazeeruddin, S.M. Zakeeruddin, U. Rothlisberger, M. Graetzel, *Ionic polarization-induced current–voltage hysteresis in $CH_3NH_3PbX_3$ perovskite solar cells*, Nature Communications **7** (2016), 10334.

[41] G. Richardson, S.E.J. O'Kane, R.G. Niemann, T.A. Peltola, J.M. Foster, P.J. Cameron, A.B. Walker, *Can slow-moving ions explain hysteresis in the current-voltage curves of perovskite solar cells?*, Energy & Environmental Science **9** (2016), p:1476-1485.

[42] N.G. Park, M. Grätzel, T. Miyasaka, *Organic-Inorganic Halide Perovskite Photovoltaics: From Fundamentals to Device Architectures*, Springer International Publishing, 2016.

[43] Z. Song, S.C. Watthage, A.B. Phillips, M.J. Heben, *Pathways toward high-performance perovskite solar cells: review of recent advances in organo-metal halide perovskites for photovoltaic applications*, Journal of Photonics for Energy **6** (2016), p:022001-022001.

[44] F. Hao, C.C. Stoumpos, D.H. Cao, R.P.H. Chang, M.G. Kanatzidis, *Lead-free solid-state organic-inorganic halide perovskite solar cells*, Nat Photon **8** (2014), p:489-494.

[45] T. Krishnamoorthy, H. Ding, C. Yan, W.L. Leong, T. Baikie, Z. Zhang, M. Sherburne, S. Li, M. Asta, N. Mathews, S.G. Mhaisalkar, *Lead-free germanium iodide perovskite materials for photovoltaic applications*, Journal of Materials Chemistry A **3** (2015), p:23829-23832.

[46] J. Burschka, N. Pellet, S.-J. Moon, R. Humphry-Baker, P. Gao, M.K. Nazeeruddin, M. Gratzel, *Sequential deposition as a route to high-*

performance perovskite-sensitized solar cells, Nature **499** (2013), p:316-319.

[47] M.A. Green, A. Ho-Baillie, H.J. Snaith, *The emergence of perovskite solar cells*, Nat Photon **8** (2014), p:506-514.

[48] M. Gratzel, *The light and shade of perovskite solar cells*, Nat Mater **13** (2014), p:838-842.

[49] B. Conings, J. Drijkoningen, N. Gauquelin, A. Babayigit, J. D'Haen, L. D'Olieslaeger, A. Ethirajan, J. Verbeeck, J. Manca, E. Mosconi, F.D. Angelis, H.-G. Boyen, *Intrinsic Thermal Instability of Methylammonium Lead Trihalide Perovskite*, Advanced Energy Materials **5** (2015), 1500477.

[50] C.C. Stoumpos, C.D. Malliakas, M.G. Kanatzidis, *Semiconducting Tin and Lead Iodide Perovskites with Organic Cations: Phase Transitions, High Mobilities, and Near-Infrared Photoluminescent Properties*, Inorganic Chemistry **52** (2013), p:9019-9038.

[51] C.K. Moller, *Crystal Structure and Photoconductivity of Caesium Plumbohalides*, Nature **182** (1958), p:1436-1436.

[52] N.J. Jeon, J.H. Noh, W.S. Yang, Y.C. Kim, S. Ryu, J. Seo, S.I. Seok, *Compositional engineering of perovskite materials for high-performance solar cells*, Nature **517** (2015), p:476-480.

[53] J.P. Correa Baena, L. Steier, W. Tress, M. Saliba, S. Neutzner, T. Matsui, F. Giordano, T.J. Jacobsson, A.R. Srimath Kandada, S.M. Zakeeruddin, A. Petrozza, A. Abate, M.K. Nazeeruddin, M. Gratzel, A. Hagfeldt, *Highly efficient planar perovskite solar cells through band alignment engineering*, Energy & Environmental Science **8** (2015), p:2928-2934.

[54] H. Choi, J. Jeong, H.-B. Kim, S. Kim, B. Walker, G.-H. Kim, J.Y. Kim, *Cesium-doped methylammonium lead iodide perovskite light absorber for hybrid solar cells*, Nano Energy **7** (2014), p:80-85.

[55] J.-W. Lee, D.-H. Kim, H.-S. Kim, S.-W. Seo, S.M. Cho, N.-G. Park, *Formamidinium and Cesium Hybridization for Photo- and Moisture-Stable Perovskite Solar Cell*, Advanced Energy Materials **5** (2015), 1501310.

[56] X. Li, D. Bi, C. Yi, J.-D. Décoppet, J. Luo, S.M. Zakeeruddin, A. Hagfeldt, M. Grätzel, *A vacuum flash–assisted solution process for high-efficiency large-area perovskite solar cells*, Science **353** (2016), p:58-62.

[57] Q. Chen, H. Zhou, Z. Hong, S. Luo, H.-S. Duan, H.-H. Wang, Y. Liu, G. Li, Y. Yang, *Planar Heterojunction Perovskite Solar Cells via Vapor-Assisted Solution Process,* Journal of the American Chemical Society **136** (2014), p:622-625.

[58] J.-P. Correa-Baena, A. Abate, M. Saliba, W. Tress, T. Jesper Jacobsson, M. Gratzel, A. Hagfeldt, *The rapid evolution of highly efficient perovskite solar cells*, Energy & Environmental Science **10** (2017), p:710-727.

[59] T. Leijtens, G.E. Eperon, N.K. Noel, S.N. Habisreutinger, A. Petrozza, H.J. Snaith, *Stability of Metal Halide Perovskite Solar Cells*, Advanced Energy Materials **5** (2015), 1500963.

[60] F. Matteocci, L. Cinà, E. Lamanna, S. Cacovich, G. Divitini, P.A. Midgley, C. Ducati, A. Di Carlo, *Encapsulation for long-term stability enhancement of perovskite solar cells*, Nano Energy **30** (2016), p:162-172.

[61] I. Mesquita, L. Andrade, A. Mendes, Perovskite solar cells: materials, configurations and stability, Renewable & Sustainable Energy Reviews 82 (2017), p:2471-2489.

[62] Q. Tai, P. You, H. Sang, Z. Liu, C. Hu, H.L.W. Chan, F. Yan, *Efficient and stable perovskite solar cells prepared in ambient air irrespective of the humidity*, Nature Communications **7** (2016), 11105.

[63] Y.S. Kwon, J. Lim, H.J. Yun, Y.H. Kim, T. Park, *A diketopyrrolopyrrole-containing hole transporting conjugated polymer for use in efficient stable organic-inorganic hybrid solar cells based on a perovskite*, Energy and Environmental Science **7** (2014), p:1454-1460.

[64] T. Leijtens, G.E. Eperon, S. Pathak, A. Abate, M.M. Lee, H.J. Snaith, *Overcoming ultraviolet light instability of sensitized TiO_2 with meso-superstructured organometal tri-halide perovskite solar cells*, Nature Communications **4** (2013), 2885.

[65] Y. Han, S. Meyer, Y. Dkhissi, K. Weber, J.M. Pringle, U. Bach, L. Spiccia, Y.-B. Cheng, *Degradation observations of encapsulated planar $CH_3NH_3PbI_3$ perovskite solar cells at high temperatures and humidity*, Journal of Materials Chemistry A **3** (2015), p:8139-8147.

[66] J. You, L. Meng, T.-B. Song, T.-F. Guo, Y. Yang, W.-H. Chang, Z. Hong, H. Chen, H. Zhou, Q. Chen, Y. Liu, N. De Marco, Y. Yang, *Improved air stability of perovskite solar cells via solution-processed metal oxide transport layers*, Nat Nano **11** (2016), p:75-81.

[67] J. Gong, S.B. Darling, F. You, *Perovskite photovoltaics: life-cycle assessment of energy and environmental impacts*, Energy & Environmental Science **8** (2015), p:1953-1968.

[68] E. Zimmermann, K.K. Wong, M. Müller, H. Hu, P. Ehrenreich, M. Kohlstädt, U. Würfel, S. Mastroianni, G. Mathiazhagan, A. Hinsch, T.P. Gujar, M. Thelakkat, T. Pfadler, L. Schmidt-Mende, *Characterization of perovskite solar cells: Towards a reliable measurement protocol*, APL Materials **4** (2016), 091901.

CHAPTER 3

TEMPERATURE IMPACT ON PEROVSKITE SOLAR CELLS UNDER OPERATION

Adapted from the peer-reviewed article

Mesquita, I., Andrade, L., Mendes, A., *Temperature Impact on Perovskite Solar Cells under Operation*, ChemSusChem **12** (2019), p:2186-2194.

3

TEMPERATURE IMPACT ON PEROVSKITE SOLAR CELLS UNDER OPERATION

Abstract

Thermal stability is still an obstacle to the PSC commercialisation and so the temperature effect on the mesoporous triple-cation perovskite solar cells with two different hole extraction materials (spiro-OMeTAD and PTAA) was assessed in this work. The cells were exposed to thermal stress between -5 °C and 80 °C and their photovoltaic performance was monitored *in-situ* to reproduce real operating conditions. At low temperatures, devices presented very stable values (average loss < 5 %), whilst as temperature increases a significant decrease in the open circuit potential and short-circuit current was observed. X-ray diffraction showed no modification of the perovskite crystal structure with temperature. On the other hand, electron scanning microscopy and X-ray photoelectron spectroscopy helped to conclude that temperature had a great impact in the hole extraction layer. The cell performance loss was attributed to the evaporation of additives added to the hole extraction layer to enhance its conductivity. Although the decrease in power conversion efficiency at 80 °C is slightly higher for PTAA cells, spiro-OMeTAD cells presented a higher irreversible loss of (21.6 ± 2.3) % after thermal-stress tests while PTAA devices showed only a loss of (8.2 ± 1.6) %.

3.1 Introduction

In less than a decade the efficiency of perovskite solar cells (PSC) raised from 3.8 % to 25.2 %.[1] This fast improvement in terms of power conversion efficiency (PCE) was mainly possible by tailoring the formation and composition of perovskite materials,[2,3,4,5] new deposition methods[6,7,8] and the use of new hole and electron extraction layers.[9,10,11,12,13,14] Although perovskites are very efficient as light absorbers and easy to produce, complete devices still presenting some stability challenges that are hampering their large-scale production. Perovskite solar cells are very sensitive to temperature, moisture and UV light and, for that reason, understanding the effect of these environmental elements in devices under operation is of crucial importance. Temperature is particularly critical since normal operating environment for photovoltaic devices is under direct sunlight, and the cell temperature can be up to 45 °C higher than the environmental temperature.[15] So far, temperature dependent studies on PSCs have been very limited compared to the numerous studies on improving their power output at room temperature.

Due to the unprecedented photovoltaic properties of the organometal halide perovskite crystals, the majority of studies focused on the chemical stability of the perovskite material as a function of the temperature. Actually, it is well known that the crystal structure is significantly affected by temperature and that perovskite crystals show three phases, namely α, β, and γ phases, depending on the crystallization temperature. According with some authors,[16,17,18] in $CH_3NH_3PbI_3$ perovskites at 100 °C an intermediate phase of the perovskite absorber, between tetragonal and cubic phase, starts appearing and the PSC device loses performance. Also, when perovskite is exposed for a long time to 85 °C it starts decomposing into PbI_2.[18] Several research groups progressed on improving the thermal stability of PSCs by developing more stable hybrid perovskites, and the addition of small amounts of inorganic cesium and rubidium cations resulted in highly monolithic grains of more pure perovskite.[2,3] In fact, it has been observed that the “cation cascade” perovskite is quite stable under dry conditions and at temperatures up to 85 °C, showing apparently no change in color neither in the X-ray diffraction (XRD) patterns of

the devices submitted to 85 °C. Following the attempt to overcome thermal instability, different architectures and deposition techniques[2,7,12,19] have been studied, which led to verify the additional thermal instability of hole extraction materials. In the best performing devices spiro-OMeTAD [2,2',7,7'-tetrakis(N,N-di-p-methoxyphenyl-amine)9,9'-spirobifluorene] is used as hole extraction layer (HEL). Although the glass transition temperature of spiro-OMeTAD is around 125 °C,[20] the use of dopants like lithium-bis(trifluoromethanesulfonyl) imide (Li-TFSI) and *tert*-butylpyridine (*t*-BP) to enhance electrical conductivity actually reduces this temperature to values below 100 °C. So, for these devices, temperature is a key factor since spiro-OMeTAD with additives crystallises when subjected to thermal-stress, responsible for reducing the hole mobility and electrical contact of perovskite/HEL interface.[21] Besides, the interface between perovskite and HEL may be also affected promoting the degradation of HEL due to the I^- migration. According to Kim *et al*.,[17] at elevated temperatures iodide ions from the perovskite layer diffuse into the spiro-OMeTAD and act as reducing agents decreasing its oxidation and, consequently, its conductivity properties. Moreover, Jena *et al*.[22] attributed the PSC performance degradation under temperature stress to crystallization and photo-oxidation of spiro-OMeTAD; they observed that when overheating a perovskite film, free of spiro-OMeTAD, to promote its degradation to PbI_2, the PSC device did not show significant performance losses. This led to the conclusion that the textural modification of the spiro-OMeTAD layer (generation of pinholes at high temperature) and certain unidentified modifications at the perovskite/spiro-OMeTAD interface seem to be the main reasons for the performance drop of the cells at high temperature. Zheng *et al*.[23] ascribed the loss of performance of formamidinium perovskite devices to the loss of dopants from the HEL. These authors observed that when using a dopant-free HEL (P3HT-poly(3-hexylthiophene-2,5-diyl)) the devices retained the initial efficiency and showed no apparent performance change after 800 h storage in the temperature range of 20- 85 °C. More recently, Magomedov *et al*.[24] showed that oxidized HEL species can interact with *t*-BP additive forming pyridinated products that influence negatively the performance of the device, even in short aging times. Moreover,

Kasparavicius *et al*.[25] also showed that oxidized HEL starts to degrade at 100 °C and part reverts back to the original unoxidized material, and other part reacts with *t*-BP. Additionally, Li-TFSI and FK209, also responsible for the oxidation of HELs, do not affect the degradation rate. Thus, the authors concluded that even if the dopants are important to oxidize the HELs to increase their conductivities and consequently to obtain higher power conversion efficiencies, the instability of the oxidized HELs can be actually responsible for the low-performing spiro-OMeTAD based-devices at elevated temperatures. Besides, high temperatures also proved to induce gold migration to inner-layers. According to Domanski *et al*.[26] a temperature of 70 °C is enough to induce gold migration from the back contact through the HEL (spiro-OMeTAD) and into perovskite layer affecting consequently the performance of the cell.

Important to mention that the aforementioned temperature tests were not made under real operating conditions; the cells were exposed to thermal-stress and the characteristic curves obtained at room temperature. In outdoor conditions, the PSC device produces electricity at the operating temperature conditions. Moreover, most of the studies concerning temperature stress were performed under nitrogen atmosphere or with cells sealed under inert atmosphere, what will be very difficult to realize in large-scale industrialisation, not only in terms of costs but also in terms of equipment limitations. The present work aims at mimicking as close as possible real operating conditions. PSC devices sealed under room conditions were submitted to thermal-stress between -5 °C to 80 °C and characterised at the stress temperature. Mesoporous triple-cation perovskite cells using a spiro-OMeTAD or PTAA (poly(triaryl amine)) HEL were prepared and then sealed under ambient conditions of oxygen and humidity. The performance degradation of the devices was investigated by photocurrent-potential (*I-V*), X-ray diffraction (XRD), scanning electron microscopy (SEM) and X-ray photoelectron spectroscopy (XPS).

3.2 Materials and Methods

3.2.1 Material and device fabrication

Triple-cation perovskites prepared by anti-solvent method were used to prepare complete devices as described elsewhere.[3] Fluorine-doped tin oxide (FTO) glass substrates (TCO 22-7, 7 $\Omega \cdot \square^{-1}$, Solaronix, Switzerland) were cleaned with KOH saturated solution and water in an ultrasonic bath, 5 min each step. The substrates were then dried with air and treated with UV-ozone for 15 min (UVO cleaner from Jelight Company, Inc.). At 5 mm from the glass edge, a scribing was made with a Versa Laser printer to electrically isolate the photo- from the counter-electrode.

Titanium dioxide (TiO_2) blocking layer was made from a precursor solution of titanium diisopropoxide bis(acetylacetonate) in anhydrous 2-propanol sprayed at 450 °C and left at that temperature for 45 min. After cooling down to room temperature, TiO_2 paste (Dyesol, 30 NR-D) was spin-coated on the blocking layer at 5000 rpm for 10 s and immediately placed at 125 °C. After drying at 125 °C for 10 min, the film was annealed at 500 °C for 30 min.

The triple-cation perovskite solution was prepared from a precursor solution containing formamidinium iodide (FAI - 1 M), lead iodide (PbI_2 - 1.1 M), methylammonium bromide (MABr - 0.2 M) and lead bromide ($PbBr_2$ - 0.2 M) in anhydrous N,N-dymethylformamide:dimethyl sulfoxide (DMF:DMSO 4:1 (v:v)). After the total dissolution of all the components, 5 % in volume of a 1.5 M cesium iodide (CsI) solution in DMSO was added to the initial solution. The perovskite layer was deposited by spin-coating at 1000 rpm during 10 s, followed by 30 s at 6000 rpm; 15 s before the end of second step, 100 μL of chlorobenzene was deposited on top of the spinning substrate and immediately a brownish colour appeared. The substrates were placed at 100 °C during 40 min to anneal. After the annealing, the substrates were cooled down for few minutes before the deposition of HEL.

The HEL solution was prepared dissolving 102 mg of spiro-OMeTAD (Chemborun, 99.57 %) in 1.116 mL of chlorobenzene, to which 40 μL of 4-*tert*-butylpyridine (*t*-BP - Acros Organic, 96 %), 23 μL of lithium bis(trifluoromethanesulfonyl)imide (Li-TSFI - Acros Organic, 99 %) solution

(520 mg Li-TSFI in 1 ml acetonitrile) and 10 μL of FK209 (Dyenamo) solution (40 μg in 100 µL of acetonitrile), were added. 40 μL of this spiro-OMeTAD solution was spin-coated on the perovskite layer at 4000 rpm for 20 s. To the samples with PTAA as HEL, the solution was prepared dissolving 10 mg of PTAA (Ossila) in 1 mL of toluene and added 2.0 μL of *t*-BP and 1.6 μL of 1.8 M of Li-TFSI solution. Finally, *ca*. 60 nm gold electrode was deposited by thermal-evaporation on the spiro-OMeTAD layer. The perovskite and spiro-OMeTAD/PTAA depositions were performed inside a nitrogen filled glove box.

Complete devices were sealed using double side Kapton® tape and the cell edges coated with high temperature epoxy resin (Original Cold-Weld® two-part epoxy steel reinforced from JB Weld®; product number: 8265-S). No effect of Kapton® and epoxy resin on devices photovoltaic performance was observed. It is important mentioning that the pressure inside the cell increases as the temperature increases. Not only the permanent gases contribute for the pressure rise but mostly the evaporation of low boiling solvents, which make the cell eventually to leak. This leak should, however, not impair the performance of cell since the amount of air entering in the cell during the experimental time is rather limited.

3.2.2 Characterisation and experimental setup

Photocurrent-potential (*I-V*) characteristics curves were obtained in a setup equipped with a 150 W xenon light source (Oriel class A simulator, Newport USA) irradiating *ca*. 98 ± 2 $mW \cdot cm^{-2}$ with an air mass filter of 1.5 (Newport, USA). The *I-V* curves were obtained by applying an external potential bias and measuring the generated photocurrent with an Autolab electrochemical station in the temperature range of -5 °C to 80 °C. The measurements were done in reverse scan (from open-circuit to short-circuit) at scan rate of 10 $mV \cdot s^{-1}$ and after stabilisation of the V_{oc}. This stabilization was fast (less than 20 s) to ensure that the characterisation is not influenced by the light-soaking effect.

The temperature of the cell was controlled using an in-house developed setup based on a peltier element (Marlow Industries, model RC12-6) connected to a Keithley DC power supply (Model 2425C) and controlled by a National Instruments LabVIEW software.[27] Three K-type thermocouples were

used to monitor the temperature: one in the cell, to read the real operation temperature, and the other two at the different sides (cold and hot sides) of peltier device - Figure 3.1. The heat dissipation side of peltier element was connected to a thermostatic water bath (Julabo model ME, Germany). The devices were submitted to 12 different temperatures, from -5 °C to 80 °C, in a step-wise process with a dwell time at each temperature of 10 min; at end of each dwell time the *I-V* was recorded. The overall experiment lasted *ca*. 4 h for each cell.

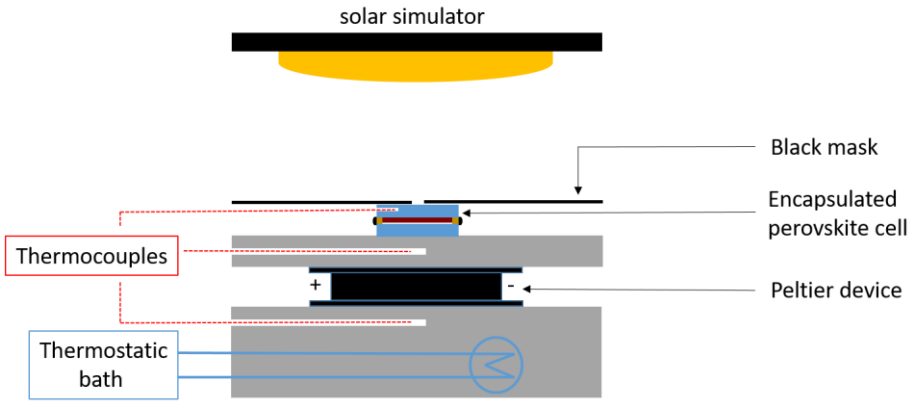

Figure 3.1. Experimental setup used for PSC temperature tests between -5 °C and 80 °C; grey components are aluminum slabs.

3.3 Results and discussion

Thermal-stress measurements were conducted in perovskite solar cells prepared from different batches and characterised in different days. The experiments performed at temperatures below room temperature (12 °C, 7 °C, 0 °C and -5 °C) were conducted first; then, these cells were stabilised at 22 °C and the corresponding photovoltaic performance assessed again. The same batch of 10 cells was used at all low-temperature experiments. The cells presented very stable results for all photovoltaic parameters with an average decrease of approximately 5 % when tested at -5 °C compared with the initial PCE at 22 °C. This loss of efficiency was mainly due to a decrease in the V_{oc} (open circuit voltage) and *FF* (fill factor) and consequently an increase of the

series resistance. Nevertheless, the observed PCE decrease at -5 °C was then fully reversible when devices were characterised again at room-temperature - Figure 3.2. Spiro-OMeTAD mobility has been characterised at different temperatures by Rana *et al*.[28] and it was observed that as temperature decreases, the charge mobility also decreases rapidly suggesting a thermally activated transport mechanism. This type of transport process has been observed in organic semiconductors by many authors.[29,30,31,32]

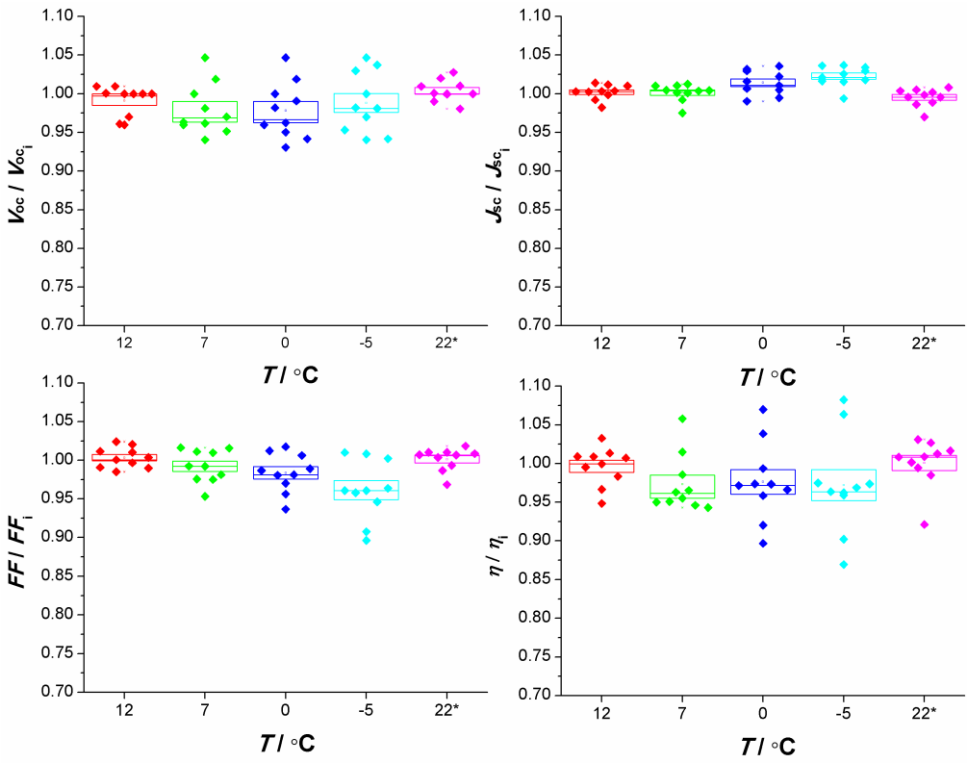

Figure 3.2. Photovoltaic performance of complete PSC devices at temperatures between -5 °C and 12 °C. The photovoltaic performance values were normalized by the initial PCE obtained at 22 °C for each cell. It was also added the normalized performance parameters of cells characterized at 22 °C after low-temperature stress tests (22*).

Since no significant changes in the performance were observed, the same batch of cells was exposed to higher temperatures, stepwise from 30 °C up to 80 °C. As temperature increases, a very significant decrease in the V_{oc} and J_{sc} (short-circuit current) was observed, leading to a decrease in the overall

performance of the devices - Figure 3.3. When the devices were tested at 80 °C the PCE diminished in average of (36.0 ± 5.5) % compared with the initial PCE of each cell at 22 °C; after bringing again the devices to 22 °C, it was observed an irreversible PCE loss of (21.6 ± 2.3) %. From the *I-V* curve of a representative device, Figure 3.4, when the cell returns to room temperature after 80 °C, it is observed a decrease in the J_{sc} and V_{oc} due to enhanced series and shunt resistances.

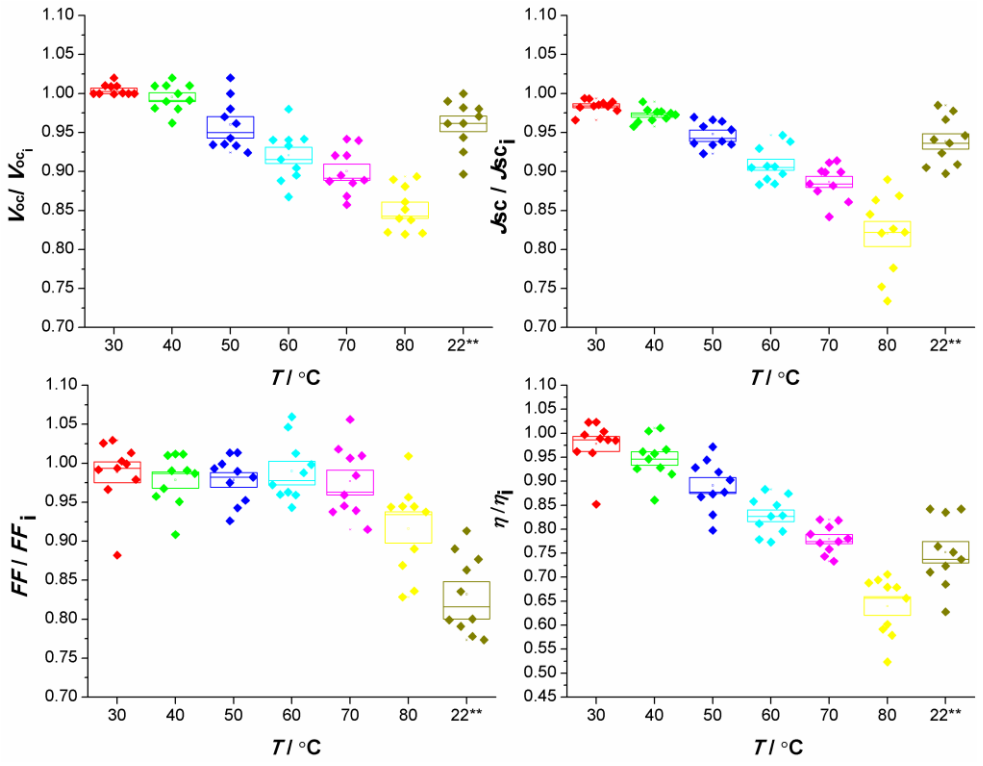

Figure 3.3. Photovoltaic performance of complete PSC devices at temperatures between 30 °C and 80 °C. The photovoltaic performance values were normalized by the initial PCE obtained at 22 °C for each cell. It was also added the normalized performance parameters of cells characterized at 22 °C after high-temperature stress tests (22**).

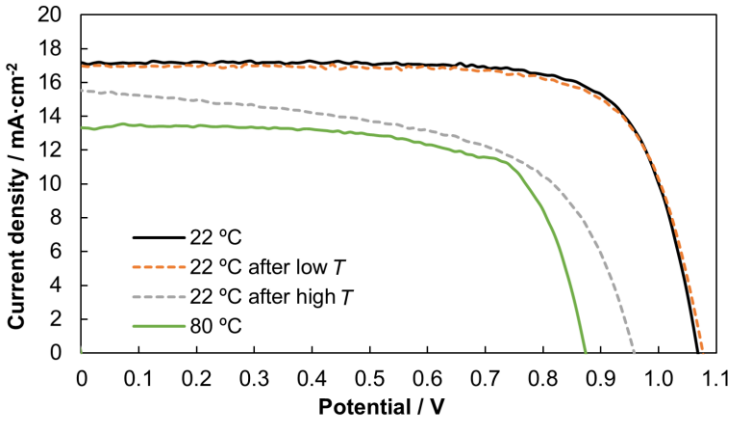

Figure 3.4. *I-V* curves of a representative device with spiro-OMeTAD as HEL operating at room temperature (22 °C) (black line) and the same cell operating at 80 °C (green line). Control characterisation were performed at 22 °C after thermal-stress at low (orange dotted line) and high temperatures (grey dotted line).

The PCE loss observed at high operating temperatures can be assigned either to spiro-OMeTAD or perovskite degradation. Scanning electron microscopy images of cells exposed to 80 °C showed pinholes on top of the HEL - Figure 3.5. According to Jena *et al.*,[33] pinholes only appear when gold is on top of spiro-OMeTAD and when Li-TFSI and *t*-BP are used together as dopants of HEL. Interestingly, Figure 3.5 shows pinholes over a spiro-OMeTAD surface region of the PSC without gold-back contact; pinholes are formed after thermal-stress test and independently of this surface area being covered or not by a gold-back contact layer.

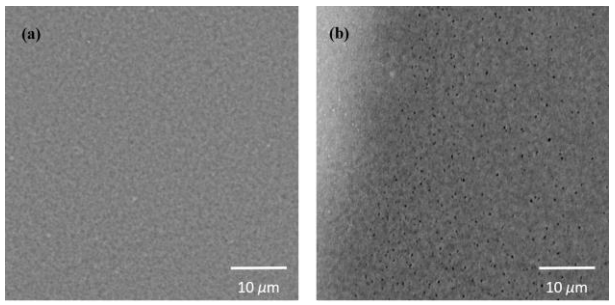

Figure 3.5. Top SEM micrographs of a mesoporous triple-cation perovskite solar cell in an area without gold-back contact on top (a) before and (b) after thermal-stress tests.

For understanding the loss of PCE of a PSC under thermal-stress, two set of experiments were conducted. First, the gold-back contact layer was peeled-off from a batch of fresh and a batch of thermally aged cells (80 °C for 4 h in a hot plate) and a new layer of gold was evaporated on top of spiro-OMeTAD. These devices were characterized at room temperature, however the degradation remained in the batch of thermally aged cells. Then, the gold back-contact and spiro-OMeTAD layers were removed from new batches of fresh and thermally aged cells and fresh layers of gold and spiro-OMeTAD were deposited - Table 3.1. Again, these devices were characterised at room temperature and the PCE recovered only after the use of a fresh layer of spiro-OMeTAD. This indicated that the loss of performance after the thermal-stress is related to HEL layer probably due to the loss of volatiles, either additives or degradation products.

Table 3.1. Photovoltaic parameters obtained at 22 °C of a PSC device thermally-aged at 80 °C and after removal and deposition of a new layer of spiro-OMeTAD and gold.

Photovoltaic parameters	Fresh cell	Thermally-aged cell	Cell with new layers
V_{oc} / mV	945	924	964
J_{sc} / mA·cm^{-2}	17.0	16.6	17.3
FF	0.644	0.558	0.649
η / %	11.4	9.40	11.9

To corroborate the effect of additives loss in the photovoltaic performance, spiro-OMeTAD without additives was used to assemble a new batch of cells. In this case, the power conversion efficiency increased with temperature, Figure 3.6, that was attributed to the heating-induced improvement of the crystallinity, promoting a more efficient charge mobility and corresponding extraction.[20] Since the glass transition temperature of the spiro-OMeTAD is 125 °C[34] and there is no degradation in pristine (not additivated) spiro-OMeTAD after being exposed to 80 ºC, it can be concluded that the performance decrease should be related to evaporation of additives. This is further supported since the

performance of spiro-OMeTAD-based PSC without additives is similar to the performance of additivated spiro-OMeTAD-based PSC, both, after thermal-stress - Table 3.2. The pinholes at the spiro-OMeTAD layer should then be formed because of the fast evaporation of additives during the thermal-stress tests. It should be emphasised that due to the pressure rise inside the cell, it should leak out during the evaporation of the low boiling point solvents. Even though *t*-BP presents a boiling point of almost 200 °C, Bailie *et al*.[35] showed that this compound in small quantities can possess an appreciable equilibrium partial pressure that allows it to evaporate at temperatures as low as 85 °C in dye-sensitized solar cells. Finally, and as discussed before, also Kasparavicius *et al*.[25] showed that oxidized HEL starts to degrade at those values of temperature and part reverts back to the original unoxidized material, and other part reacts with *t*-BP.

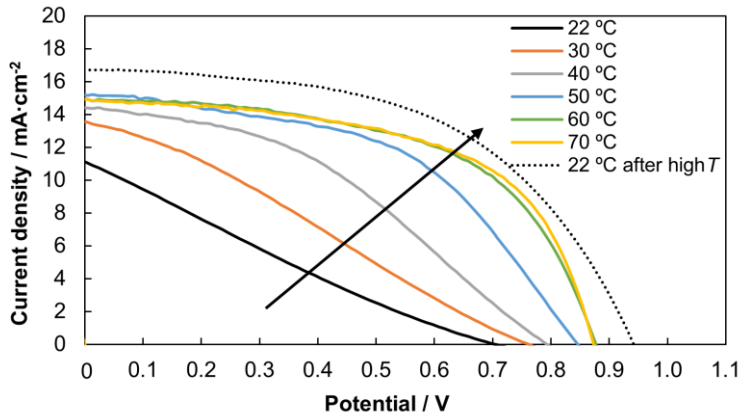

Figure 3.6. *I-V* curves of a representative device, prepared with pristine spiro-OMeTAD, operating at different temperatures, during the thermal-stress tests.

Table 3.2. Photovoltaic parameters of spiro-OMeTAD cells as HEL, with and without additives at 22 °C, both, after thermal-stress test at 80 °C.

Photovoltaic parameters	Additivated spiro-OMeTAD (*t*-BP + Li-TFSI + FK209)	Pristine Spiro-OMeTAD
V_{oc} / mV	940	955
J_{sc} / mA·cm^{-2}	16.5	15.5
FF	0.551	0.583
η / %	9.69	9.61

XPS analysis of pristine and additivated spiro-OMeTAD before and after thermal-stress tests were performed. This analysis allows to assess possible migration to the surface of additives species when additivated spiro-OMeTAD is thermally aged - Figure 3.7.

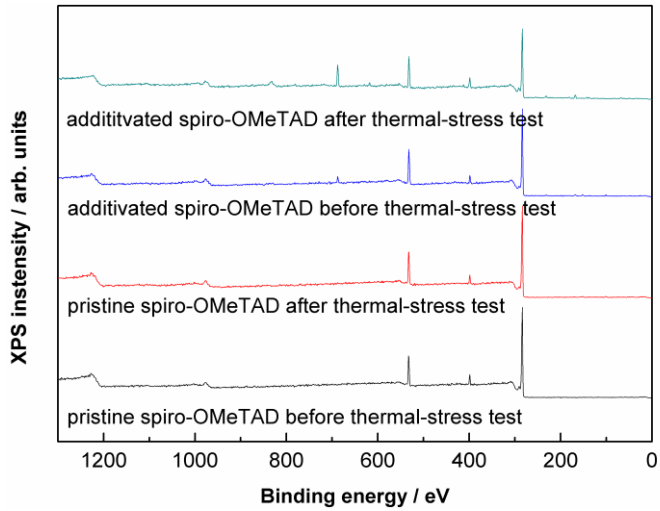

Figure 3.7. XPS survey spectra (Al Kα = 1486.6 eV) of pristine and additivated spiro-OMeTAD before and after thermal-stress tests.

The spectrum of pristine spiro-OMeTAD before thermal stress shows C 1s, O 1s and N 1s XPS peaks similar to those of the pristine spiro-OMeTAD spectrum after thermal stress. This means that no significant changes occur in the non-additivated HEL during tests. When comparing fresh pristine and additivated spiro-OMeTAD, it is observed a small peak at ~688 eV in this

sample, corresponding to the F 1s peak, attributed to the -CF_3 groups of Li-TFSI and FK209-TFSI additives. On the other hand, lithium, sulfur and cobalt (from FK209) should also display a detectable signature. Figure 3.8 zooms the spectra of the additivated sample, before and after thermal stress, for assessing Li 1s, Co 2p, F 1s and S 2p. The overlapping signals of C-H, C-C and C-N from spiro-OMeTAD and *t*-BP turns difficult the detection of *t*-BP additive in the XPS spectrum.[36]

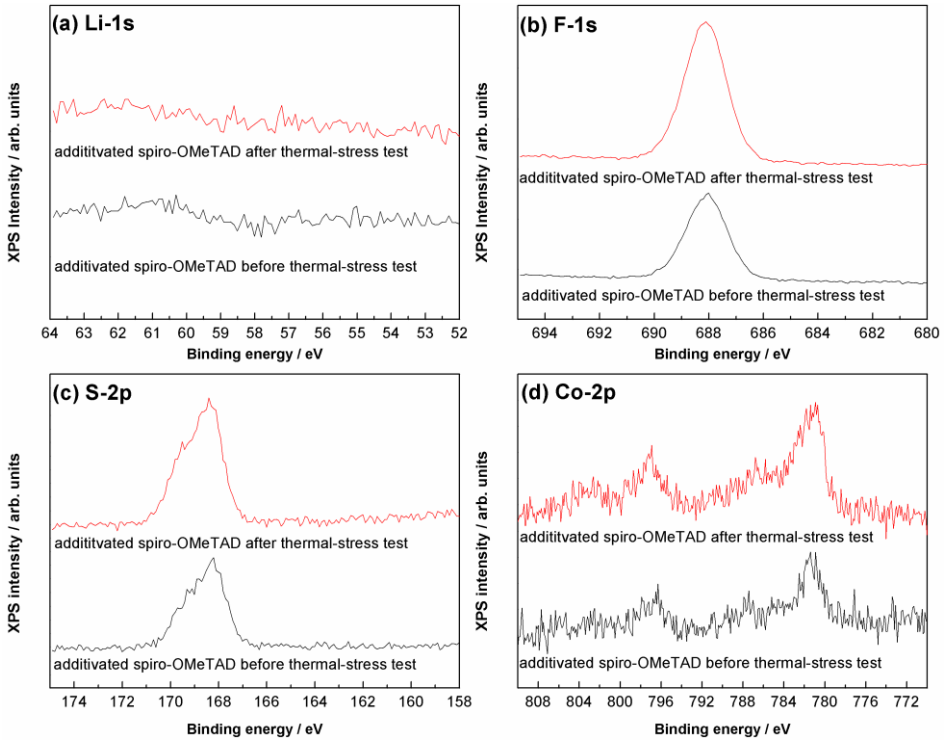

Figure 3.8. XPS spectra (Al Kα = 1486.6 eV) corresponding to (a) Li-1s, (b) F-1s, (c) S-2p and (d) Co-2p core levels of the spiro-OMeTAD films at room temperature before and after thermal-stress tests.

Changes in Li 1s region are undetectable because of low response sensitivity factor of lithium (RSF = 0.025) compared to the other elements (1 to F 1s, 0.668 to S 2p and 3.59 to Co 2p). In additivated spiro-OMeTAD, clear XPS signals of F 1s, S 2p and Co 2p are observed and their intensity increases after thermal stress. In particular, the atomic percentage of F increases from 6.5 % to 10.9 %; this increase evidences a migration phenomenon of these

elements to the surface of spiro-OMeTAD, promoted during the evaporation of volatiles during the thermal-stress tests.

Figure 3.9 shows the characteristic curves of a fresh cell using PTAA as hole extraction layer at room temperature (22 °C), under thermal stress at 80 °C, 70 °C, 60 °C and 50 °C, and back to room temperature. It can be seen that with PTAA the cell recovers mostly its original performance. Actually, this explains why PTAA has been reported to produce very stable cells with minimal PCE losses, even when running at 85 °C for 500 h, since these aged devices are then characterised at room temperature.[2] The photovoltaic performance as a function of the temperature shows no significant impact in J_{SC} for PTAA device but a strong decrease in the *FF* and V_{oc} is observed, as a consequence of an increase of series resistance. Khadka *et al*.[37] reported similar behavior mentioning that this can happen because a number of factors such as accelerated interfacial recombination, bulk defect activities or contact limited transport. When devices are submitted to high temperatures and then returned back to the room temperature, the additives evaporate and so the mobility of these aged HELs becomes closer to the pristine values. In fact, hole mobility of pristine PTAA (≈1 × 10^{-2} – 1 × 10^{-3} $cm^2 \cdot V^{-1} \cdot s^{-1}$)[38] is higher than pristine spiro-OMeTAD (1.6 × 10^{-5} $cm^2 \cdot V^{-1} \cdot s^{-1}$)[39] and so it is understandable that the irreversible loss is higher for the spiro-OMeTAD-based devices.

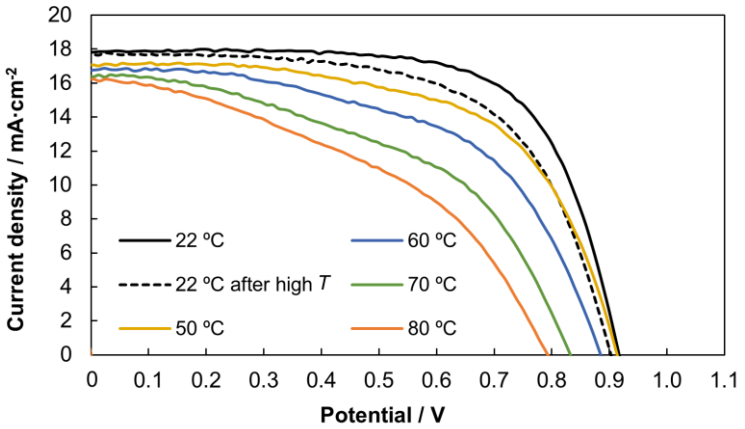

Figure 3.9. *I-V* curves of a representative device, with PTAA as HEL, operating at room temperature (22 °C) in the beginning of the test (black line) and after working at 80 °C (dashed line); and operating at 80 °C, 70 °C, 60 °C and 50 °C (coloured lines).

PTAA-based cells displayed an irreversible loss of PCE after thermal-stress of (8.2 ± 1.6) % which compares very favorably with the loss of (21.6 ± 2.3) % observed for the spiro-OMeTAD-based cells - Table 3.3. Interestingly, the PTAA-based cells display a higher decrease in PCE under 80 °C compared with spiro-OMeTAD-based cells.

Table 3.3. Loss and recovery of power conversion efficiency in different HEL tested in thermal stress-studies.

HEL	Decrease at 80 °C [%] - average	Irreversible loss[a] [%] - average
Spiro - OMeTAD	36.0 ± 5.5	21.6 ± 2.3
PTAA	48.2 ± 9.3	8.2 ± 1.6

[a] values at 22 °C, after high-temperature thermal-stress tests.

Similarly, to spiro-OMeTAD-based cells, pinholes were also visible in thermally stressed PTAA-based cells - Figure 3.10. PTAA also contains *t*-BP and Li-TFSI additives, so they will also volatilise with temperature. However, this may occur in less extension since additives are added to PTAA at lower concentration.

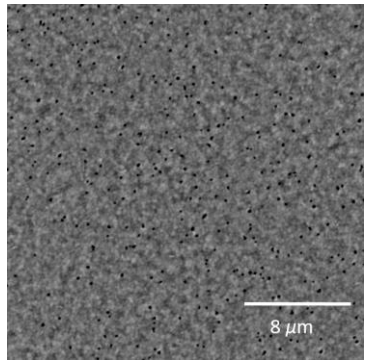

Figure 3.10. Top SEM micrographs of a mesoporous triple-cation perovskite solar cell with PTAA as HEL after thermal-stress tests.

After assessing the role of the HEL additives loss on the photovoltaic performance, it is now important to assess the role of the perovskite after the thermal-stress test and a possible degradation. According to some

authors,[40,41] the presence of additives and moisture exacerbates the degradation of perovskite absorber when the layer is in direct contact with spiro-OMeTAD. XRD diffractogram of devices with spiro-OMeTAD and PTAA after thermal-stress did not show any differences compared with XRD diffractogram at room temperature performed before encapsulation - Figure 3.11. Several devices were analyzed and none of them displayed PbI_2 peak, corresponding to (0 0 2) diffraction peak, common sign associated to the degradation of the perovskite crystal. These results indicate that there is no degradation on perovskite layer.

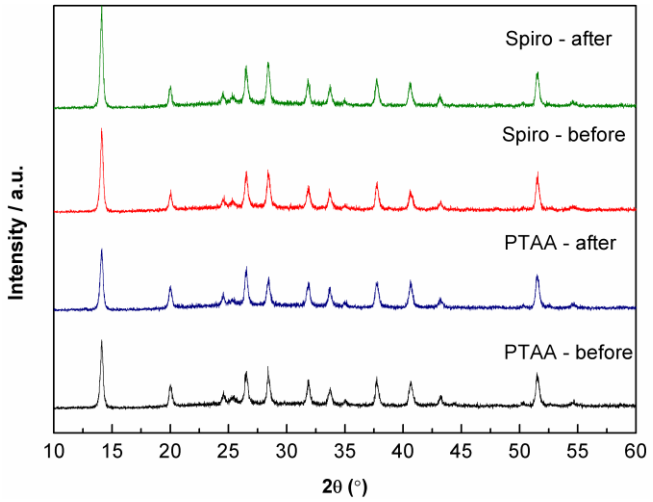

Figure 3.11. XRD diffractogram of triple-cation perovskite devices using PTAA and spiro-OMeTAD as HEL, before and after thermal-stress tests at 80 C°.

3.4 Conclusions

Temperature influence is critical for perovskite solar cells since during real conditions of outdoor operation the device can easily reach temperatures 45 °C higher than room temperature. Within this work PSC devices are exposed to thermal-stress in a range of temperatures between -5 °C and 80 °C to reproduce real operating conditions, allowing to investigate the temperature effect on the devices performance. The performance of mesoporous triple-cation perovskite cells displayed *ca*. 5 % less PCE at -5 °C when compared to 22 °C, which indicates a small sensitivity of this technology to low

temperatures; the thermally-stressed samples were then characterised at 22 °C, displaying essentially the same photovoltaic performance. However, at 80 °C it was observed a significant decrease in the V_{oc} and J_{sc}, leading to an average PCE decrease of (36.0 ± 5.5) %. Also, these thermally-stressed samples when characterised at 22 °C displayed an irreversible performance loss of (21.6 ± 2.3) %.

The roots of this performance loss were investigated. It was concluded that temperatures between -5 °C and 80 °C do not affect the perovskite layer since no peak of PbI_2 was observed in the XRD diffractogram; instead, the high-temperature stress test originates the evaporation of the additives presented in the HEL that is responsible for the irreversible performance loss. This conclusion was supported by the appearance of pinholes in the spiro-OMeTAD layer, observed by SEM, and by the percentage increase of elements like F, S and Co (characteristic XPS peaks of Li-TFSI and FK209 compounds) on the top surface of spiro-OMeTAD after thermal-stress test, observed by XPS. The migration of elements derived from volatiles evaporation. Also, it was observed at 80 °C that a PSC prepared with a spiro-OMeTAD layer without additives displays the same photovoltaic performance of a device prepared with additivated spiro-OMeTAD. Besides spiro-OMeTAD, PTAA is often used as HEL in PSC. The PTAA needs less additives when compared with spiro-OMeTAD, indicating a potentially better thermal stability. Actually, it was concluded that PTAA-based devices displayed an irreversible performance loss of only (8.2 ± 1.6) %. This reinforces the role of the additives on the PSC performance loss upon thermal-stress. Therefore, more efforts need to be done to devise thermally stable and highly conductive HELs.

Acknowledgements

I. Mesquita is grateful to FCT (Fundação para a Ciência e a Tecnologia) for her Ph.D. fellow (ref.: PD/PB/105985/2014). L. Andrade also acknowledges FCT for funding (IF/01331/2015). The research leading to these results has received funding from: European Union's Horizon 2020 Programme through a FET Open research and innovation action under Grant agreement no. 687008; project SolarPerovskite - NORTE-01-0145-FEDER-028966 funded by FEDER funds through NORTE 2020 - Programa Operacional Regional do NORTE - and by national funds (PIDDAC) through FCT/MCTES; project WinPSC (POCI-01-0247-FEDER-017796) co-funded by the European Regional Development Fund(ERDF), through the Operational Programme for Competitiveness and Internationalization (COMPETE 2020), under PORTUGAL 2020 Partnership Agreement; project BI-DSC: Building Integrated Dye Sensitized Solar Cells supported by the European Commission through the Seventh Framework Programme, the Specific Programme "Ideas" of the European Research Council for research and technological development as part of an Advanced Grant under grant agreement No.321315; POCI-01-0145-FEDER-006939 (LEPABE- UID/EQU/00511/2013), funded by the ERDF, through COMPETE 2020 and by national funds through FCT; and NORTE-01-0145-FEDER-000005 LEPABE-2-ECO-INNOVATION, supported by North Portugal Regional Operational Programme (Norte 2020), under the Portugal2020 Partnership Agreement, through the ERDF. The authors thank to Professor M. Grätzel for hosting I. Mesquita at EPFL to deepen the knowledge about PSC fabrication, to Rita Arnaldo and Bogdan Postolnyi for assisting SEM and XRD analysis, respectively, CEMUP and Prof. Carlos Sá for assisting the XPS analysis and Dr Cecilia Pedrero for help in XPS discussion.

References

[1] National Renewable Energy Laboratory, *www.nrel.gov/pv/cell-efficiency.html*, 2019.

[2] M. Saliba, T. Matsui, K. Domanski, J.-Y. Seo, A. Ummadisingu, S.M. Zakeeruddin, J.-P. Correa-Baena, W.R. Tress, A. Abate, A. Hagfeldt,

M. Grätzel, *Incorporation of rubidium cations into perovskite solar cells improves photovoltaic performance*, Science **354** (2016), p:206-209.

[3] M. Saliba, T. Matsui, J.-Y. Seo, K. Domanski, J.-P. Correa-Baena, M.K. Nazeeruddin, S.M. Zakeeruddin, W. Tress, A. Abate, A. Hagfeldt, M. Gratzel, *Cesium-containing triple cation perovskite solar cells: improved stability, reproducibility and high efficiency*, Energy & Environmental Science **9** (2016), p:1989-1997.

[4] H.S. Kim, C.R. Lee, J.H. Im, K.B. Lee, T. Moehl, A. Marchioro, S.J. Moon, R. Humphry-Baker, J.H. Yum, J.E. Moser, M. Grätzel, N.G. Park, *Lead iodide perovskite sensitized all-solid-state submicron thin film mesoscopic solar cell with efficiency exceeding 9%*, Scientific Reports **2** (2012), 591.

[5] M.M. Lee, J. Teuscher, T. Miyasaka, T.N. Murakami, H.J. Snaith, *Efficient hybrid solar cells based on meso-superstructured organometal halide perovskites*, Science **338** (2012), p:643-647.

[6] J.C.S. Costa, J. Azevedo, L.M.N.B.F. Santos, A. Mendes, *On the Deposition of Lead Halide Perovskite Precursors by Physical Vapor Method*, The Journal of Physical Chemistry C **121** (2017), p:2080-2087.

[7] X. Li, D. Bi, C. Yi, J.-D. Décoppet, J. Luo, S.M. Zakeeruddin, A. Hagfeldt, M. Grätzel, *A vacuum flash–assisted solution process for high-efficiency large-area perovskite solar cells*, Science 353 (2016), p:58-62.

[8] S.G. Hashmi, D. Martineau, X. Li, M. Ozkan, A. Tiihonen, M.I. Dar, T. Sarikka, S.M. Zakeeruddin, J. Paltakari, P.D. Lund, M. Grätzel, *Air Processed Inkjet Infiltrated Carbon Based Printed Perovskite Solar Cells with High Stability and Reproducibility*, Advanced Materials Technologies **2** (2017), 1600183.

[9] X. Jiang, Z. Yu, Y. Zhang, J. Lai, J. Li, G.G. Gurzadyan, X. Yang, L. Sun, *High-Performance Regular Perovskite Solar Cells Employing Low-Cost Poly(ethylenedioxythiophene) as a Hole-Transporting Material,* Scientific Reports **7** (2017), 42564.

[10] E.H. Anaraki, A. Kermanpur, L. Steier, K. Domanski, T. Matsui, W. Tress, M. Saliba, A. Abate, M. Gratzel, A. Hagfeldt, J.-P. Correa-Baena, *Highly*

efficient and stable planar perovskite solar cells by solution-processed tin oxide, Energy & Environmental Science **9** (2016), p:3128-3134.

[11] J. Liu, Y. Wu, C. Qin, X. Yang, T. Yasuda, A. Islam, K. Zhang, W. Peng, W. Chen, L. Han, *A dopant-free hole-transporting material for efficient and stable perovskite solar cells*, Energy and Environmental Science **7** (2014), p:2963-2967.

[12] N. Arora, M.I. Dar, A. Hinderhofer, N. Pellet, F. Schreiber, S.M. Zakeeruddin, M. Grätzel, *Perovskite solar cells with CuSCN hole extraction layers yield stabilized efficiencies greater than 20%*, Science **358** (2017), p:768-771.

[13] J. Song, L. Liu, X.-F. Wang, G. Chen, W. Tian, T. Miyasaka, *Highly efficient and stable low-temperature processed ZnO solar cells with triple cation perovskite absorber*, Journal of Materials Chemistry A **5** (2017), p:13439-13447.

[14] X. Li, J. Yang, Q. Jiang, H. Lai, S. Li, J. Xin, W. Chu, J. Hou, *Low-Temperature Solution-Processed ZnSe Electron Transport Layer for Efficient Planar Perovskite Solar Cells with Negligible Hysteresis and Improved Photostability*, ACS Nano **12** (2018), p:5605-5614.

[15] M.C. Alonso García, J.L. Balenzategui, *Estimation of photovoltaic module yearly temperature and performance based on Nominal Operation Cell Temperature calculations*, Renewable Energy **29** (2004), p:1997-2010.

[16] K.W. Tan, D.T. Moore, M. Saliba, H. Sai, L.A. Estroff, T. Hanrath, H.J. Snaith, U. Wiesner, *Thermally induced structural evolution and performance of mesoporous block copolymer-directed alumina perovskite solar cells*, ACS Nano **8** (2014), p:4730-4739.

[17] S. Kim, S. Bae, S.-W. Lee, K. Cho, K.D. Lee, H. Kim, S. Park, G. Kwon, S.-W. Ahn, H.-M. Lee, Y. Kang, H.-S. Lee, D. Kim, *Relationship between ion migration and interfacial degradation of $CH_3NH_3PbI_3$ perovskite solar cells under thermal conditions*, Scientific Reports **7** (2017), 1200.

[18] N.-K. Kim, Y.H. Min, S. Noh, E. Cho, G. Jeong, M. Joo, S.-W. Ahn, J.S. Lee, S. Kim, K. Ihm, H. Ahn, Y. Kang, H.-S. Lee, D. Kim, *Investigation of Thermally Induced Degradation in $CH_3NH_3PbI_3$ Perovskite Solar*

Cells using In-situ Synchrotron Radiation Analysis, Scientific Reports **7** (2017), 4645.

[19] Y. Han, S. Meyer, Y. Dkhissi, K. Weber, J.M. Pringle, U. Bach, L. Spiccia, Y.-B. Cheng, *Degradation observations of encapsulated planar $CH_3NH_3PbI_3$ perovskite solar cells at high temperatures and humidity*, Journal of Materials Chemistry A **3** (2015), p:8139-8147.

[20] Y. Fang, X. Wang, Q. Wang, J. Huang, T. Wu, *Impact of annealing on spiro-OMeTAD and corresponding solid-state dye sensitized solar cells*, Physica Status Solidi (A) Applications and Materials Science **211** (2014), p:2809-2816.

[21] T. Malinauskas, D. Tomkute-Luksiene, R. Sens, M. Daskeviciene, R. Send, H. Wonneberger, V. Jankauskas, I. Bruder, V. Getautis, *Enhancing Thermal Stability and Lifetime of Solid-State Dye-Sensitized Solar Cells via Molecular Engineering of the Hole-Transporting Material Spiro-OMeTAD*, ACS Applied Materials & Interfaces **7** (2015), p:11107-11116.

[22] A.K. Jena, Y. Numata, M. Ikegami, T. Miyasaka, *Role of spiro-OMeTAD in performance deterioration of perovskite solar cells at high temperature and reuse of the perovskite films to avoid Pb-waste*, Journal of Materials Chemistry A **6** (2018), p:2219-2230.

[23] H. Zheng, G. Liu, C. Zhang, L. Zhu, A. Alsaedi, T. Hayat, X. Pan, S. Dai, *The influence of perovskite layer and hole transport material on the temperature stability about perovskite solar cells*, Solar Energy **159** (2018), p:914-919.

[24] A. Magomedov, E. Kasparavičius, K. Rakstys, S. Paek, N. Gasilova, K. Genevičius, G. Juška, T. Malinauskas, M.K. Nazeeruddin, V. Getautis, *Pyridination of hole transporting material in perovskite solar cells questions the long-term stability*, Journal of Materials Chemistry C **6** (2018), p:8874-8878.

[25] E. Kasparavicius, A. Magomedov, T. Malinauskas, V. Getautis, *Long-Term Stability of the Oxidized Hole-Transporting Materials used in Perovskite Solar Cells*, Chemistry – A European Journal **24** (2018), p:9910-9918.

[26] K. Domanski, J.-P. Correa-Baena, N. Mine, M.K. Nazeeruddin, A. Abate, M. Saliba, W. Tress, A. Hagfeldt, M. Grätzel, *Not All That Glitters Is Gold: Metal-Migration-Induced Degradation in Perovskite Solar Cells,* ACS Nano **10** (2016), p:6306-6314.

[27] J. Macaira, I. Mesquita, L. Andrade, A. Mendes, *Temperature Role in the Recombination Reaction on Dye-Sensitized Solar Cells*, Physical Chemistry Chemical Physics **17** (2015), p:22699-22710.

[28] O. Rana, R. Srivastava, R. Grover, M. Zulfequar, M. Husain, M.N. Kamalasanan, *Charge transport studies in thermally evaporated 2,2',7,7'-tetrakis-(N,N-di-4-methoxyphenylamino)-9,9'-spirobifluorene (spiro-MeOTAD) thin film,* Synthetic Metals **161** (2011), p:828-832.

[29] D.M. Pai, *Transient Photoconductivity in Poly(N-vinylcarbazole)*, The Journal of Chemical Physics **52** (1970), p:2285-2291.

[30] W.D. Gill, *Drift mobilities in amorphous charge-transfer complexes of trinitrofluorenone and poly-n-vinylcarbazole,* Journal of Applied Physics **43** (1972), p:5033-5040.

[31] H. Bässler, Charge Transport in Disordered Organic Photoconductors a Monte Carlo Simulation Study, physica status solidi (b) **175** (1993), p:15-56.

[32] W. Brütting, S. Berleb, A.G. Mückl, *Device physics of organic light-emitting diodes based on molecular materials*, Organic Electronics **2** (2001), p:1-36.

[33] A.K. Jena, M. Ikegami, T. Miyasaka, S*evere Morphological Deformation of Spiro-OMeTAD in* $(CH_3NH_3)PbI_3$ *Solar Cells at High Temperature*, ACS Energy Letters **2** (2017), p:1760-1761.

[34] T. Leijtens, I.K. Ding, T. Giovenzana, J.T. Bloking, M.D. McGehee, A. Sellinger, *Hole transport materials with low glass transition temperatures and high solubility for application in solid-state dye-sensitized solar cells*, ACS Nano **6** (2012), p:1455-1462.

[35] C.D. Bailie, E.L. Unger, S.M. Zakeeruddin, M. Gratzel, M.D. McGehee, *Melt-infiltration of spiro-OMeTAD and thermal instability of solid-state dye-sensitized solar cells*, Physical Chemistry Chemical Physics **16** (2014), p:4864-4870.

[36] Z. Hawash, L.K. Ono, S.R. Raga, M.V. Lee, Y. Qi, *Air-Exposure Induced Dopant Redistribution and Energy Level Shifts in Spin-Coated Spiro-MeOTAD Films,* Chemistry of Materials **27** (2015), p:562-569.

[37] D.B. Khadka, Y. Shirai, M. Yanagida, J.W. Ryan, K. Miyano, *Exploring the effects of interfacial carrier transport layers on device performance and optoelectronic properties of planar perovskite solar cells*, Journal of Materials Chemistry C **5** (2017), p:8819-8827.

[38] W. Zhang, Y.-C. Wang, X. Li, C. Song, L. Wan, K. Usman, J. Fang, *Recent Advance in Solution-Processed Organic Interlayers for High-Performance Planar Perovskite Solar Cells*, Advanced Science **5** (2018), 1800159.

[39] J. Burschka, A. Dualeh, F. Kessler, E. Baranoff, N.-L. Cevey-Ha, C. Yi, M.K. Nazeeruddin, M. Grätzel, *Tris(2-(1H-pyrazol-1-yl)pyridine)cobalt(III) as p-Type Dopant for Organic Semiconductors and Its Application in Highly Efficient Solid-State Dye-Sensitized Solar Cells*, Journal of the American Chemical Society **133** (2011), p:18042-18045.

[40] J. Kim, N. Park, J.S. Yun, S. Huang, M.A. Green, A.W.Y. Ho-Baillie, *An effective method of predicting perovskite solar cell lifetime–Case study on planar $CH_3NH_3PbI_3$ and $HC(NH_2)_2PbI_3$ perovskite solar cells and hole transfer materials of spiro-OMeTAD and PTAA*, Solar Energy Materials and Solar Cells **162** (2017), p:41-46.

[41] Y. Dkhissi, H. Weerasinghe, S. Meyer, I. Benesperi, U. Bach, L. Spiccia, R.A. Caruso, Y.B. Cheng, *Parameters responsible for the degradation of $CH_3NH_3PbI_3$-based solar cells on polymer substrates*, Nano Energy **22** (2016), p:211-222.

CHAPTER 4

EFFECT OF RELATIVE HUMIDITY DURING THE PREPARATION OF PEROVSKITE SOLAR CELLS: PERFORMANCE AND STABILITY

Adapted from the article

Mesquita, I., Andrade, L., Mendes, A., *Effect of Relative Humidity during the Preparation of Perovskite Solar Cells: Performance and Stability*, submited to Solar Energy, June 2019.

4

EFFECT OF RELATIVE HUMIDITY DURING THE PREPARATION OF PEROVSKITE SOLAR CELLS: PERFORMANCE AND STABILITY

Abstract

Humidity is one of the main environmental factors that limits performance and stability of perovskite solar cells (PSC); it plays a critical role during the preparation of the perovskite film, influencing the crystal growth. In this work, it is investigated the effect of the relative humidity (RH) and type of atmosphere (nitrogen *vs* air) used during the deposition of both perovskite layer and hole extraction layer (HEL). While humidity and oxygen seem not to affect the HEL deposition step, the perovskite layer is notoriously influenced by the RH and by the presence of oxygen during its deposition. Until 10 % of RH, the performance of devices prepared with a triple-cation perovskite layer deposited under a nitrogen environment was mostly unaffected, whilst for devices deposited in air that limit is lower. On the other hand, for high RH values (above 30 %), devices prepared with a triple-cation perovskite layer deposited under N_2 presented slightly better stability over time than the ones prepared under air. Surprisingly, the best-performing device was prepared with a triple cation perovskite layer deposited under dry air, presenting a power conversion efficiency of 16.7 %. These results are of critical value when designing a plant for fabricating PSC, showing that the perovskite layer may be deposited under a simple dry air atmosphere (RH < 1 %).

4.1 Introduction

Power conversion efficiency (PCE), long-term stability and manufacturing costs represent the three vertices of the golden triangle for photovoltaic technologies. More than 90 % of the share on the commercialised photovoltaics (PV) is dominated by silicon panels presenting efficiencies of *ca*. 20 %, a lifetime of more than 25 years and low manufacturing costs of 0.3 $\$\cdot W^{-1}$.[1] PSC is probably the only PV technology that might rival the silicon monopoly; this technology emerged a decade ago and reached already a certified PCE of over 25 % at lab size.[2] Perovskite solar cells promise to display lower production costs than crystalline silicon with similar PCE.[3] However, PSC technology still needs to overcome the present major drawback: long-term stability. According to many authors, relative humidity (RH), temperature, oxygen and UV-light seem to play an important role on the device degradation, and for that reason it is very important to understand their degradation mechanisms.[4,5,6]

While some research groups allege that humidity is a problem for perovskite films, showing that at high levels of moisture the perovskite starts to degrade with formation of hydrate phases,[7,8] other groups defend that a certain level of humidity can actually improve the crystallinity of perovskite layer.[9,10] In the fabrication of high performance PSCs the quality of the grain boundaries at the perovskite layer can affect not only the PCE, but also the hysteresis. The formation of a high-quality perovskite layer depends on the deposition process but also on the atmosphere during the crystals growth. So, due to the hygroscopic nature of the most common perovskites, RH is a key factor controlling the crystal growth and later on the PSC performance.

The presence of humidity can affect the quality of the perovskite solar cell in different stages: the precursors solutions used to prepare the devices, during the fabrication of the cells and during the devices operation over time. Liu *et al*.[11] showed that the use of water-containing perovskite precursors ($CH_3NH_3PbI_{3-x}Cl_x$) and the exposure to high water content (25 vol.%) during the fabrication in air allow to obtain high performance cells with low moisture sensitivity and enhanced crystallisation. They also concluded that the water

contained in the precursor solution only limits the solubility of the precursors, but it does not influence the device performance.[11,12] Contreras-Bernal *et al*.[4] also observed this same effect for aged $CH_3NH_3PbI_3$ cells when prepared under high relative humidity, *ca*. 50 %, compared to the ones prepared under dry-conditions. On the other side, Wozny *et al*. [13] assessed the humidity effect during preparation of $FAPbI_3$ planar devices and concluded that the increase of the relative humidity during the preparation of the devices decreased the performance of fresh cells – from 16.4 % to 8.6 % of PCE at 40 % of RH. The humidity leads to the formation of voids at the perovskite layer, decreasing the open-circuit voltage and recombination resistance, leading to shorter carrier lifetimes. Similarly, Salado *et al*.[14] studied the moisture-induced degradation of triple-cation perovskite solar cells and concluded that aging devices by exposing them to moisture enhances interfacial charge accumulation that can accelerate the charge recombination rate. Emami *et al*.[15] proposed the hermetic encapsulation of the PSC devices based on a laser-assisted glass-frit sealing process performed at a process temperature of 120 °C. The sealing procedure was compatible with the requirements of the PSC, which displayed thermal stability after five cycles of a humidity-freeze between -40 °C and 85 °C, according to the IEC61646 standard.

As a result of these studies, concerning humidity-induced degradation of complete PSC devices, many researchers tried to overpass this problem by proposing new preparation methods that allow to prepare devices less-sensitive to moisture. Wang *et al*. [16] showed that the anti-solvent method using diethyl ether can be humidity insensitive since the fast solvent removal minimize the influence of humidity on the crystallization process. Troughton *et al*.[17] obtained similar results using ethyl acetate as anti-solvent, which can also protect the perovskite precursor intermediate phase during the spin-coating step due to its ability to sequester airborne moisture. Liu *et al*. [18] also increased the stability of the PSC to the humidity by improving the perovskite crystallisation step: a perovskite-like metal formate (PLMF) was used into the perovskite precursor solution as a scaffold additive to achieve a well-organised crystalline and compact morphology. As a consequence, improved grain boundaries were formed, suppressing hole-electron recombination and defect

points usually originated by humidity exposure. PSCs with 3 $mg \cdot ml^{-1}$ of PLMF maintained 85 % of their initial performance after 1000 h of exposure to (40 ± 5) % of RH. Another strategy considers the use of passivation layers of organic polymers and Al_2O_3 deposited on top of the perovskite layer as a way to protect it from moisture.[19,20,21]

The majority of studies reported until now assess single-cation perovskite ($CH_3NH_3PbI_3$ or MAPI) stability against moisture during aging experiments. Moreover, triple-cation perovskite based solar cells start now to be the standard configuration as it allows obtaining efficient, stable and reproducible devices. Therefore, it is important to understand how humidity affects triple cation based-devices, still during preparation. This work analyses three different scenarios, all relevant for designing a production plant of PSC: i) water content in the solvents used for preparing the devices, resulting from the contact with a humidified atmosphere; ii) different levels of ambient humidity during preparation of devices (0-50 % of RH) and; iii) effect of ambient humidity on the long term stability of prepared cells (~1000 h). Besides, it was also investigated the combination of humidity with nitrogen and air atmospheres in the glove box. Two perovskite compositions were tested, $CH_3NH_3PbI_3$ and $Cs_{0.05}(MA_{0.17}FA_{0.83})_{0.95}Pb(I_{0.83}Br_{0.17})_3$, both prepared by anti-solvent method with chlorobenzene. The effect of RH and carrier gas in the hole extraction layer, spiro-OMeTAD, was also studied. The humidity effect was assessed based on the photovoltaic performance of several batches of devices, and the morphology and crystallinity were analysed by SEM and XRD, respectively. The relation between photovoltaic performance, morphology and structural analysis allowed to conclude about the main degradation pathways of devices prepared under different humid environments, but also about the boundary conditions that can be used until the perovskite films start to degrade or the device performance starts to significantly decrease.

4.2 Materials and Methods

4.2.1 Preparation of Perovskite Solar Cells

The preparation procedure of the perovskite solar cells were similar to those outlined by the authors elsewhere.[6] Fluorine-doped tin oxide (FTO) glass substrates (TCO -7, 7 $\Omega \cdot \square^{-1}$, Solaronix, Switzerland) were cleaned with a 10 % Hellmanex III (Hellma GmbH, Germany) solution, then with a potassium hydroxide saturated solution and finally with water in an ultrasonic bath, 15 min each step, followed by drying under a stream of air and treatment with UV-ozone for 15 min (UVO cleaner from Jelight Company, Inc.). A thin and compact layer of TiO_2 was deposited by spray-pyrolysis at 450 °C, using a precursor solution of titanium diisopropoxide bis(acetylacetonate) in anhydrous 2-propanol. The compact layer was then kept at 450 ºC for 45 min for the formation of anatase phase. Once the substrates achieved the room temperature, TiO_2 paste (Dyesol, 30 NR-D) was spin-coated on top of the compact layer at 5000 rpm for 10 s and immediately placed at 125 °C. After drying at 125 °C for 10 min, the film was annealed at 500 °C for 30 min. After the TiO_2 sintering, the samples were immediately placed inside the glove box before cooling down, in order to prevent moisture adsorption.

Two types of perovskite were used in this study. The triple-cation perovskite ($Cs_{0.05}(MA_{0.17}FA_{0.83})_{0.95}Pb(I_{0.83}Br_{0.17})_3$) was prepared from a precursor solution containing formamidinium iodide (FAI - 1 M), lead iodide (PbI_2 - 1.1 M), methylammonium bromide (MABr - 0.2 M) and lead bromide ($PbBr_2$ - 0.2 M) in anhydrous N,N-dymethylformamide:dimethyl sulfoxide (DMF:DMSO 4:1 (v:v)). After the total dissolution of all the components, 5 % in volume of a 1.5 M cesium iodide (CsI) solution in DMSO was added to the initial solution. The $CH_3NH_3PbI_3$ perovskite precursor was prepared mixing 1.4 M of PbI_2 with MAI (1:1 mol.%) in DMSO. In both cases the perovskite layer was deposited by spin-coating at 1000 rpm during 10 s, followed by 30 s at 6000 rpm; 15 s before the end of second step, 150 μL of chlorobenzene was deposited on top of the spinning substrate. In the triple-cation perovskite a brownish colour immediately appears, whilst for $CH_3NH_3PbI_3$ the darkening of the layer only occurs when the substrate is placed in the hot plate. After spinning, the

substrates were placed in a hot-plate at 100 °C during 40 min. During the preparation of perovskite layer, different RH (0 - 50 %) and different carrier gas (N_2 and air) were tested.

On top of perovskite layer, a thin layer of spiro-OMeTAD (102 mg of spiro-OMeTAD, 40 μL of 4-*tert*-butylpyridine (*t*-BP), 23 μL of lithium bis(trifluoromethanesulfonyl)imide (Li-TFSI) solution (520 mg of Li-TFSI in 1 mL of acetonitrile) and 40 μL of FK209 (tris(2-(1H-pyrazol-1-yl)-4-tert-butyl pyridine)cobalt(III)tri[bis(trifluoromethane)sulfonimide]) solution (40 μg in 100 μL of acetonitrile) dissolved in 1.116 mL of chlorobenzene) was deposited by spin-coating at 4000 rpm for 20 s. The deposition of HEL in devices with perovskite layer prepared with different RH was performed inside a N_2 dry glove box (MBraun, Germany). However, the effect of RH and carrier gas on the HEL deposition was also studied. Finally, *ca*. 60 nm gold electrode was thermally-evaporated on top of spiro-OMeTAD layer.

4.2.2 Characterisation and experimental setup

The devices were characterised right after their preparation, at room temperature and ambient air. For stability tests, the best-performing devices were selected and tested along 6 weeks (~1000 h). Two batches of cells prepared at same humidity were always kept in two different places: inside the dry glove box with N_2 and outside with ambient atmosphere. The devices were always kept in the dark. The simulator was calibrated using a single crystal Si photodiode (Newport, USA). The *I-V* curves were obtained by applying an external potential load and measuring the generated photocurrent using a Zennium (Zahner Elektrik, Germany) workstation controlled by the Thales software package (Thales XT 5.1.4).

Scanning electron microscopy (SEM) was carried out on a Quanta 400 FEG (FEI Company, USA); the acceleration voltage was 15 keV while an in-lens detector was employed with a working distance of about 10 nm. The surface of samples was examined in order to identify and analyse modifications in their morphology. X-ray diffraction (XRD) patterns of perovskite layers were

acquired in a PANalytical X'Pert MPD (Spectris plc, England) equipped with an X'Celerator detector and secondary monochromator (Cu Kα λ = 0.154 nm, 40 kV, 30 mA; data recorded at a 0.017 step size, 10 s·step^{-1}).

4.3 Results and discussion

4.3.1 Effect of humidity on precursor solutions

The effect of water content on the precursor solutions was assessed. For that, the solvents used to prepare the perovskite layer, namely DMF, DMSO and chlorobenzene, were left opened under dry conditions (RH < 0.5 ppmv) and under 15 %, 45 % and 60 % of relative humidity inside a hermetically sealed chamber during 52 h. The required humidity inside the chamber were achieved with saturated salt aqueous solutions: potassium hydroxide, sodium bromide and potassium bromide for 15 %, 45 % and 60 % of RH, respectively.[22] The relative humidity inside the chamber was measured with a hygrometer (Vaisala, DryCap® hand-held dewpoint meter DM70). After that, the solvents were used to prepare the triple-cation perovskite deposited inside a nitrogen dry glove box as described in the experimental section. The contact of these solvents with humidified atmospheres does not seems to affect the performance of the prepared devices, as observed in Table 4.1.

Table 4.1. Photovoltaic parameters of complete PSC devices prepared with humidified solvents at different RH (0, 15, 45 and 60 %).

% of RH	V_{oc} / V	J_{sc} / mA·cm^{-2}	*FF*	η / %
0	1.04 ± 0.02	18.4 ± 0.6	0.720 ± 0.020	14.6 ± 0.7
15	1.02 ± 0.01	18.4 ± 0.2	0.708 ± 0.023	14.1 ± 0.5
45	1.03 ± 0.02	18.8 ± 0.7	0.722 ± 0.015	14.8 ± 0.8
60	1.02 ± 0.01	18.8 ± 0.5	0.700 ± 0.022	14.0 ± 0.6

4.3.2 Effect of humidity during the preparation of perovskite layer

To investigate the role of the atmosphere humidity during the perovskite deposition step, it is important to distinguish its effect on the perovskite film

crystallisation or the repercussion on subsequent device degradation. Actually, the presence of moisture may influence not only the formation of perovskite film during the crystallisation phase, but it may also have a long-term detrimental effect in a fully crystallised film, leading to its degradation. So, different levels of humidity were used during the preparation of triple-cation perovskite layer deposited inside an in-house built glove box fed with a mixture of two streams of N_2: one dry and one saturated with humidity, for obtaining relative humidity values between 0 and 40 % - Figure 4.1. A hygrometer was used to measure the humidity inside the glove box and a water bubbler was placed at the exit to prevent the gas to return back to the glove box.

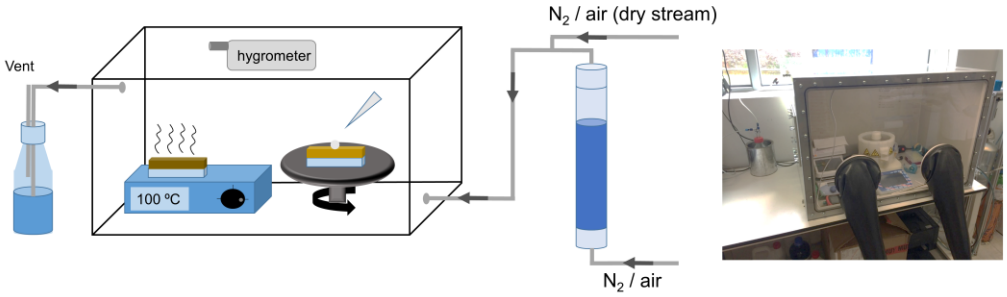

Figure 4.1. Scheme of the in-house built glove box used to control the RH during the perovskite layer deposition and sintering.

After achieved the required humidity level, the triple-cation perovskite layer was deposited by anti-solvent method using chlorobenzene. All other layers were deposited inside the N_2 dry glove box as described in the experimental section. The corresponding photovoltaic performance parameters for the range of RH studied are shown in Figure 4.2. For all batches prepared at different RH, it was also prepared a batch of cells made inside the dry glove box for reference, noted in Figure 4.2 as “0 %”. No significant performance differences are noticed for 5 % and 10 % under nitrogen atmosphere, being the average PCE of *ca*. 14 %. However, at relative humidity higher than 10 %, short-circuit current density, J_{sc}, and open-circuit voltage, V_{oc}, of the devices drastically decrease, reaching PCE values of about half of the PCE value obtained at 0 %

of RH. This means that until 10 % it is possible to produce devices with no performance changes.

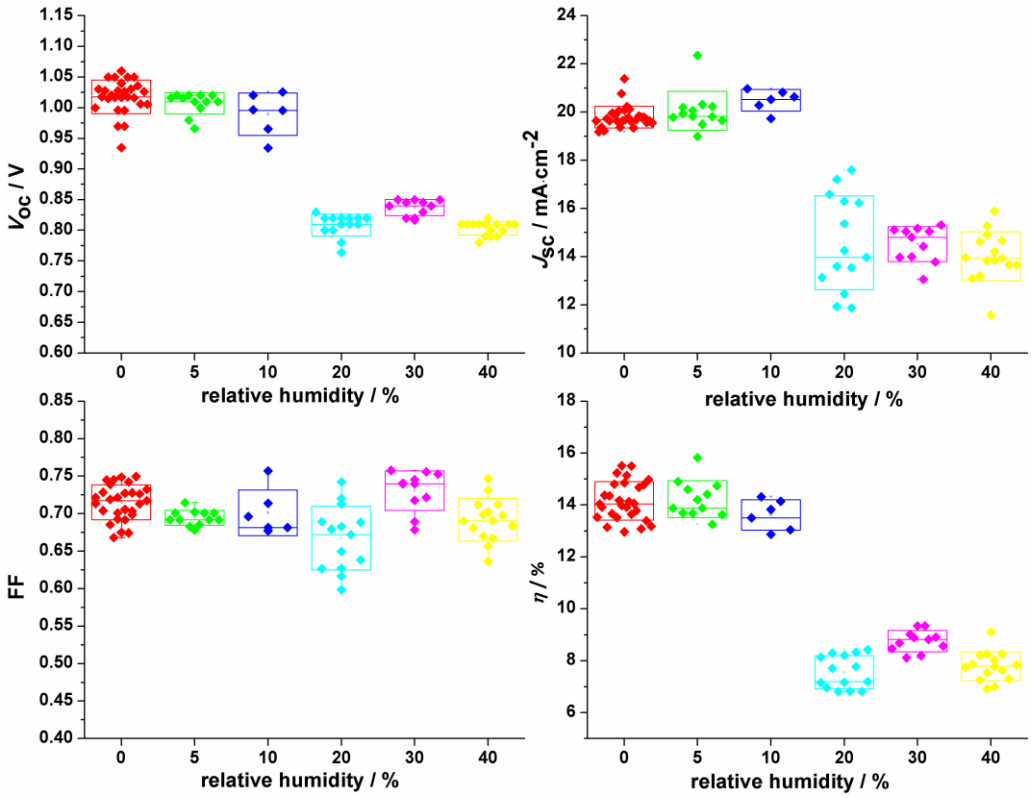

Figure 4.2. Photovoltaic performance of complete PSC devices with triple-cation perovskite layer prepared at different relative humidity (0 - 40 %) under nitrogen atmosphere.

The SEM image of the perovskite layer prepared at 0 % of RH under nitrogen atmosphere shows very distinct cubic crystallites with good connectivity between the grains and grain size between 100 and 200 nm - Figure 4.3. On the other hand, the perovskite layer prepared at 40 % of RH shows melted grain boundaries. This grain boundary blurry is due to the high humidity (~9840 ppmv) during the deposition and sintering of the perovskite layer, that also forms large gaps between crystals. Those gaps in the perovskite layer expose the mesoporous TiO_2 scaffold to the direct contact

with the HEL, enabling internal shunts that decrease the performance of the device.[13]

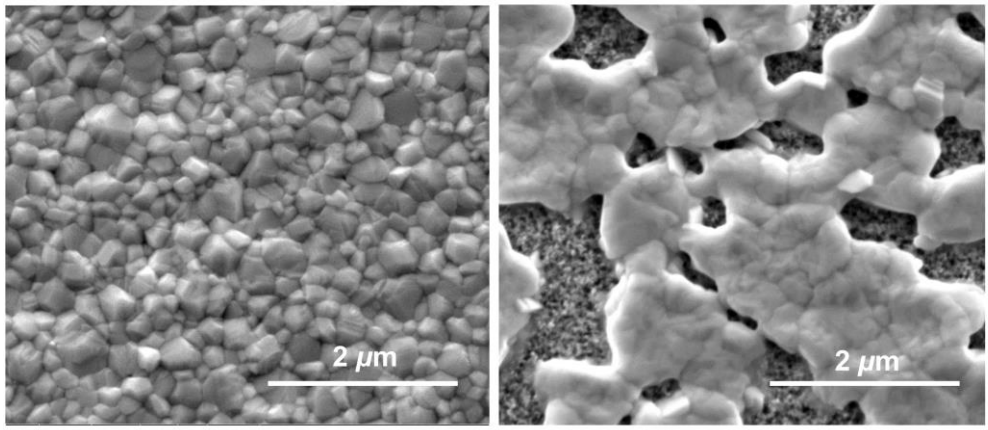

Figure 4.3. Top SEM micrographs of triple-cation perovskite layer prepared under nitrogen atmosphere at 0 % (left) and at 40 % (right) of RH.

Remarkably, the preparation of perovskite layer under high relative humidity seems to have a stabilizing effect on the device performance over time - Figure 4.4. It is possible to observe that at high relative humidity (40 %) the cells kept inside – Figure 4.4a - and outside – Figure 4.4b - the glove box show very stable PCE. Devices prepared in a more humid environment tend to keep their electric original properties better than those prepared at lower moisture conditions.[4] Devices prepared with 0 % and 5 % of RH also present very stable performance over time. The majority of the devices presented in Figure 4.4b suffer from a slight loss in the PCE after one week (168 h); however, that loss is more pronounced in the devices with perovskite layer deposited at 20 % of RH, which loose almost 35 % of the initial PCE. Triple-cation cells prepared under low relative humidity (0 and 5 %) and nitrogen atmosphere, present no sensitivity to oxygen environment along the time, since no differences are observed between devices kept inside or outside the dry glove box. Surprisingly, for RH of 30 % and 40 % the cells kept inside the glove box were very stable when compared with devices stored under ambient conditions. On

the other hand, the loss of performance for 10 % and 20 % of RH samples, independently of the storage conditions, is quite severe.

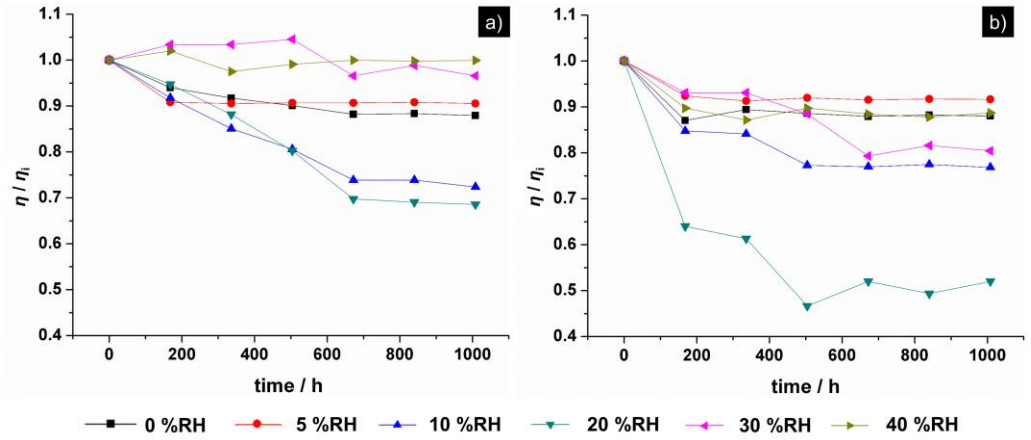

Figure 4.4. Performance history of the devices with perovskite layers prepared with different values of relative humidity and under nitrogen atmosphere. The devices were kept under dark: a) inside the glove box (dry N_2) and b) outside the glove box (air with 30 - 40 % of RH) - average values.

The use of an inert atmosphere during the preparation of the perovskite layer, allowed to conclude that the increase in the RH affects the crystal growth of the triple-cation perovskite, decreasing the uniformity of the layer and consequently the performance of the device. However, devices prepared with 40 % of RH present better stability over time, not only in an inert environment, but also under ambient conditions. The use of a completely dry environment is not necessary to achieve good performances with triple-cation PSC; up to 10 % of RH it was possible to achieve good performing devices with average PCE of (13.6 ± 0.5) %.

4.3.3 Combined effect of humidity and oxygen during the preparation of perovskite layer

To assess the effect of using air instead of dry and inert atmosphere in the production of PSCs is very important since it may allow a simpler deposition process. Figure 4.5 shows the performance values and statistics of the devices

prepared with perovskite layer deposited under atmospheric air and RH between 0 and 50 %.

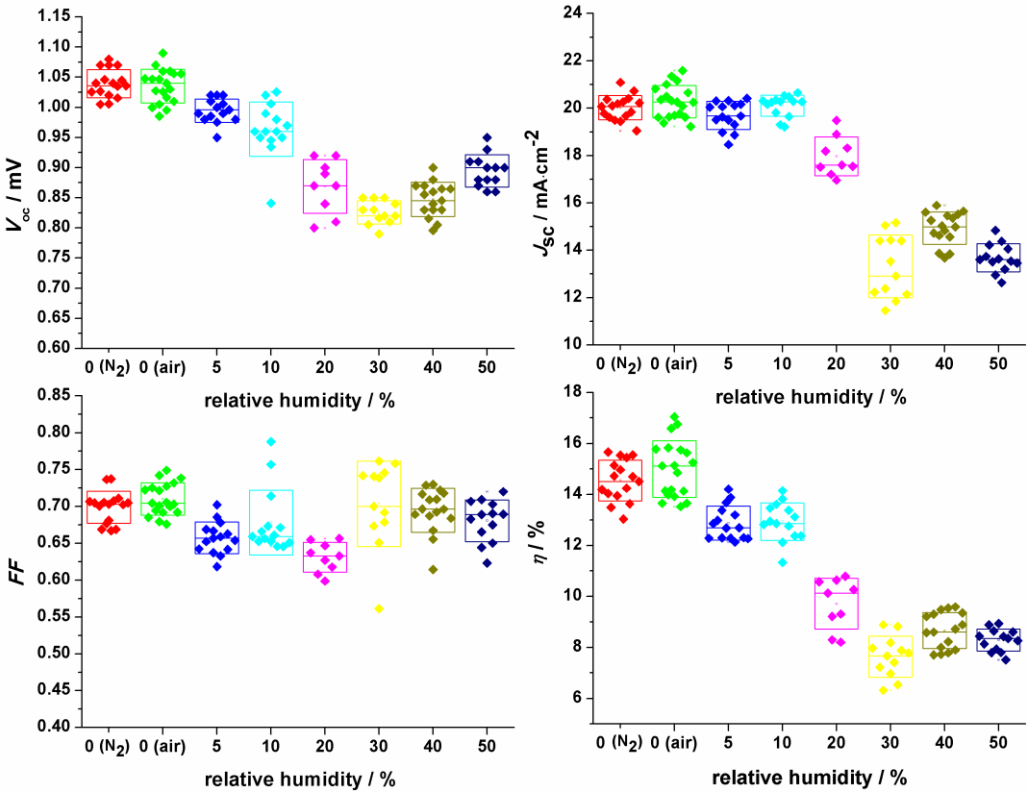

Figure 4.5. Photovoltaic performance of complete PSC devices with triple-cation perovskite prepared under different relative humidity air conditions (0 - 50 %). The values of devices prepared under dry N_2 were also included in the figure.

Although the use of dry air as carrier gas improves slightly the PCE of the triple-cation PSC; the humidity increase is responsible for a PCE decrease, even for 5 % of RH. The PCE difference obtained for 0 % of RH [(15.0 ± 1.1) %)] and 5 % of RH [(12.9 ± 0.6) %] air atmosphere is more pronounced. As it is possible to conclude from Figure 4.6 the decrease in the PCE can be attributed to changes in the perovskite film crystallinity and morphology. At 5 % of RH the film presents smaller crystals than in dry air, with numerous grain boundaries, resulting in a lower carrier transport and consequently lower PCE.[23] As observed before, when nitrogen was used as carrier gas at high RH (Figure 4.3), it is also possible to see the mesoporous

underlayer, which in contact with the HEL promotes recombination. In the case of air, 50 % of RH was also tested since it was observed a slight improvement in the performance of the PCS prepared at 40 % compared to the ones prepared at 30 % of RH; however, the performance does not increase and it was similar as for 40 % of RH.

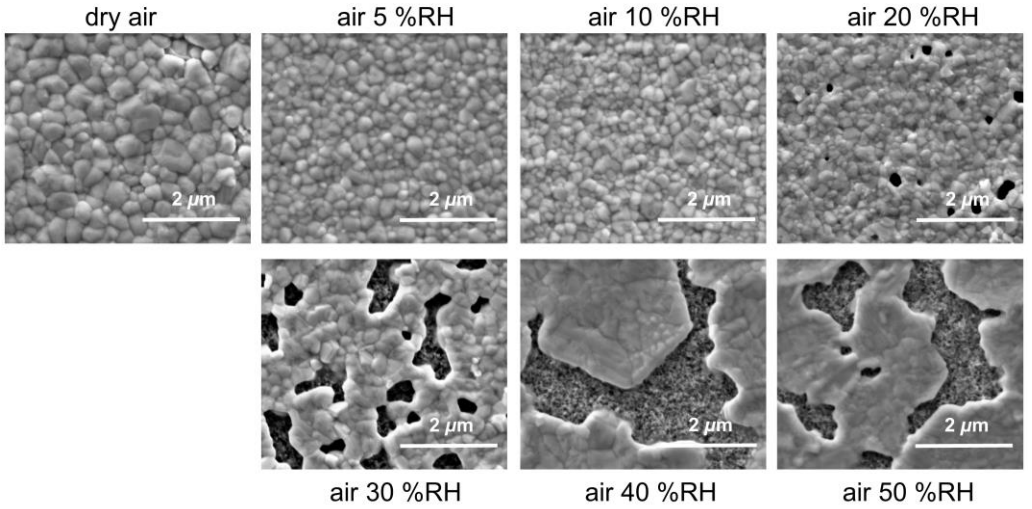

Figure 4.6. Top SEM micrographs of triple-cation perovskite layer prepared in air with different RH.

The UV-vis absorption spectra for all the RH were recorded and plotted in Figure 4.7. Higher RH is responsible for lower light absorption; at naked eye, it was indeed possible to observe that at higher RH the films were more transparent and lighter brownish. Close to the band edge – Figure 4.7inset – all the films show a sharp decrease in the absorbance; however, at RH higher than 40 % it is possible to observe a more gradual decay in the absorbance, which is consistent with the reduced crystallinity shown by the lower XRD peak intensities – Figure 4.8. In Figure 4.8, (0 0 2) diffraction peak at 12.7° related to PbI_2 is not present in none of the samples, meaning that the decrease in the PSC performance is not related to the perovskite decomposition. The major difference observed in Figure 4.8 is on the intensity decrease of the characteristic diffraction peaks of the tetragonal perovskite phase (14.1°, 28.5°

and 31.9°)[14] with the humidity; this is related to the decrease in the size of the coherent scattering domains,[24] and thus the formation of smaller grain crystals. The conclusion is in straight agreement with SEM images - Figure 4.6.

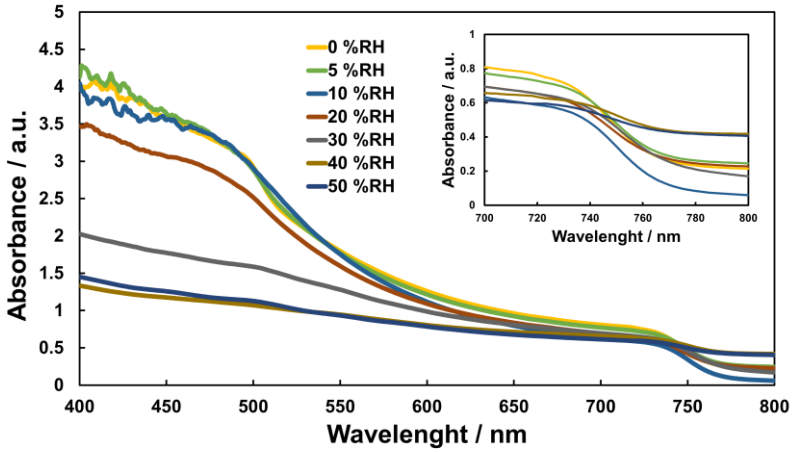

Figure 4.7. UV- vis absorption spectra for triple-cation perovskite films prepared under air and different RH.

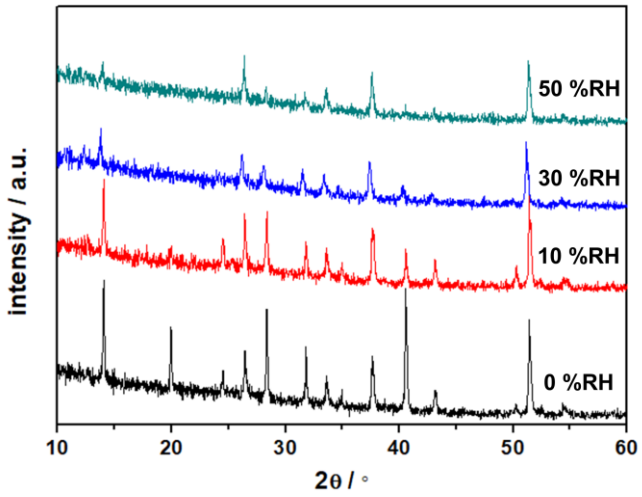

Figure 4.8. XRD diffractogram of triple-cation perovskite prepared under air and at different RH.

The stability of the devices prepared under air at different RH is plotted in Figure 4.9. Devices prepared with higher RH (40 % and 50 %) and kept inside

the glove box showed better stability over time. However, for low RH, the devices degrade faster when compared with devices prepared under inert atmosphere; losses of *ca*. 15 % against *ca*. 10 %.

For the devices kept outside the glove box, it is evident that they degrade easily and without any specific trend.

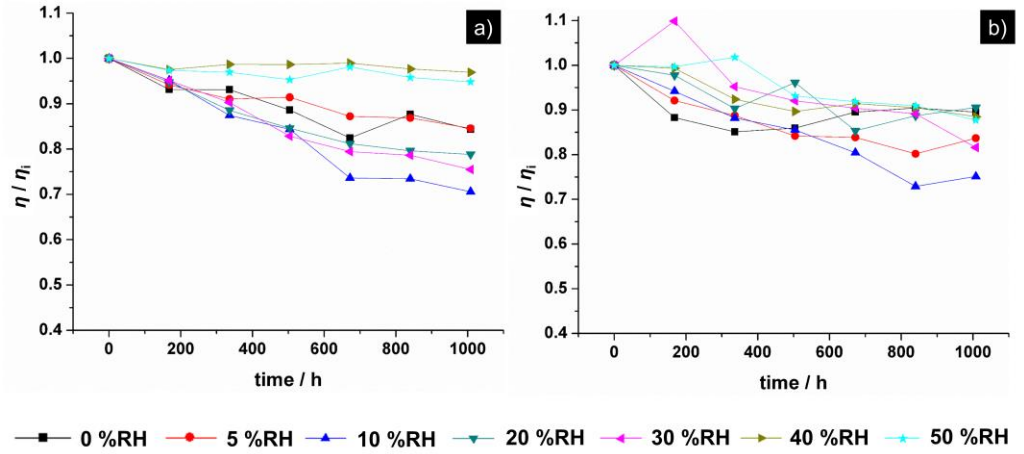

Figure 4.9. Performance history of the devices prepared with perovskite layer prepared under different values of relative humidity with air as carrier gas. The devices were kept under dark: a) inside the glove box (dry N_2) and b) outside the glove box (air with 30-40 % of RH) – average values.

4.3.4 Combined effect of humidity and oxygen on the HEL

The humidity affects mostly the perovskite layer, however the HEL used in this work, spiro-OMeTAD, is highly hydrophilic due to the Li-TFSI additive used to increase its hole conductivity. Although, many other HEL emerged as substitutes,[25,26] spiro-OMeTAD is still the most used HEL in the high-performing PSCs. Therefore, it is important to understand the role of oxygen and humidity during the deposition step of the spiro-OMeTAD. To assess the impact of these two factors, the triple-cation perovskite layer was prepared in the N_2 dry glove box and only the spiro-OMeTAD layer was deposited in the in-house built glove box. Figure 4.10 compares the *I-V* curves of the devices prepared under the two limiting scenarios: with spiro-OMeTAD layer deposited under dry N_2 atmosphere and under humidified air at 50 % of RH. As it is

possible to see, even in the worst-case scenario of high RH and presence of oxygen the performance of the devices was not affected. This means that spiro-OMeTAD does not need to be deposited in a dry and inert atmosphere.

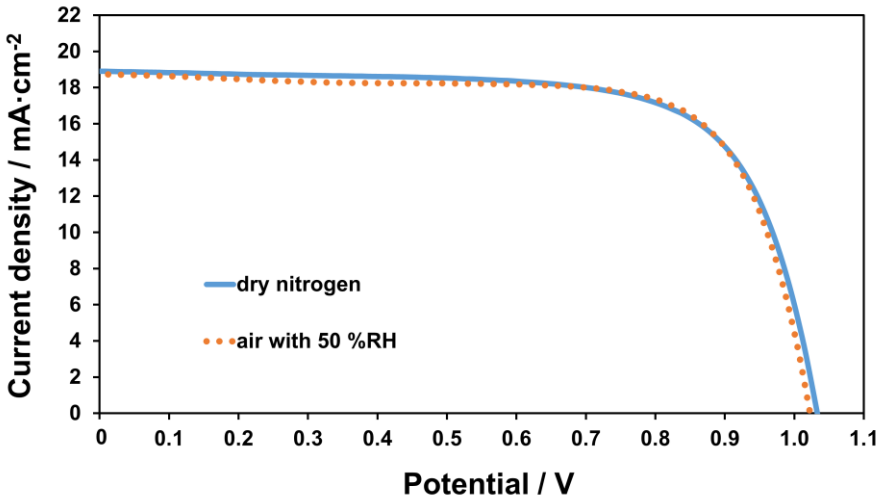

Figure 4.10. *I-V* curves of representative devices prepared with spiro-OMeTAD layer deposited under dry N_2 atmosphere (blue solid line) and in air with 50 % of RH (orange dashed line).

Spiro-OMeTAD suffers from low hole mobility and conductivity in its pristine form and to circumvent this drawback, researchers use additives that modify the electrical properties of this material. The most used additives are *t*-BP, Li-TFSI and FK209; while *t*-BP improves the formation of the HEL layer reducing the pinholes and avoiding the aggregation of Li-TFSI salt by favoring its distribution,[27] Li-TFSI oxidise the spiro-OMeTAD increasing its conductivity.[28] Later on, the spiro-OMeTAD was formulated also with FK209 since it produces an effective electron transfer to the electron acceptor, leaving the HEL partially oxidized (radical cation).[29] This formation of additional holes, with consequently higher carriers density, allows to obtain devices with better performances. However, from the present results, the use of FK209 did not affect the performance of the devices, neither in N_2 - Figure 4.11a nor in air - Figure 4.11b. This may indicate that for moderate PCE this additive might not be essential.

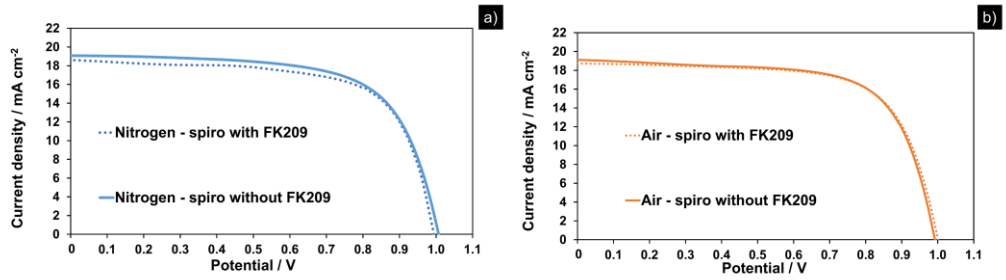

Figure 4.11. *I-V* curves of representative devices prepared with spiro-OMeTAD layer deposited in: a) dry N_2 with FK209 (blue dashed line) and without FK209 (blue solid line); and in b) dry air with FK209 (orange dashed line) and without FK209 (orange solid line).

4.3.5 Combined effect of humidity and oxygen in $CH_3NH_3PbI_3$ perovskite

Triple-cation based devices prepared under 10 % of RH in inert atmosphere or under dry air exhibited good and stable performances. So, it is important to understand if a similar behaviour is also observed for other types of perovskites. $CH_3NH_3PbI_3$ (normally called MAPI) devices were prepared under air and RH of 0 %, 10 %, 30 % and 50 % and the corresponding photovoltaic performance assessed. Figure 4.12 shows the photovoltaic parameters and statistics of the devices prepared; the results of the devices prepared under dry N_2 are also included.

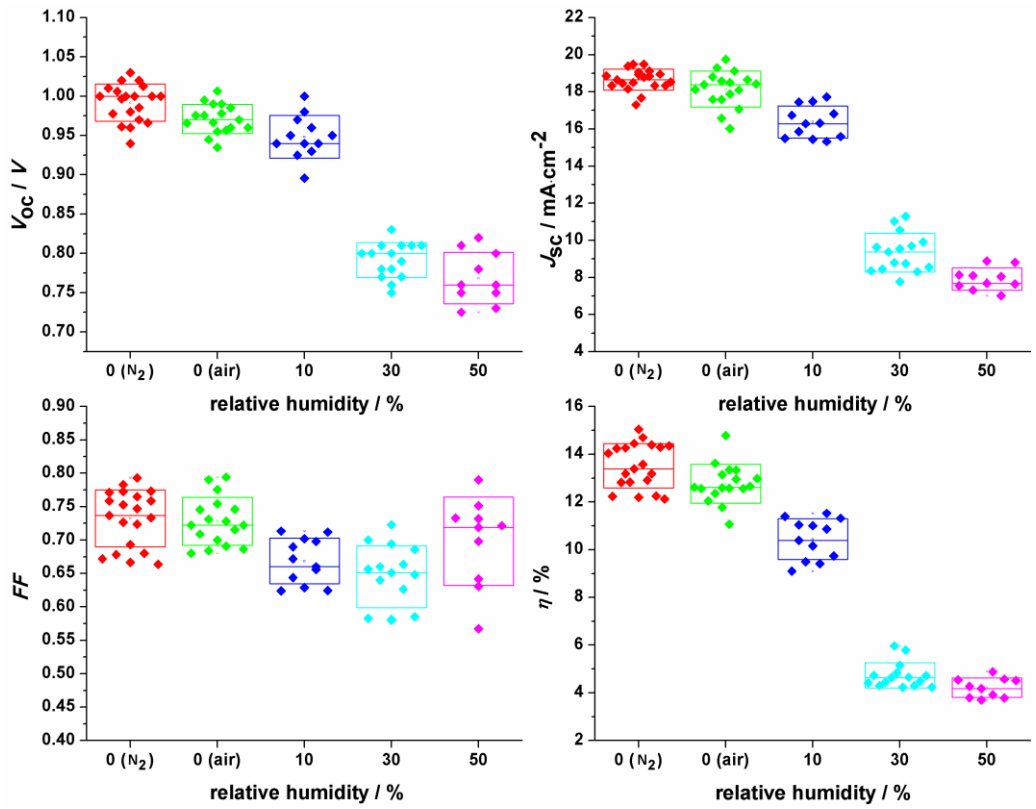

Figure 4.12. Photovoltaic performance of complete PSC devices with MAPI perovskite layer prepared at different RH (0 % - 50 %) under air and dry nitrogen atmospheres.

It is possible to conclude from Figure 4.5 and Figure 4.12 that MAPI devices are globally much more sensitive to the ambient moisture and oxygen presence; they also show lower PCE than triple cation. MAPI devices reached PCE of (13.5 ± 0.9) % under dry nitrogen and (12.8 ± 0.8) % under dry air, while for triple cation devices the PCE was higher, (14.5 ± 0.8) % and (15.0 ± 1.1) %, respectively.

Figure 4.13 shows the top SEM micrographs of MAPI perovskite layer prepared under air and different relative humidity. As the humidity increases, poorer MAPI coverage is observed, indicating that the increase of humidity reduces the film coverage density. The observed pinholes introduce a greater number of shunt pathways, which may explain the reduction of J_{sc} and V_{oc} for devices with MAPI deposited at higher RH. According to Clegg *et al.*,[10] larger

grain sizes may be followed by increased film roughening in the z-direction, leading to incomplete coverage by the spiro-OMeTAD layer and therefore recombination at the interface between the MAPI layer and the gold contact. These were actually the arguments to develop the triple-cation perovskite, which became a standard material, enabling simultaneously high performance and stability against moisture. The cesium cation suppresses yellow phase impurities and induces highly uniform perovskite grains even at not fully dry atmospheres.[30]

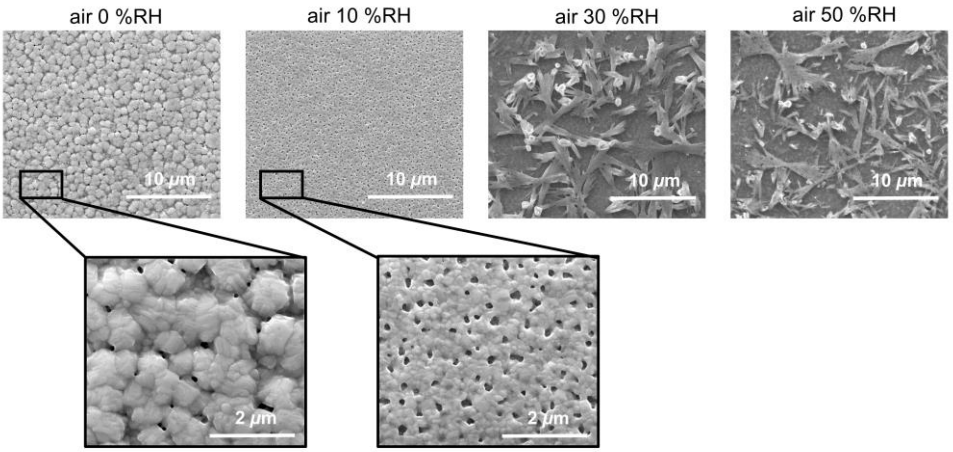

Figure 4.13. Top SEM micrographs of MAPI perovskite layer prepared under air and different relative humidity.

At naked eye it was observed that the colour of the perovskite layer during sintering changes from brown to yellow, for higher RH, evidencing the presence of PbI_2. Cronin *et al*.[31] had demonstrated that the sintering time in the presence of moisture (*e.g*. in ambient air) should be different of the time normally used for the sintering under inert atmospheres; still, and in order to allow comparisons, it was used the same sintering time for preparing both perovskite structures (~40 min). Right after placing the substrate on the hot-plate it changes for brownish colour, what is expectable when the crystals start forming. However, at the end of the sintering step the device presented a yellowish appearance. This means that during the sintering step and in the presence of moisture the perovskite layer started to decompose. This

corroborates the idea that the RH inside the glove box not only influences the crystals growth, but also their decomposition.

Regarding the stability of MAPI devices, once again PSCs were divided in two groups and some were kept inside the glove box under dry N_2 and another group kept outside the glove box in ambient air. The performance history of the cells was recorded - Figure 4.14. For devices prepared in air and at low values of RH, MAPI is more stable than triple-cation devices when kept inside the glove box. On the other hand, for high RH levels, it is possible to observe the continuous and accentuated performance loss independently of the storage conditions, whilst in Figure 4.9b that trend was not noticeable. Thus, for MAPI devices, the deposition of the perovskite layer under a humidified environment is strongly detrimental. The devices not only showed lower initial photovoltaic performance, as they lose more performance as a function of the time.

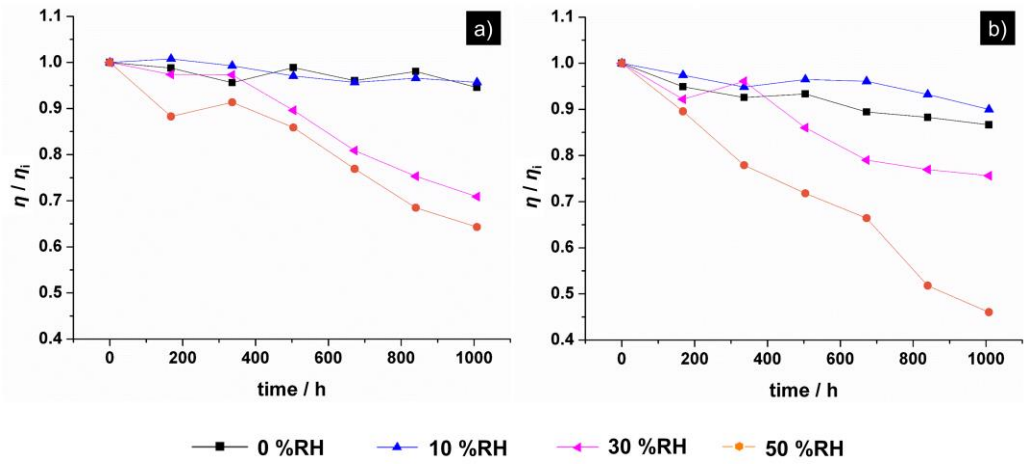

Figure 4.14. Performance history of the devices with MAPI perovskite layer prepared under different values of relative humidity with air as carrier gas. The devices were kept under dark: a) inside the glove box (dry N_2) and b) outside the glove box (air with 30-40 % of RH) – average values.

4.4 Conclusions

Perovskite solar cell technology is close to industrialisation; it is important now to study the cheapest fabrication design and conditions to produce an efficient and stable product. This work addresses the fabrication ambient conditions to produce efficient and stable devices.

The use of humidified solvents to prepare the precursor solutions of triple-cation perovskite displayed a minor effect on the device PCE, demonstrating that to obtain moderate performing PSCs there is no need of using anhydrous solvents. Moreover, when the triple-cation perovskite layer was prepared under inert atmosphere and RH up to 10 %, no instantaneous PCE loss was observed; when the devices were prepared up to 5 % of RH, the PCE loss after 1000 h in dry inert atmosphere was *ca*. 10 %. For higher humidity values, the PCE dive to values as low as half of the initial PCE values.

Devices with perovskite layer prepared under air and RH values higher than 40 %, demonstrate great stability after 1000 h. Devices kept inside the glove box displayed greater stability when compared with devices kept under ambient conditions. The triple-cation perovskite layer prepared in a dry air presented better performance [(15.0 ± 1.1) %] than devices prepared under dry N_2 [(14.5 ± 0.8) %]. However, the devices degrade faster when compared with devices prepared under inert atmosphere; losses of *ca*. 15 % against *ca*. 10 %. Since, only the perovskite layer was prepared inside the humidified glove box and the other layers were prepared in a dry nitrogen glove box, it was possible to conclude that the humidity is actually affecting the crystallisation step of the perovskite layer.

Concerning the deposition of the HEL, spiro-OMeTAD, neither oxygen nor humidity seem to display any influence under atmospheres up to 50 % of RH. The inclusion of FK209 in the spiro-OMeTAD formulation did not improve the performance of the devices, independently of the atmosphere used for depositing the HEL. Since FK209 is the most expensive additive used, avoiding its use is advantageous to decrease the manufacturing costs of the PSC.

This work shows that the restricted conditions normally used to prepare high efficient PSCs, like dry inert atmospheres,[32,33] are not actually needed if triple-cation formulation is used. The best device prepared in this work displayed a PCE of 16.7 % (V_{oc} = 1.09 V, J_{sc} = 20.5 mA·cm^{-2} and *FF* = 0.742), and it was formulated using triple-cation perovskite applied under dry air.

Acknowledgements

I. Mesquita is grateful to FCT (Fundação para a Ciência e a Tecnologia) for her Ph.D. fellow (ref.: PD/PB/105985/2014). L. Andrade also acknowledges FCT for funding (IF/01331/2015). The research leading to these results has received funding from: European Union's Horizon 2020 Programme through a FET Open research and innovation action under Grant agreement no. 687008; project SolarPerovskite - NORTE-01-0145-FEDER-028966 funded by FEDER funds through NORTE 2020 - Programa Operacional Regional do NORTE – and by national funds (PIDDAC) through FCT/MCTES; project WinPSC (POCI-01-0247-FEDER-017796) co-funded by the European Regional Development Fund(ERDF), through the Operational Programme for Competitiveness and Internationalization (COMPETE 2020), under PORTUGAL 2020 Partnership Agreement; POCI-01-0145-FEDER-006939 (LEPABE - UID/EQU/00511/2013), funded by the ERDF, through COMPETE 2020 and by national funds through FCT; and NORTE-01-0145-FEDER-000005 LEPABE-2-ECO-INNOVATION, supported by North Portugal Regional Operational Programme (Norte 2020), under the Portugal2020 Partnership Agreement, through the ERDF. The authors also thank to Professor Pedro Tavares and Doctor Mafalda Pereira for assisting the XRD and UV-vis analysis, respectively, CEMUP for assisting SEM analysis and Doctor Margarida Catarino for help in the assembling of the in-house built glove box

References

[1] L. Meng, J. You, Y. Yang, *Addressing the stability issue of perovskite solar cells for commercial applications,* Nature Communications **9** (2018), 5265.

[2] National Renewable Energy Laboratory, *www.nrel.gov/pv/cellefficiency.html,* 2019.

[3] Z. Song, C.L. McElvany, A.B. Phillips, I. Celik, P.W. Krantz, S.C. Watthage, G.K. Liyanage, D. Apul, M.J. Heben, *A technoeconomic analysis of*

perovskite solar module manufacturing with low-cost materials and techniques, Energy & Environmental Science **10** (2017), p:1297-1305.

[4] L. Contreras-Bernal, C. Aranda, M. Valles-Pelarda, T.T. Ngo, S. Ramos-Terrón, J.J. Gallardo, J. Navas, A. Guerrero, I. Mora-Seró, J. Idígoras, J.A. Anta, *Homeopathic Perovskite Solar Cells: Effect of Humidity during Fabrication on the Performance and Stability of the Device*, The Journal of Physical Chemistry C **122** (2018), p:5341-5348.

[5] L. Zheng, Y. Xuan, *Suppressing the negative effect of UV light on perovskite solar cells via photon management*, Solar Energy **173** (2018), p:1216-1224.

[6] I. Mesquita, L. Andrade, A. Mendes, *Temperature Impact on Perovskite Solar Cells Under Operation*, ChemSusChem **12** (2019), p:2186-2194.

[7] J. Yang, B.D. Siempelkamp, D. Liu, T.L. Kelly, *Investigation of CH3NH3PbI3 Degradation Rates and Mechanisms in Controlled Humidity Environments Using in Situ Techniques*, ACS Nano **9** (2015), p:1955-1963.

[8] Z. Song, A. Abate, S.C. Watthage, G.K. Liyanage, A.B. Phillips, U. Steiner, M. Graetzel, M.J. Heben, *Perovskite Solar Cell Stability in Humid Air: Partially Reversible Phase Transitions in the PbI2-CH3NH3I-H2O System*, Advanced Energy Materials **6** (2016), 1600846.

[9] W. Zhou, Y. Zhao, C. Shi, H. Huang, J. Wei, R. Fu, K. Liu, D. Yu, Q. Zhao, *Reversible Healing Effect of Water Molecules on Fully Crystallized Metal–Halide Perovskite Film*, The Journal of Physical Chemistry C **120** (2016), p:4759-4765.

[10] C. Clegg, I.G. Hill, *Systematic study on the impact of water on the performance and stability of perovskite solar cells*, RSC Advances **6** (2016), p:52448-52458.

[11] D. Liu, C.J. Traverse, P. Chen, M. Elinski, C. Yang, L. Wang, M. Young, R.R. Lunt, *Aqueous-Containing Precursor Solutions for Efficient Perovskite Solar Cells*, Advanced Science **5** (2018), 1700484.

[12] B. Conings, A. Babayigit, T. Vangerven, J. D'Haen, J. Manca, H.-G. Boyen, *The impact of precursor water content on solution-processed*

organometal halide perovskite films and solar cells, Journal of Materials Chemistry A **3** (2015), p:19123-19128.

[13] S. Wozny, M. Yang, A.M. Nardes, C.C. Mercado, S. Ferrere, M.O. Reese, W. Zhou, K. Zhu, *Controlled Humidity Study on the Formation of Higher Efficiency Formamidinium Lead Triiodide-Based Solar Cells*, Chemistry of Materials **27** (2015), p:4814-4820.

[14] M. Salado, L. Contreras-Bernal, L. Caliò, A. Todinova, C. López-Santos, S. Ahmad, A. Borras, J. Idígoras, J.A. Anta, *Impact of moisture on efficiency-determining electronic processes in perovskite solar cells*, Journal of Materials Chemistry A **5** (2017), p:10917-10927.

[15] S. Emami, J. Martins, R. Madureira, D. Hernandez, G. Bernardo, J. Mendes, A. Mendes, *Development of hermetic glass frit encapsulation for perovskite solar cells*, Journal of Physics D: Applied Physics **52** (2018), 074005.

[16] F. Wang, Z. Ye, H. Sarvari, S.M. Park, A. Abtahi, K. Graham, Y. Zhao, Y. Wang, Z.D. Chen, S. Li, *Humidity-insensitive fabrication of efficient perovskite solar cells in ambient air,* Journal of Power Sources **412** (2019), p:359-365.

[17] J. Troughton, K. Hooper, T.M. Watson, *Humidity resistant fabrication of $CH_3NH_3PbI_3$ perovskite solar cells and modules*, Nano Energy **39** (2017), p:60-68.

[18] G. Liu, L. Zhu, H. Zheng, X. Xu, A. Alsaedi, T. Hayat, X. Pan, S. Dai, *Highly efficient and humidity stable perovskite solar cells achieved by introducing perovskite-like metal formate material as the nanocrystal scaffold*, Journal of Power Sources **402** (2018), p:229-236.

[19] M. Kim, S.G. Motti, R. Sorrentino, A. Petrozza, *Enhanced solar cell stability by hygroscopic polymer passivation of metal halide perovskite thin film*, Energy & Environmental Science **11** (2018), p:2609-2619.

[20] I. Hwang, I. Jeong, J. Lee, M.J. Ko, K. Yong, *Enhancing Stability of Perovskite Solar Cells to Moisture by the Facile Hydrophobic Passivation*, ACS Applied Materials & Interfaces **7** (2015), p:17330-17336.

[21] D. Koushik, W.J.H. Verhees, Y. Kuang, S. Veenstra, D. Zhang, M.A. Verheijen, M. Creatore, R.E.I. Schropp, *High-efficiency humidity-stable planar perovskite solar cells based on atomic layer architecture*, Energy & Environmental Science **10** (2017), p:91-100.

[22] L. Greenspan, *Humidity Fixed Points of Binary Saturated Aqueous Solutions, Journal of Research of the National Bureau of Standards* - A. Physics and Chemistry **81**A (1977), p:89-96.

[23] F. Arabpour Roghabadi, M. Alidaei, S.M. Mousavi, T. Ashjari, A.S. Tehrani, V. Ahmadi, S.M. Sadrameli, *Stability progress of perovskite solar cells dependent on the crystalline structure: From 3D ABX_3 to 2D Ruddlesden–Popper perovskite absorbers*, Journal of Materials Chemistry A **7** (2019), p:5898-5933.

[24] M.K. Gangishetty, R.W.J. Scott, T.L. Kelly, *Effect of relative humidity on crystal growth, device performance and hysteresis in planar heterojunction perovskite solar cells*, Nanoscale **8** (2016), p:6300-6307.

[25] K. Rakstys, S. Paek, P. Gao, P. Gratia, T. Marszalek, G. Grancini, K.T. Cho, K. Genevicius, V. Jankauskas, W. Pisula, M.K. Nazeeruddin, *Molecular engineering of face-on oriented dopant-free hole transporting material for perovskite solar cells with 19% PCE*, Journal of Materials Chemistry A **5** (2017), p:7811-7815.

[26] R. Xue, M. Zhang, G. Xu, J. Zhang, W. Chen, H. Chen, M. Yang, C. Cui, Y. Li, Y. Li, *Molecular design with silicon core: toward commercially available hole transport materials for high-performance planar p–i–n perovskite solar cells*, Journal of Materials Chemistry A **6** (2018), p:404-413.

[27] S. Wang, M. Sina, P. Parikh, T. Uekert, B. Shahbazian, A. Devaraj, Y.S. Meng, *Role of 4-tert-Butylpyridine as a Hole Transport Layer Morphological Controller in Perovskite Solar Cells*, Nano Letters **16** (2016), p:5594-5600.

[28] A. Abate, T. Leijtens, S. Pathak, J. Teuscher, R. Avolio, M.E. Errico, J. Kirkpatrik, J.M. Ball, P. Docampo, I. McPherson, H.J. Snaith, *Lithium salts as "redox active" p-type dopants for organic semiconductors and*

their impact in solid-state dye-sensitized solar cells, Physical Chemistry Chemical Physics **15** (2013), p:2572-2579.

[29] J. Urieta-Mora, I. García-Benito, A. Molina-Ontoria, N. Martín, *Hole transporting materials for perovskite solar cells: a chemical approach*, Chemical Society Reviews **47** (2018), p:8541-8571.

[30] J.-W. Lee, D.-H. Kim, H.-S. Kim, S.-W. Seo, S.M. Cho, N.-G. Park, *Formamidinium and Cesium Hybridization for Photo- and Moisture-Stable Perovskite Solar Cell*, Advanced Energy Materials **5** (2015), 1501310.

[31] H.M. Cronin, K.D.G.I. Jayawardena, Z. Stoeva, M. Shkunov, S.R.P. Silva, *Effects of ambient humidity on the optimum annealing time of mixed-halide Perovskite solar cells*, Nanotechnology **28** (2017), 114004.

[32] A. Senocrate, T. Acartürk, G.Y. Kim, R. Merkle, U. Starke, M. Grätzel, J. Maier, *Interaction of oxygen with halide perovskites*, Journal of Materials Chemistry A **6** (2018), p:10847-10855.

[33] H.J. Jung, D. Kim, S. Kim, J. Park, V.P. Dravid, B. Shin, *Stability of Halide Perovskite Solar Cell Devices: In Situ Observation of Oxygen Diffusion under Biasing*, Advanced Materials **30** (2018), 1802769.

CHAPTER 5

GENERAL CONCLUSIONS AND OUTLOOK

5

GENERAL CONCLUSIONS AND OUTLOOK

Among researchers it is consensual the great opportunity for perovskite solar cells (PSCs) to stablish as a competitive photovoltaic technology. PSCs experienced a great power conversion efficiency (PCE) increase in the pasted 10 years, from 3.8 % in 2009 to 25.2 % in 2019,[1] already very close to Shockley-Queisser limit value.[2] Moreover, PSCs are easy to produce and display a great potential for BIPV allowing colour and transparency.

The huge amount of contradicting and incomplete information about PSC fabrication is limiting researchers to reproduce the reported PCEs, making difficult to implement the technology in their laboratories and to perform comparable tests with new materials developed. Therefore, it is important to have facile and complete fabrication and characterisation protocols that allow to achieve reproducible and stable values of PCE. PSCs are made of several thin layers and interfaces, which play important roles in the power conversion efficiency and stability of the devices. So, each layer was analysed and optimised and, as a consequence, it was demonstrated their influence on the entire PSC device. This step-by-step study gave clues for the following works developed within this thesis, supporting the need of more detailed and in-deep comprehension of PSC inner-components. Spray pyrolysis revealed to be the best technique for blocking layer deposition, even if the use of oxygen or air as carrier gas do not affect the performance of the devices. On the other hand, the atmosphere composition during the perovskite layer deposition demonstrated to be of critical relevance, which was then deeply analysed in Chapter 4. Spiro-OMeTAD evidenced to be more efficient hole extraction layer than P3HT but the later presented superior long-term stability, which from an industrial perspective might be more important. Again, following this preliminary study, a detailed thermal-stability study of different HELs was performed in Chapter 3. Thermal evaporation technique is clearly a better back-contact deposition technique. Plasma used during sputtering allows

deeper penetration of the deposited gold into the PSC layers, creating recombination centers. An innovative and versatile method of electrochemical reduction of the TCO was used, being a powerful substitute of laser scribing technique to prepare clean and effective substrate scribing in the FTO substrates. All these studies resulted in the implementation of a systematic fabrication protocol that allows to achieve reproducible, stable and moderately efficient PSCs with (14.8 ± 1.0) % power conversion efficiency.

The long-term stability is a critical factor for market penetration of all photovoltaic technologies and perovskite solar cells are not an exception. The scientific community is more aware of this requirement since PSC technology presents now the needed maturity for being scaled-up. Temperature, oxygen and humidity are the three main environmental factors that influence the operation and stability of the PSCs. To assess the temperature impact on the performance of PSCs, triple-cation devices were prepared using two different HELs, spiro-OMeTAD and PTAA, submitted to thermal-stress in a temperature range of -5 °C to 80 °C and characterised during temperature test operation. At low temperatures (-5 °C), the average performance loss was less than 5 %, indicating poor sensitivity to low temperatures. On the other hand, at high temperatures (80 °C) a significant decrease in the V_{oc} and J_{sc} was observed with a consequent photovoltaic performance loss of (36.0 ± 5.5) %. Since no modifications were observed in XRD diffractogram of the perovskite layer, this performance loss was ascribed to the evaporation of additives present in the HEL. This conclusion was supported by the presence of pinholes in the spiro-OMeTAD layer and by the increase of atomic percentage of chemical elements like F, S and Co on the HEL top surface after thermal-stress. At 80 ºC a device prepared with additivated spiro-OMeTAD displayed the same performance of non-additivated spiro-OMeTAD. PTAA showed better thermal stability than spiro-OMeTAD, with only (8.2 ± 1.6) % of irreversible performance loss compared with (21.6 ± 2.3) % for spiro-OMeTAD. Since PTAA presents less additives concentration, these observations reinforce the additives role on the PSC performance loss upon thermal-stress.

Regarding humidity and oxygen impact in the preparation and stability of PSCs, a systematic study was done with two different deposition atmospheres

(N_2 and air) with a wide range of relative humidity values (0 - 50 %) on two types of perovskite, $CH_3NH_3PbI_3$ and $Cs_{0.05}(MA_{0.17}FA_{0.83})_{0.95}Pb\ (I_{0.83}Br_{0.17})_3$. The use of humidified solvents in the preparation of precursor solutions of triple-cation perovskite did not affect the PCE of the device, concluding that the use of anhydrous solvents to prepare PSC displaying moderate efficiencies (~15 %) is not required. In terms of humidity concentration in the atmosphere during the perovskite deposition step, the scenario is different. When triple-cation perovskite layer is prepared under N_2 and RH up to 10 %, no performance loss is observed, whilst above this value the increase of the RH causes a decrease in the performance of the devices. For devices prepared up to 5 % of RH and stored inside a dry N_2 glove box, the PCE loss after 1000 h is *ca*. 10 %. Triple-cation perovskite layer prepared under dry air presented better average PCE (15.0 ± 1.1) % than devices prepared under dry N_2 (14.5 ± 0.8) %; however, under dry air showed higher performance loss after 1000h, *ca*. 15 % *vs*. *ca*. 10 %. Surprisingly, devices prepared under high humidity values presented better stability during time than the ones prepared under low RH and devices stored inside the glove box displayed greater stability when compared with devices kept under ambient conditions. For MAPI devices this trend is the opposite: the devices prepared with low RH values are those with better stability performance after 1000 h. Concerning the HEL deposition, neither oxygen nor humidity (up to 50 %) displayed any influence. The best device prepared displayed a PCE of 16.7 % (V_{oc} = 1.09 V, J_{sc} = 20.5 mA·cm^{-2} and *FF* = 0.742) and it was assembled under dry air atmosphere. Thus, it is possible to conclude that the restricted atmospheres and anhydrous materials usually reported are not so important to obtain efficient and stable PSCs. Since this type of technology is getting closer to the industrialisation step, the standardisation of cheaper designs and preparation conditions is of major importance.

PSC power conversion efficiencies are being pushed forward by improving the absorption spectrum range of the perovskite absorbers, by replacing the

typical spiro-OMeTAD by thermal stable HELs with high mobility to improve the fill factor and by interface engineering for allowing better efficient charge transfer. The study of different architectures will lead to better understanding the role of each active layer and how they contribute for the device overall performance. Although planar and mesoporous devices show similar results in terms of energy conversion efficiency, the planar architecture is indeed the most appropriate for upscaling, since it presents good PCE and stability with less fabrication complexity. The substitution of spin-coating technique is a matter of great importance. Among the deposition methods available for the devices scale-up, slot-die and blade-coating seem to present interesting advantages over other processes. The most relevant is the fact that slot-die and blade-coating can print large areas of softly irregular surfaces and in any type of substrate, leaving the surroundings clean; they can operate at very high deposition rates displaying very low costs. Slot-die and blade-coating were used to prepare PSC modules with good energy conversion performance PSC of 13.8 % (144 cm^2 active area)[3] and 14.6 % (57.2 cm^2 active area)[4], respectively.

Future improvements on the stability of PSCs can be possible if a proper encapsulation method is used. The host laboratory developed a low temperature laser sealing method that has already demonstrated to be compatible with scribing and blocking layer steps.[5] The next stage is to understand the type of atmosphere that should be used during the encapsulation: an inert atmosphere or a less restrictive one. The stability of the devices under real outdoor conditions should also be assessed.

The photovoltaic community is aware of the toxicity associated with the lead content in the highly performing perovskite solar cells. However, the metal content per square meter of a solar panel is only few hundred milligrams, and so no extra concerns may arise when compared to contending solar cells technologies. In case of catastrophic perovskite module failure, the added amount of lead to the ambient is very small in comparison to the natural occurrence of lead in soils; 1 m^2 PSC module has the equivalent amount of

lead to 1 cm-thick natural soil with the same area.[6] Nevertheless, the actual environmental awareness concerning toxic elements as lead is increasing. Even though the lead content is very low, this might not be enough to be well accepted by the restrictive guidelines given by Europe to the PV producers. So, the natural trend might be to fully eliminate lead from PV devices, which makes Pb substitution a matter of extreme urgency in perovskite solar cells.

Besides all efforts for developing efficient and stable PSC devices it is critical the standardisation of the energy conversion efficiency and stability characterisation protocols with the adoption of MPP tracking. The standardisation is crucial for realistic comparative assessment of the performance of PCSs prepared by different research groups and companies.

Finally, only few groups have focused in the economic assessment of perovskite modules manufacture.[7,8,9] Song *et al*.[9] presented a comprehensive study evaluating the direct manufacturing cost of a perovskite module, using low cost materials and methods that demonstrated high efficiencies in lab devices. The authors calculated a cost per module of 31.7 $\$\cdot m^{-2}$ and a minimum sustainable price (MSP) of 0.41 $\$\cdot W_p^{-1}$. The MSP is defined as the minimum price charged to cover all variable and fixed costs and to pay back to the investors at their minimum rate of return. Based in a PCE of 16 %, a 30 years' lifetime and no incentives, the LCOE (Levelized Cost of Electricity) was estimated to be 4.93-7.90 $¢\$\cdot kWh^{-1}$. These values evidence that perovskite can emerge as a cost leader in the market competing with other PV technologies.

References

[1] National Renewable Energy Laboratory, *https://www.nrel.gov/pv/cell-efficiency.html*, 2019.

[2] A.A.B. Baloch, M.I. Hossain, N. Tabet, F.H. Alharbi, *Practical Efficiency Limit of Methylammonium Lead Iodide Perovskite ($CH_3NH_3PbI_3$) Solar Cells,* The Journal of Physical Chemistry Letters **9** (2018), p:426-434.

[3] PV-Magazine, *Solliance achieves 14.5% cell efficiency on perovskite module*, *https://www.pv-magazine.com/2018/04/09/solliance-achieves-14-5-cell-effici ency-on-perovskite-module/*, May 2019.

[4] Y. Deng, X. Zheng, Y. Bai, Q. Wang, J. Zhao, J. Huang, *Surfactant-controlled ink drying enables high-speed deposition of perovskite films for efficient photovoltaic modules*, Nature Energy **3** (2018), p:560-566.

[5] S. Emami, J. Martins, R. Madureira, D. Hernandez, G. Bernardo, J. Mendes, A. Mendes, *Development of hermetic glass frit encapsulation for perovskite solar cells*, Journal of Physics D: Applied Physics **52** (2018), 074005.

[6] N.-G. Park, M. Grätzel, T. Miyasaka, K. Zhu, K. Emery, *Towards stable and commercially available perovskite solar cells*, Nature Energy **1** (2016), 16152.

[7] M. Cai, Y. Wu, H. Chen, X. Yang, Y. Qiang, L. Han, *Cost-Performance Analysis of Perovskite Solar Modules*, Advanced Science **4** (2017), 1600269.

[8] N.L. Chang, A.W. Yi Ho-Baillie, P.A. Basore, T.L. Young, R. Evans, R.J. Egan, *A manufacturing cost estimation method with uncertainty analysis and its application to perovskite on glass photovoltaic modules*, Progress in Photovoltaics: Research and Applications **25** (2017), p:390-405.

[9] Z. Song, C.L. McElvany, A.B. Phillips, I. Celik, P.W. Krantz, S.C. Watthage, G.K. Liyanage, D. Apul, M.J. Heben, *A technoeconomic analysis of perovskite solar module manufacturing with low-cost materials and techniques*, Energy & Environmental Science **10** (2017), p:1297-1305.